VOLUME 32, NUMBER 1 MARCH 2015

ALGEBRAS, GROUPS AND GEOMETRIES

ALGEBRAS, GROUPS & GEOMETRIES Volume 32, Number 1, March 2015

EDITORIAL BOARD

M.R. ADHIKARI
A.K. ARINGAZIN
A. BAYOUMI
G. CARICATO
QING-MING CHENG
A. HARMANCY
L. P. HORWITZ
C. P. JOHNSON
S.L. KALLA
L. KEXI
N. KAMIYA
A. U. KLIMYK
J. A. LESLIE*
J. LOHMUS*
R. MIRON
M.R. MOLAEI
P. NOWOSAD
KAR-PING SHUM
S. SILVESTROV
H. M. SRIVASTAVA
G.T. TSAGAS*

* In memoriam

FOUNDER AND EDITOR IN CHIEF
R.M. SANTILLI

FOUNDED IN 1984. SOME OF THE PAST EDITORS INCLUDE PROFESSORS: A. A. ANDERSEN, V. V. DEODHAR, J. R. FAULKNER, M. GOLDBERG, N. IWAHORI, M. KOECHER, M. MARCUS, K. M. MCCRIMMON, R. V. MOODY, R. H. OHEMKE, J. M. OSBORN, J. PATERA, H. RUND, T. A. SPRINGER, G. S. TSAGAS.

HADRONIC PRESS, INC.

ALGEBRAS GROUPS AND GEOMETRIES

VOLUME 32, NUMBER 1, MARCH 2015

QUALITATIVE ANALYSIS OF MATHEMATICAL MODELS OF RELAXING MEDIA WITH SPATIAL AND TEMPORAL NONLOCALITY, 1

Danylenko V.A., Danevich T.B., Makarenko O.S., Skurativisky S.I. and Vladimirov V.A.
Subbotin Institute of Geophysics of the National Academy of Sciences of Ukraine
Palladin Av. 32, Kyiv, Ukraine, UA-03680

MATHEMATICAL MODELLING IN HYDRODYNAMICS WITH MEMORY, 53

Danylenko V.A., Danevich T.B., Makarenko O.S., Skurativisky S.I. and Vladimirov V.A.
Subbotin Institute of Geophysics of the National Academy of Sciences of Ukraine
Palladin Av. 32, Kyiv, Ukraine, UA-03680

QUALITATIVE ANALYSIS OF MATHEMATICAL MODELS OF RELAXING MEDIA WITH SPATIAL AND TEMPORAL NONLOCALITY[1]

Danylenko V.A., Danevich T.B., Makarenko O.S.[2], Skurativisky S.I. and Vladimirov V.A.
Subbotin Institute of Geophysics of the National Academy of Sciences of Ukraine
Palladin Av. 32
Kyiv, Ukraine, UA-03680
makalex@i.com.ua

Received October 30, 2014

Abstract

In this article we study the following objects:

1. The model of the relaxing medium, which is representative of models with temporal nonlocality.
2. The model taking into account effects of spatial nonlocality.
3. The generalization of the models obtained above by means of incorporation of the spatial and temporal nonlocalities.
4. The model of the medium with physical nonlinearity, temporal and spatial nonlocalities.

[1]Based on invited talks given by A. Makarenko at the 6th Petrov International Symposium on *High Energy Physics, Cosmology and Gravity*, Kyiv–Kosivska Poliana (Ukraine), September 5–20, 2013.

[2]On leave from the National Technical University of Ukraine (KPI), Ukraine.

Copyright © 2015 by Hadronic Press Inc., Palm Harbor, FL 34682, U.S.A

1. Analysis of the relaxing hydrodynamics equations invariant solutions (Eulerian coordinates)

Using the methods of the phenomenological thermodynamics presented in [1–3], the state of the medium can be described with the help of additional internal variable (denote it as λ), which satisfies some phenomenological integro-differential relations

$$\Phi(\lambda, \dot{\lambda}, \bigtriangledown\lambda, ...; s, \dot{s}, \bigtriangledown s, ...) = 0, \tag{1}$$

where s_i are external parameters (volume, temperature). Using different modeling cases of equation (1), we obtain the dynamical equations of state of the structured medium, which concretely define its mathematical model.

One of the simplest dynamical equations of state, taking into account relaxation, has the following form:

$$\tau\left(\frac{dp}{dt} - \chi\frac{d\rho}{dt}\right) = \kappa\rho - p, \tag{2}$$

where function ρ is density of medium, p is pressure, u is velocity, $d(\cdot)/dt = \partial(\cdot)/\partial t + u\,\partial(\cdot)/\partial x$ is a substantial derivative, parameters τ, κ, χ are nonnegative constants. Together with the balance equations for mass and momentum

$$\rho\frac{du}{dt} + \frac{\partial p}{\partial x} = \gamma\rho, \qquad \frac{d\rho}{dt} + \frac{\partial u}{\partial x} = 0, \tag{3}$$

equation (2) forms a closed system of PDE. Using the Lie symmetry methods [4,5], one can be convinced, that system (2)–(3) admits the one-parametric Lie group, generated by the operator

$$\hat{Z} = \frac{\partial}{\partial t} + D\frac{\partial}{\partial x} + \xi\left(\rho\frac{\partial}{\partial\rho} + p\frac{\partial}{\partial p}\right). \tag{4}$$

Based on the invariants of operator (4), we construct the ansatz

$$u = U(\omega) + D, \quad \rho = \rho_0 \exp\{\xi t + S(\omega)\}, \quad p = Z(\omega)\,\rho, \quad \omega = x - Dt \tag{5}$$

enabling to perform the self-similar reduction of the initial system of PDE's. Equations (5) describe the invariant wave pack, moving with velocity D. It is easy to check that system (2) has the stationary invariant solution

$$u_1 = 0, \quad \rho = \rho_0 \exp\left\{\xi x D^{-1}\right\}, \quad p_1 = \kappa\rho_1, \tag{6}$$

if $\gamma = \kappa\xi D^{-1}$. Note that, parameter ξ determines the slope of the inhomogeneity of the stationary invariant solution (6), when the remaining parameters are fixed. Inserting ansatz (5) into system (2) - (3), we obtain one quadrature and two-dimensional dynamical system, which after some algebraic manipulation can be presented as follows:

$$\begin{aligned} U\Delta\frac{dU}{d\omega} &= U\left(\tau\gamma U + \sigma Z - \kappa\right) = Uf, \\ U\Delta\frac{dZ}{d\omega} &= \left(Z - U^2\right) f + \Delta\left(\gamma U + \xi Z\right). \end{aligned} \tag{7}$$

Here $\Delta = \tau\left(U^2 - \chi\right)$, $\sigma = 1 + \tau\xi$. System (7) has only one critical point A

$$U = -\frac{\kappa\xi}{\gamma} \equiv -D, \quad Z = \kappa, \tag{8}$$

which belongs to the physical parameters range. Note that, this critical point represents the stationary invariant solution (6). Other critical points are

$$O\left(0;0\right), \quad B\left(0;\kappa + \chi\xi/\sigma\right), \quad H_{1,2}\left(\pm\sqrt{\frac{\chi}{\tau}};\frac{\kappa}{\sigma}\left(1 \mp \frac{\tau\gamma}{\kappa}\sqrt{\frac{\chi}{\tau}}\right)\right).$$

Let us analyze the conditions leading to the limit cycle appearance in the vicinity of critical point $A\left(-D;\kappa\right)$. In coordinates $x = U + D$, $y = Z - \kappa$ the linear part of system (7) takes on the following form:

$$\begin{pmatrix} x \\ y \end{pmatrix}' = \begin{bmatrix} -\kappa\xi\tau & \sigma U_1 \\ \gamma\tau\left(\kappa - \chi\right) & \kappa\sigma - \xi\tau\chi - U_1^2 \end{bmatrix} \begin{pmatrix} x \\ y \end{pmatrix} \equiv \hat{R}\begin{pmatrix} x \\ y \end{pmatrix}, \tag{9}$$

where $U_1 = -D$, $(\cdot)' = U\Delta d\left(\cdot\right)/d\omega$. As it is well known, the Hopf bifurcation could take place in the nonlinear system if the eigenvalues of the

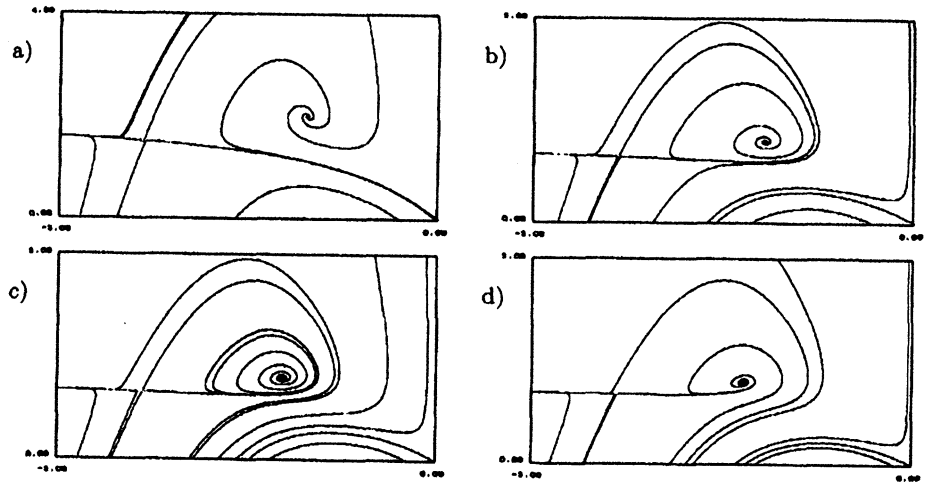

Fig. 1: Phase portraits of system (7), obtained at the following values of parameters $\kappa = 2$, $\xi = -0.5$, $\chi = 5$, $\tau = 0.33$, $D = D_{cr} + \mu$ and a) $\mu = -0.4$, b) $\mu = -0.165$, c) $\mu = -0.1$, d) $\mu = 0.1$

linearization matrix $\hat{R}$ are purely imaginary. This is so if Sp $\hat{R}$ nullifies, while Det $\hat{R}$ is positive. The condition Sp $\hat{R} = 0$ is fulfilled if

$$D = D_{cr} = \sqrt{\kappa - \chi\tau\xi}. \tag{10}$$

The fulfillment of the condition Det $\hat{R} > 0$ depends on the sign of parameter ξ. We choose the sign in such a way that condition $\chi > \kappa$, suggested by the physical reason be satisfied. Since the constants τ, κ, χ are non-negative, then the only way to fulfil the inequality is to take $\xi < 0$. With this choice inequality Det $\hat{R} > 0$ can be written as follows

$$\chi > \frac{\kappa}{\sigma} > \kappa. \tag{11}$$

Note that, we have an additional inequalities $0 < \sigma = 1 + \tau\xi < 1$ from above. In order to study solutions that arise when parameter D differs from critical value (10), we pass to the variables v, w, defined as follows

$$v = x, \quad w = (y - Ex)\, L^{-1}, \tag{12}$$

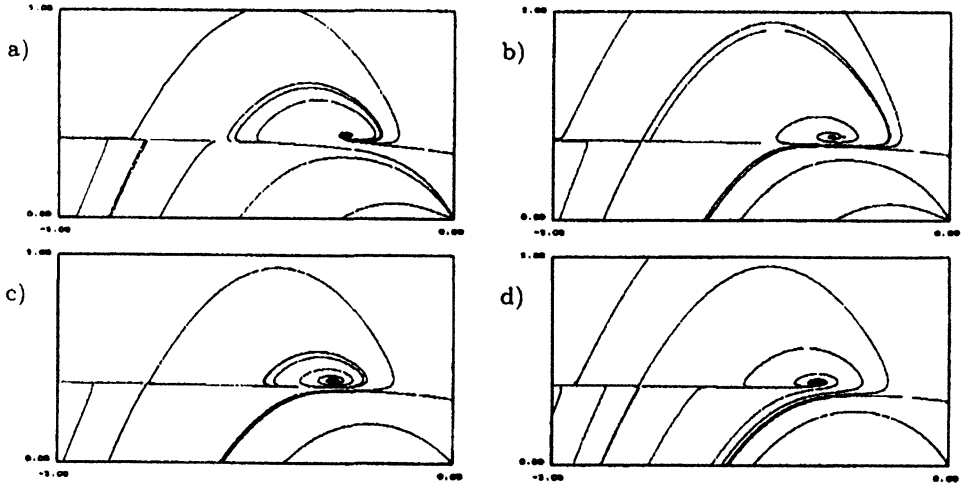

Fig. 2: Phase portraits of system (7), obtained at the following values of parameters $\kappa = 2$, $\xi = -0.1$, $\chi = 5$, $\tau = 0.33$, $D = D_{cr} + \mu$ and a) $\mu = -0.25$, b) $\mu = -0.1135$, c) $\mu = -0.07$, d) $\mu = 0.07$

where

$$E = \frac{\tau\kappa\xi}{\sigma U_1}, \quad L = -\frac{\Omega}{\sigma U_1}, \quad \Omega = \sqrt{\kappa\xi\tau\left(\kappa - \chi\sigma\right)}$$

and use parameter $\mu = D - D_{cr}$ as the parameter of bifurcation. In new coordinates, system (7) takes on the form

$$\begin{aligned} v' &= a_1(\mu)\, v - \Omega_1(\mu)\, w + F(v, w), \\ w' &= \Omega_2(\mu)\, v + a_2(\mu)\, w + G(v, w), \end{aligned} \tag{13}$$

where $a_1(\mu) = -\mu\sigma E$, $a_2(\mu) = \mu(\sigma E - 2D)$, $\Omega_i(\mu) = \Omega + O(|\mu|)$, $i = 1, 2$,

$$\begin{aligned} F &= -\Omega U_1^{-1} vw + O(|\mu|), \\ G &= \frac{1}{L}\left\{(Ev + Lw)\left(\sigma Lw - 2U_1 v - v^2\right) + E\Omega U_1^{-1} vw\right\} + O(|\mu|). \end{aligned} \tag{14}$$

Using the standard transformation we can pass to the canonical represen-

tation:

$$\begin{pmatrix} Z_1 \\ Z_2 \end{pmatrix}' = \begin{pmatrix} a(\mu) & -\Omega(\mu) \\ \Omega(\mu) & a(\mu) \end{pmatrix} \begin{pmatrix} Z_1 \\ Z_2 \end{pmatrix} + \\ + \begin{pmatrix} \mathrm{Re}C_1(\mu) & -\mathrm{Im}C_1(\mu) \\ \mathrm{Im}C_1(\mu) & \mathrm{Re}C_1(\mu) \end{pmatrix} \begin{pmatrix} Z_1 \\ Z_2 \end{pmatrix} |Z|^2 + O\left(|Z|^3\right), \tag{15}$$

where $a(\mu) = (a_1(\mu) + a_2(\mu))/2 \equiv -D\mu$, $\Omega(\mu) = \Omega + O(|\mu|)$, $C_1(\mu)$ is the first Floquet index [6]. If $\mathrm{Re}C_1(0) \neq 0$, then the limit cycle exists as $|a(\mu)| \ll 1$ and $a(\mu)\,\mathrm{Re}C_1(0) < 0$. For small μ, the stability of the limit cycle is defined by the sign of $\mathrm{Re}C_1(0)$, which is calculated on the basis of the well known formula. For the case under consideration it reduces to

$$16\Omega \mathrm{Re}C_1(0) = \Omega G_{vvw} - G_{vw}(G_{vv} + G_{ww}) = \\ = -2\Omega - \frac{1}{L^2}\left(E\sigma L - 2U_1 L + E\frac{\Omega}{L}\right)\left(2\sigma L^2 - 4U_1 E\right),$$

where lower indices denote the partial derivatives over the subsequent variables. Inserting E and L into this equation and taking (10) and (14) into account we finally obtain:

$$\mathrm{Re}C_1(0) = -\frac{\kappa|\xi|}{8\Omega^2}\left(3\chi + \tau U_1^2\right). \tag{16}$$

In order to formulate the main result of this section, we must estimate the sign of factor $U\Delta$, standing at the LHS of system (7). In the proximity of the critical point, the value of $|U - U_1|$ has the same order of magnitude as $|\mu| = |D - D_{cr}|$, therefore

$$\mathrm{sgn}\left[\tau U\left(U^2 - \chi\right)\right] = \mathrm{sgn}\left[\tau D\left(\chi - D^2\right) + O(|\mu|)\right] = \mathrm{sgn}\left[\chi\sigma - \kappa + O(|\mu|)\right] = 1,$$

as $|\mu| \ll 1$. Thus, the following statement holds.

Theorem 1..1. *Let $\xi < 0$ and inequalities (11) take place. Then there is an open interval J in the proximity of critical value $D = D_{cr} = \sqrt{\kappa - \chi\tau\xi}$, so that system (7) possesses stable periodic solutions whenever $D \in J$.*

The results obtained were backed by the direct numerical simulation carried out for $\xi = -0.5$, $\kappa = 2$, $\tau = 0.33$, $\chi = 5$ (Fig.1). When the

bifurcation parameter $\mu = D - D_{cr}$ is negative and its absolute value is sufficiently large, critical point $A(-D;\kappa)$ is an unstable focus, and all the trajectories but one go to infinity (Fig. 1a). At $\mu \approx -0.165$ the stable and unstable separatrices of saddle point $B(0;\kappa + \chi\xi/\sigma)$ join together, forming the homoclinic loop (Fig. 1b), and this way the limit cycle of a finite radius is created (Fig.1c). The radius of the limit cycle tends to zero as $\mu \to -0$.

For $\mu > 0$ critical point $A(-D;\kappa)$ is a stable focus (Fig.1d). On analyzing the coordinates of critical point $B(0;\kappa + \chi\xi/\sigma)$, one can easily conclude that, depending on the values of the parameters, the point B lying on the OZ axis can belong either to the upper or to the lower half-plane. This circumstance is sufficiently important, since the lower half-plane corresponds to physically meaningless values of parameter Z.

The phase portraits corresponding to the second option are obtained for $\kappa = 2, \chi = 5, \xi = -0.1$ (Fig.2). Numerical simulations show that the pattern of bifurcations does not differ from that of the previous case, yet critical point $O(0;0)$ now becomes a stable node, attracting some trajectories of the dynamical system. Like in the previous case, the limit cycle is created as a result of the homoclinic bifurcation, and its maximal radius is of the same order as the distance between critical point A and saddle point B, lying in the left half-plane.

1.1. Travelling wave solutions of the model of relaxing medium, in the case when $\chi = 0$

It is interesting to consider invariant solutions of system (2)–(3) when $\chi \to 0$. In this case, one characteristic velocity nullifies and the criteria of the periodic solutions appearance, as well as the bifurcation patterns, become completely different from that discussed in the previous section. When $\chi = 0$, inserting ansatz (5) into system (2)–(3) we again obtain one quadrature and the dynamical system:

$$\begin{aligned} \tau U^3 \frac{dU}{d\omega} &= U(\tau\gamma U + \sigma Z - \kappa) = Uf, \\ \tau U^3 \frac{dZ}{d\omega} &= U^2(\kappa - Z) + Zf. \end{aligned} \tag{17}$$

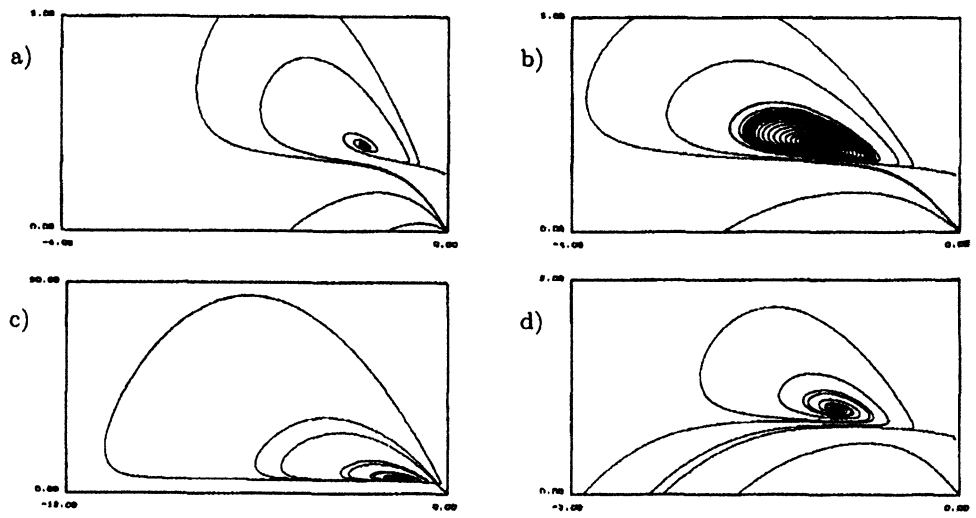

Fig. 3: Phase portraits of system (17), obtained at the following values of parameters $\kappa = 2$, $\xi = 0.5$, $\tau = 1$, $D = D_{cr} + \mu$ and a) $\mu = -0.1$, b) $\mu = 0.03$, c) $\mu = 0.08299515$, d) $\mu = 0.15$

System (17) has the following critical points $O\,(0;0)$, $B\,(0;\kappa/\sigma)$, $A\,(-D;\kappa)$ (it represents the stationary invariant solution (6)).

We are going to state the conditions leading to the appearance of the periodic solution in the proximity of critical point $A\,(-D;\kappa)$ and study the bifurcations of this solution. To begin with, let us write down the linear part of the system in coordinates $X = U + D$, $Y = Z - \kappa$:

$$\tau U^3 \frac{d}{d\omega}\begin{pmatrix} X \\ Y \end{pmatrix} = \begin{bmatrix} -\kappa\xi\tau & \sigma U_1 \\ \kappa\gamma\tau & \kappa\sigma - U_1^2 \end{bmatrix}\begin{pmatrix} X \\ Y \end{pmatrix} \equiv \hat{R}\begin{pmatrix} X \\ Y \end{pmatrix}, \qquad (18)$$

where $U_1 = -D = -\kappa\xi/\gamma$. The matrix $\hat{R}$, standing in the RHS of equation (18) has a pair of pure imaginary eigenvalues if

$$D = D_{cr} = \sqrt{\kappa} \qquad (19)$$

and the inequality

$$\tau\xi\kappa^2 > 0$$

holds. Since parameter τ is non-negative by its physical meaning, then the above inequality could be true, only when $\xi > 0$.

In order to study the conditions leading to the limit cycle creation, we would pass to the canonical representation and find the expression for the real part of the first Floquet index $C_1(\mu)$. We can perform this passage, using transformation (12), where, in accordance with (19), we put

$$\Omega = \kappa\sqrt{\xi\tau} \equiv \sqrt{\kappa\xi\tau}\,|U_1|\,. \tag{20}$$

Since the procedure of the Floquet index calculation for the considered case is not changed, equation (16) is still valid. Putting in formula $\chi = 0$, and taking account of (19), we have:

$$\mathrm{Re}C_1(0) = \frac{\kappa\xi\tau U_1^2}{8\Omega^2} = \frac{1}{8}. \tag{21}$$

Thus, the real part of the Floquet index is positive when χ nullifies.

In order that the analysis be consistent, we should take into consideration the sign of factor τU^3 standing on the LHS of system (17) (which was temporarily ignored). To do this, let us note that critical point $A(-D;\kappa)$ lies in the half-plane $U \leq 0$, which is separated from the right half-plane by the separatrices, completely filling the vertical axis. Therefore $\mathrm{sgn}(\tau U^3) = \mathrm{sgn}\,U = -1$ on each phase trajectory starting at the left half-plane. Taking this into account, we can formulate the following statement:

Theorem 1..2. *If $\xi > 0$, then an open interval $J \in R^1$ exists, containing the critical value of the parameter D_{cr}, given by formula (19), so that system (18) possesses a stable periodic solution whenever $D \in J$.*

Figures 3 show system's (17) phase trajectories, obtained by the direct numerical simulation, in which the following values of the parameters were used: $\tau = 1$, $\kappa = 2$, $\xi = 0.5$. As a bifurcation parameter we took the parameter $\mu = D - D_{cr}$. Thus, for $\mu < 0$ critical point $A(-D;\kappa)$ is a stable focus (see Fig.3 a). A stable limit cycle softly arises, when μ becomes positive (Fig.3b). The radius of this cycle grows as the bifurcation parameter approaches the second critical value $\mu_{cr} = 0.082995155$ from the left. The right edge of the periodic trajectory becomes sharper and tends to critical

point $B\,(0;\kappa/\sigma)$ as $\mu \to \mu_{cr}^{-}$. When the bifurcation parameter differs from μ_{cr} at a very small addend of the order of 10^{-9} then its further growth causes a rapid growth of sizes of the periodic trajectory (Fig. 3c), which seem to become unbounded at certain value of μ_3, which is a bit larger than μ_{cr}. From this observation we can guess that the periodic trajectory tends to the heteroclinic cycle, connecting critical point $B\,(0;\kappa/\sigma)$ with the critical points in infinity as $\mu \to \mu_3^{-}$. Finally, when $\mu > \mu_3$, the critical point becomes an unstable focus (Fig.3d).

To realize what really happens when the bifurcation parameter approaches μ_3 from the left, it is necessary to study the critical points in infinity. Before we start this study, let us note that the formation of the unbounded heteroclinic cycle is a consequence of the fact that one of the separatrices of the saddle point $B\,(0;\kappa/\sigma)$ coincides with segment $[\kappa/\sigma;\infty)$ of the vertical axis, and therefore is immovable. Thus, the usual homoclinic bifurcation which would result in the destruction of the limit cycle is impossible in this case. To study the points in infinity, we use the coordinates

$$U = \frac{1}{W}, \quad Z = \frac{V}{W} \tag{22}$$

and

$$U = \frac{R}{S}, \quad Z = \frac{1}{S}. \tag{23}$$

The first transformation gives all the critical points lying on the equator of the Poincare sphere except those, corresponding to the "ends" of the OZ axis.

So, performing transformation (22), we obtain the following system

$$\begin{aligned} W^2V' &= V - \kappa W, \\ W^2W' &= W^2\left(\tau\gamma + \sigma V - \kappa W\right). \end{aligned} \tag{24}$$

The only critical point of system (24) corresponding to the initial system's points "in infinity" is critical point $O\,(0;\,0)$. This point is of the saddle-node type, its saddle sector being located in the left half-plane. Now, let us analyze the critical points located at the "ends" of the OZ axis. Using the change of coordinates (23), we get the following system:

$$\begin{aligned} S^2R' &= -R^3 + \kappa R^3 S, \\ S^2S' &= (\kappa S - 1)\,SR^2 - S^2\left(\kappa S - \sigma - \tau\gamma R\right). \end{aligned} \tag{25}$$

The critical point we are interested in, is point $O\,(0;\,0)$. This critical point occurs to be more complicated than that of system (24), since its linear part completely nullifies. Therefore the standard classification scheme is of no use here and we should analyze this point "by hand". To begin with, let us note that the coordinate axes OR and OS play the role of separatrices. The trajectory starting at any point lying on the OR axis tends to zero as the independent variable grows, the trajectories starting at the negative part of the OS axis also tend to the origin, while the trajectories starting at its positive part move away from the origin. The negative half-plane $S \leq 0$ contains a stable nodal sector, as stated below.

Lemma 1..1. *All the trajectories placed at the some neighborhood of the origin in the half-plane $S \leq 0$ cross a circle $K\,(0;\rho)$ from the outside, provided that the radius ρ is sufficiently small.*

Proof. Let us consider function $V\,(R,S) = R^2 + S^2$. Calculating the derivative of function $V\,(R\,(\omega)\,,\,S\,(\omega))$ along the direction of the vector field defined by the RHS of system (25) at the points of set $V\,(R,S) = \rho$, $S < 0$, $0 < \rho \ll 1$, we obtain:

$$\left.\frac{dV}{d\omega}\right|_{\substack{R^2+S^2=\rho^2,\\ S<0}} = -2\left[R^2\rho^2 + \sigma\left(\rho^2 - R^2\right)^{3/2}\right] + O\left(\rho^3\right) < 0.$$

Therefore, every phase trajectory intersecting the level curve $V\,(R,S) = \rho$ at the lower half-plane for a sufficiently small p is directed "inwards" to the circle. ■

Now, let us analyze the upper half-plane. One easily gets convinced by the straightforward verification, that phase trajectories from the small neighborhood of the origin, placed above line $S = R^2/\sigma$, are directed "upwards", i.e. a saddle sector exists on the upper half-plane. So, the only thing remaining unknown is whether there are some nodal sectors between line $S = R^2/\sigma$ and the horizontal axis. But, if any such sector does exist, then the invariant trajectory L, separating the nodal sectors from the saddle one should exist. This trajectory should be tangent to the OR axis at the origin and therefore its asymptotics must be as follows:

$$S\,(R) \sim \alpha_2 R^2 + \alpha_3 R^3 + \ldots \tag{26}$$

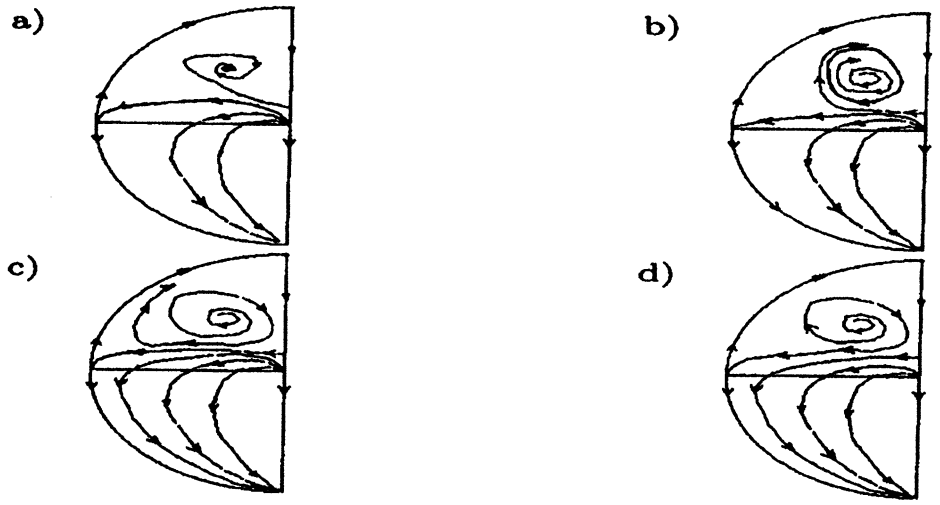

Fig. 4: Global phase portraits of system (17), corresponding to a) $\mu < 0$, b) $0 < \mu < \mu_{cr2}$, c) $\mu = \mu_{cr2}$, d) $\mu > \mu_{cr2}$

Inserting (26) into equation

$$\frac{dS}{dR} = \frac{S}{R} + \frac{S^2\left(\kappa S - \sigma - \tau\gamma R\right)}{R^3\left(1 - \kappa S\right)} \tag{27}$$

and equating to zero the coefficient at the lowest order of R, we obtain:

$$\alpha_2\left(1 + \sigma\alpha_2\right).$$

So, either $\alpha_2 = 0$ or $\alpha_2 = -1/\sigma$. However, in the second case the separatrice has the asymptotics $S\left(R\right) \sim -1/\sigma R^2$ at the origin, and therefore it lies at the half-space $S < 0$.

Let us then assume that the first case takes place and $S\left(R\right) \sim \alpha_{3+\nu} R^{3+\nu}$ with $\nu \geq 0$. Inserting this approximation into equation (27), we obtain in the lowest order that $\alpha_{3+\nu} = 0$. Since the index ν is arbitrary, then the saddle separatrice coincides with the horizontal axis and the following statement holds:

Lemma 1..2. *Critical point* $O\left(0;\ 0\right)$ *is a saddle-node, with the saddle sector lying in the upper half-plane and the stable nodal sector filling the lower one.*

On the basis of the above analysis we are able to construct the bifurcation diagrams showing how the limit cycle is destroyed. Since we are merely interested in the behaviour of the phase trajectories on the half-plane $U < 0$, we do not show the remaining part of phase space $(U; Z)$ (in fact, we are able to ignore the presence of the right half-plane, because it is completely separated from the left one by the separatrices, lying on the vertical axis). The subsequent phase portraits are shown in Figures 4.

2. Peculiarities of stochastic invariant solutions of a hydrodynamic system accounting for non-local effects

To describe the mechanism of relaxation in more detail, the dynamical equation of state (2) should be supplemented. For these purposes the following relation is proposed:

$$\tau\left(\frac{dp}{dt} - \chi\frac{d\rho}{dt}\right) = \kappa\rho - p - h\left\{\frac{d^2p}{dt^2} + \left[\frac{2}{\rho}\left(\frac{d\rho}{dt}\right)^2 - \frac{d^2\rho}{dt^2}\right]\right\}, \qquad (28)$$

where h is a coefficient of structural relaxation, which is connected with the effect of temporal nonlocality.

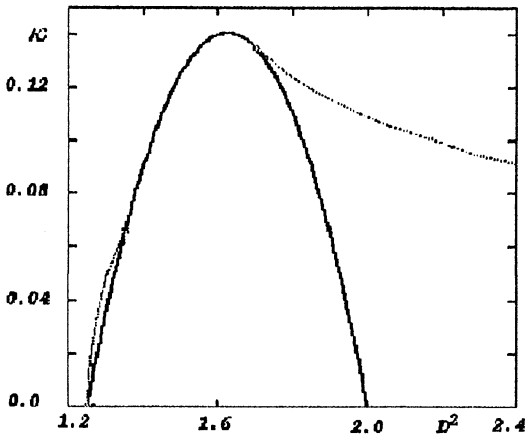

Fig. 5: Bifurcation diagram of system (29) in plane (D^2, κ), obtained for $h = 0.8$ and $\xi = -1.25$. The solid line corresponds to a Hopf bifurcation while the dotted lines correspond to a twin cycle bifurcation.

To get a closed system we affiliate system (3) to equation (28):

$$\rho\frac{du}{dt}+\frac{\partial p}{\partial x}=\gamma\rho, \qquad \frac{d\rho}{dt}+\frac{\partial u}{\partial x}=0,$$

and will try to find the structure of subset (5) of invariant solutions. Note that the introduced model with the high derivatives with respect to the temporal variable keeps its hyperbolic type.

Inserting relation (5) into the presented system, we obtain an ODE system of three equations:

$$\begin{aligned} &U\dot{U}=UW,\\ &U\dot{Z}=\gamma U+\xi Z+W(Z-U^2),\\ &U\dot{W}=[h(U^2-1)]^{-1}\{M\Phi+Z-\kappa+W(1-MZ)\}-W^2, \end{aligned} \tag{29}$$

where $M=1+h\xi$.

The only critical point of system (29) belonging to the physical parameter range (i.e., lying in the half-space $Z>0$ beyond the manifold $U(U^2-1)=0$) is point A with the coordinates

$$U_0=-\kappa\xi/\gamma\equiv -D, \qquad Z_0=\kappa, \qquad W_0=0. \tag{30}$$

We are going to analyze localized solutions of system (29) in the vicinity of this point. Let us introduce new variables $X=U-U_0$, $Y=Z-\kappa$. In coordinates X, Y, W, system (29) may be rewritten as follows:

$$U\frac{d}{d\omega}\begin{pmatrix}X\\Y\\W\end{pmatrix}=\begin{pmatrix}0, & 0, & U_0\\ \gamma, & \xi, & \Delta\\ L\gamma, & L\xi+G_1, & \sigma\end{pmatrix}\begin{pmatrix}X\\Y\\W\end{pmatrix}+O\left(|X|^2,|Y|^2,|W|^2\right), \tag{31}$$

where $L=M/K, G_1=K^{-1}$, $K=h(D^2-1)$, $\Delta=\kappa-D^2$, $\sigma=(1-MD^2)/K$.

We are going to analyze the case where matrix $\hat{M}$ standing on the RHS of equation (31) has one negative eigenvalue $\lambda_1=a<0$ and a pair of pure imaginary eigenvalues $\lambda_{2,3}=\pm\Omega$. Taking into account that function $U(\omega)$ standing on the LHS of equation (29) is negative in the vicinity of the

critical point, we can write the above conditions as follows:

$$a = \text{tr } \hat{M} = (D^2 - 1 + \xi h)/K < 0, \tag{32}$$

$$\Omega^2 = \Sigma_{i=1}^{3} M_{i,i} = (\xi - \kappa + D^2)/K > 0, \tag{33}$$

$$a\Omega^2 - \text{ Det } \hat{M} = a\Omega^2 - \kappa\xi/K = 0. \tag{34}$$

On analyzing relations (32) – (34), one concludes that positivity of ξ leads to the inequality $\kappa > D^2$. However, this relation is unacceptable since it implies the instability of the corresponding wave pack in the limiting case where $h = 0$ [14,15]. So, let $\xi < 0$ (and, hence, $K > 0$). We may then rewrite relations (32)-–(34) as

$$1 - \xi h > D^2 > \kappa - \xi, \tag{35}$$

$$\kappa = \frac{(\xi\beta + 1 - D^2)(\xi + D^2)}{D^2(\xi\beta - 1) + 1}. \tag{36}$$

Equation (36) was solved numerically for $h = 0.8$ and $\xi = -1.25$ (see Fig.5, where function $\kappa(D^2)$) is plotted by the solid line). One can easily get convinced that, for the given values of parameters ξ and h, the segment of curve (36) lying in the positive half-plane $\kappa > 0$ belongs to the open set defined by inequalities (35). We employed the curve given by equation (36) (a Hopf bifurcation curve [6]) as a starting point for our numerical study. On the opposite sides of this curve the stability types of the critical point are different. It is a stable focus beneath the curve and an unstable focus above the curve. The local change of stability can be induced by different global processes: by the unstable limit cycle disappearance (subcritical Hopf bifurcation) or by the stable limit cycle creation (supercritical Hopf bifurcation).

A local stability analysis based on the central manifold theorem and Poincare normal forms technique [6,7] shows that the neutral stability curve (36) may be divided into three parts. The domain lying between values $D_1^2 = 1.354076$ and $D_2^2 = 1.693168$ correspond to the subcritical Hopf bifurcation while two other segments correspond to the supercritical one. Thus, the dynamic system's solutions change in a different way with the growth of parameter κ when D^2 is fixed. If $1.354076 < D^2 < 1.693168$, then solutions of the system become globally unstable and tend to infinity

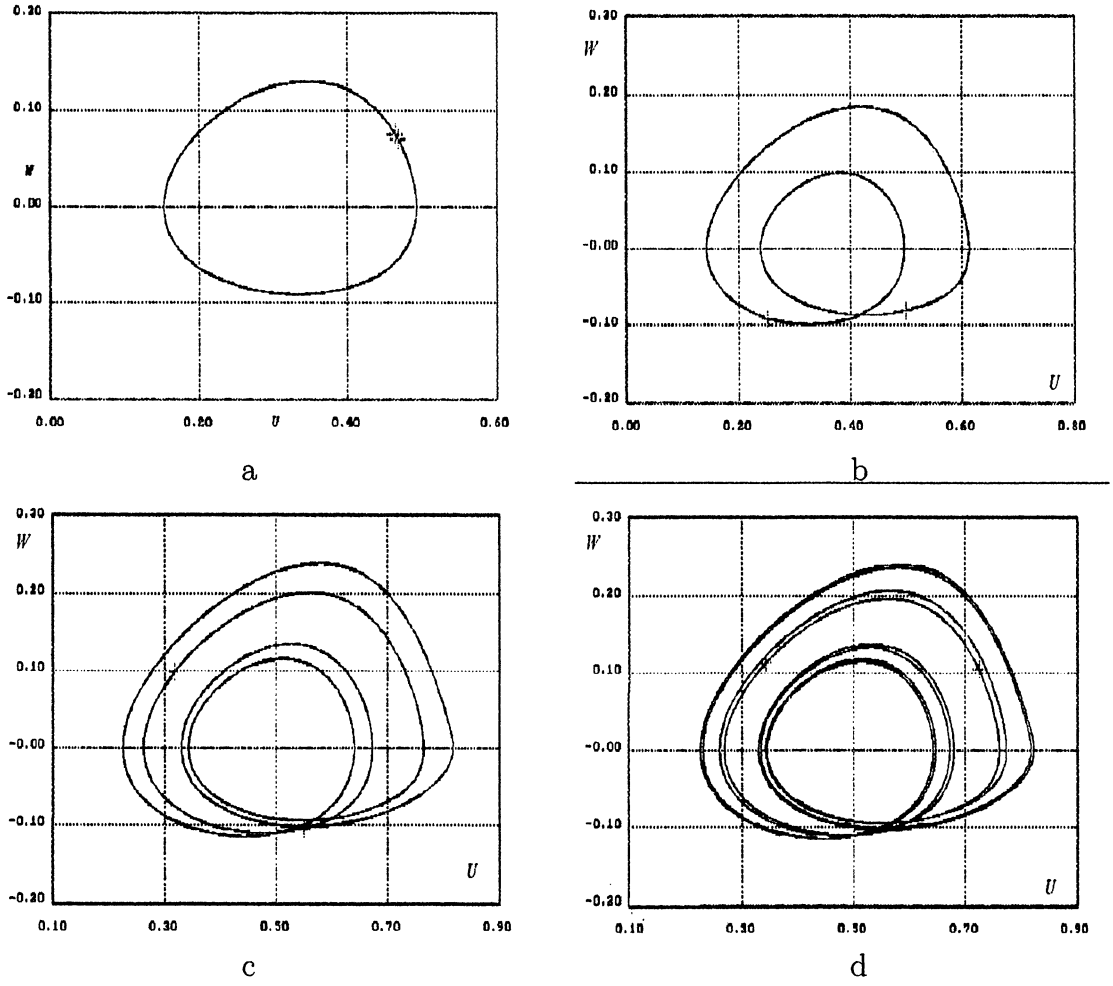

Fig. 6: Period doubling bifurcation in system (29) $h = 0.8$, $\xi = -1.25$, $\kappa = 0.05$. For the case a: $D^2 = 3$, b: $D^2 = 3.2$, c: $D^2 = 3.7$, d: $D^2 = 3.71$.

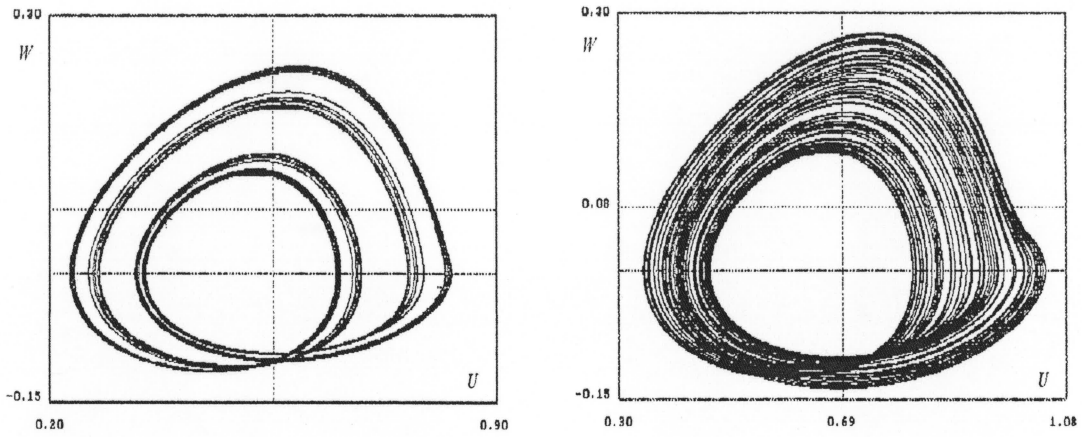

a b

Fig. 7: Patterns of chaotic trajectories of system (29) $h = 0.8$, $\xi = -1.25$, $\kappa = 0.05$. For the case a: $D^2 = 3.73$, b: $D^2 = 4.299$

after the Hopf bifurcation takes place. In the case where D^2 is beyond this interval, the growth of parameter κ leads to the self-oscillating solutions appearance. The amplitudes of oscillations grows with parameter's κ growth until one of the twin cycle bifurcation curves (shown on Fig.5 as dotted lines) is attained. Above these curves, system (29) again becomes globally unstable.

Numerical experiments show that twin cycle bifurcation curves are attached by one end to the Hopf bifurcation curve (36) at the point where the type of the Hopf bifurcation is changed. In addition, it was shown that system (29) has stable limit cycles surrounded by unstable ones in these points. These unstable attractors cannot be associated with the self-oscillating regimes -– in contrast, they are not manifested explicitly. On the other hand, the unstable cycles restrict the development of self-oscillations that grow with the growth of parameter κ. The domain of the unstable limit cycle existence in the parameter space (κ, D^2) is restricted by the subcritical branch of the Hopf bifurcation curve from one side and the bifurcation curves of twin cycles (having one of the multipliers equal to unity) from another. At the intersection of the system's parameters of both of these

curves, the unstable limiting cycle disappears (note that when the parameters approach the Hopf bifurcation curve, a radius of the periodic trajectory tends to zero, while the cycle disappears with non-zero amplitude on the dotted curves).

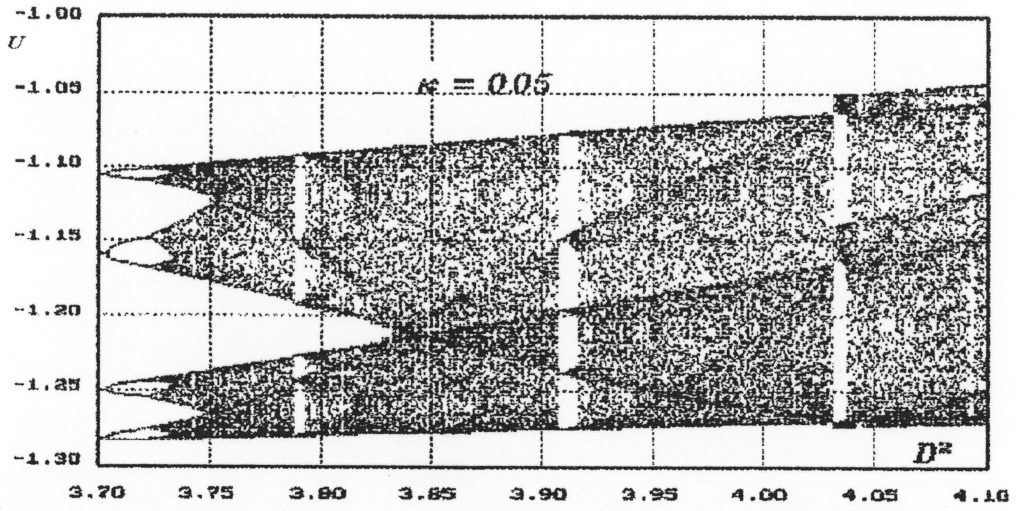

Fig. 8: Bifurcation diagram of system (29) in the plane in the plane (D^2, U), obtained for $h = 0.8$, $\xi = -1.25$, $\kappa = 0.05$.

The above analysis suggests that another direction of movement in the parametric space should be tried. Below, we describe a scenario obtained in the case where parameter D^2 is varied, while the rest of the parameters are fixed as follows:

$$h = 0.8,\ \xi = -1.25,\ \kappa = 0.05.$$

So, at $D^2 = 1.927178$, a stable limit cycle appears. The amplitude of the limit cycle grows within some interval when D^2 grows (for $D^2 = 3$, shown in Fig.6a). Finally, the limit cycle loses stability giving rise to another cycle with an approximately two times greater period ($2T$-cycle). The $2T$ cycle obtained for $D^2 = 3.2$ is shown in Fig.6b. This cycle also loses stability when D^2 approaches a certain critical value at which the $4T$-period cycle arises (Fig.6c shows $4T$ cycle obtained for $D^2 = 3.7$). Further growth of parameter

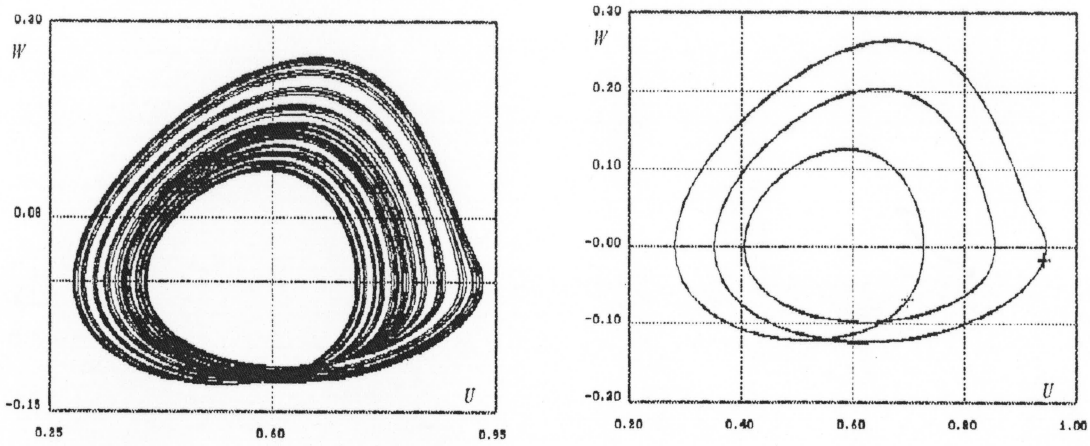

Fig. 9: Coexistence of the attractors in the phase space of system (29) at $D^2 = 4.005$.

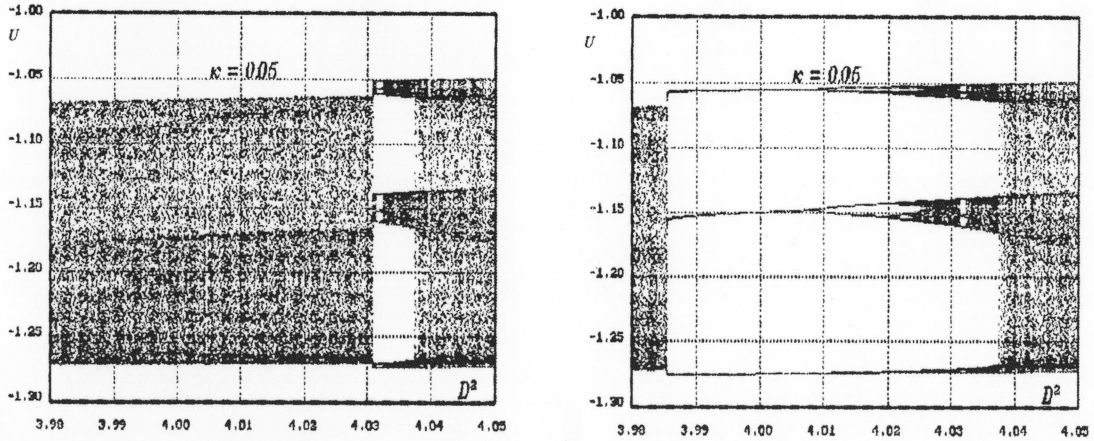

Fig. 10: Bifurcation diagrams of system (29) in the vicinity of period $3T$ window obtained when (a) parameter D^2 increases and (b) parameter D^2 decreases.

D^2 is accompanied by the creation of a series of cycles having periods $8T$ (Fig.6d at $D^2 = 3.71$), $16T$, . . ., 2^nT. The period-doubling cascade of bifurcation is well known in the theory of non-linear oscillation [7, 8]. It often leads to the appearance of stochastic regimes (strange attractors).

In fact, system (29) has a strange attractor. Within interval $3.7288 < D^2 < 3.8328$, it has a band structure. Four bands may be seen in Fig.7a corresponding to $D^2 = 3.73$, while at $D^2 = 3.75$ the trajectories form only two bands. On further growth of parameter D^2, narrow chaotic bands join together (this process is known as a "reverse" period-doubling cascade) and finally give rise to a Rössler-type attractor, covering a certain domain of the phase space. An outlook of the strange attractor just before destruction taking place at $D^2 = 4.3$ is shown in Fig.7b. A specific hump on the right edge of the attractor suggests that its destruction results from the interaction with a homoclinic loop.

The detailed investigation of the zone of chaotic oscillations enables us to see (Fig.8) that chaotic patterns are inhomogeneous, including domains with periodic movements where the system has cyclic solutions with periods that are different from 2^nT. To investigate a fine structure of the chaotic zone, the bifurcation diagrams technique [8, 9] is employed.

A plane $W = 0$ was chosen as a Poincare section plane in numerical experiments. Only those points were taken into consideration that correspond to the trajectories moving from the half–space $W > 0$ towards its supplement.

Employment of the Poincare sections technique enables to state the existence of well-known period $5T$ and $6T$ domains (the windows of periodicity in Fig.8 for $D^2 = 3.91$ and $D^2 = 3.789$, respectively) predicted by the Sharkovskij theorem [7]. In addition, it was stated another features of the chaotic domain inherent to the system were stated. The most characteristic property of this attractor is as follows. The period $3T$ domain of system (29) manifests hysteresis features. Two attractors exist there simultaneously: a chaotic attractor and a period $3T$ attractor (seen in Fig.9, both obtained for $D^2 = 4.005$). Scenario of the patterns' development at this interval depends on the direction of movement along parameter D^2 values. Parameter D^2 increasing causes a supercritical bifurcation (Fig.10a) in period $3T$. The attractor created in this way has a band structure. When parameter D^2

decreases, the 3-band chaotic attractor undergoes to the inverse cascade of period doubling bifurcations $3 \cdot 2^n \cdot T$, $3 \cdot 2^{n-1} \cdot T$, ..., $6T$, $3T$, finally giving rise to the twin cycle bifurcation resulting in the stable and unstable period $3T$ attractor creations followed by the passage to the advanced chaotic regime (Fig.10b).

Thus, the domain of the coexistence of two attractors is restricted by the twin cycle bifurcation curve from one side and the crisis of the strange attractor [12, 13] from another.

For $\kappa = 0.03$ and $\kappa = 0.02$, a similar scenario was observed, this time for significantly greater values of parameter D^2. It seems that a chaotic attractor does not exist when $\kappa < 0.01$.

From both the qualitative analysis and the numerical simulations, it has been observed that dynamical system (29) can exhibit the periodic, multiperiodic and chaotic regimes. The existence of these complicated regimes occurs to be possible due to the complex interaction of non-linear terms with terms describing relaxing properties of the medium within the united mathematical model (28).

To see the influence of relaxing features on the patterns formation, it is useful to compare the results of this section with investigations, where relaxing processes are described by the governing equations with the spatial nonlocality.

3. Autowave solutions of a model of structured medium with spatial nonlocality

Every structural element of the non-equilibrium multi-component medium interacts not only with the nearest neighbors, but with more distant surrounding elements as well. Such spatial nonlocality of interaction is displayed in the dynamical equation of state in the form of high derivatives with respect to the spatial coordinates [?]. Affiliating system (3), we get the

model of structured medium with spatial nonlocality:

$$\rho\dot{u} + p_x = \rho\gamma, \qquad \dot{\rho} + \rho u_x = 0,$$
$$\tau\left(\dot{p} - \chi\dot{\rho}\right) = \kappa\rho - p + \sigma\left\{p_{xx} + \tfrac{1}{\rho}p_x\rho_x - \chi\left(\rho_{xx} - \tfrac{1}{\rho}\left(\rho_x\right)^2\right)\right\}, \tag{37}$$

where parameter σ describes the influence of spatial non-locality.

3.1. Analysis of the quantitative characteristics of periodic and chaotic invariant solutions

It easy to verify that the invariance of system (37) is kept with respect to operator (4). Therefore, we can find solutions of system (37) again in form (5):

$$u = U(\omega) + D, \quad \omega = x - Dt, \quad \rho = \rho_0 exp(\xi t + S(\omega)), \quad p = \rho Z(\omega), \tag{38}$$

Inserting (38) into (37), we obtain one quadrature and the following dynamical system:

$$U\frac{dU}{d\omega} = UW, \qquad U\frac{dZ}{d\omega} = \gamma U + \xi Z + W(Z - U^2),$$
$$U\frac{dW}{d\omega} = \{U^2[\tau(\gamma U + \xi Z - WU^2) + \chi\tau W + Z - \kappa] + \tag{39}$$
$$+ \sigma[(\xi + W)(2U(\gamma - UW) + \chi W) + (UW)^2]\}\left[\sigma(\chi - U^2)\right]^{-1}$$

First of all, we state the conditions leading to the limiting cycle appearance in the vicinity of the critical point

$$U_0 = -D, \quad Z_0 = \frac{\kappa}{1 - 2\sigma(\xi/D)^2}, \quad W_0 = 0. \tag{40}$$

which is the only one lying in the physical parameter range under additional assumption $\gamma = \xi Z_0/D$. Note that critical point (40) defines a stationary solution

$$u = 0, \quad \rho = \rho_0 \exp\left[\frac{\xi x}{D}\right], \quad p = Z_0\rho,$$

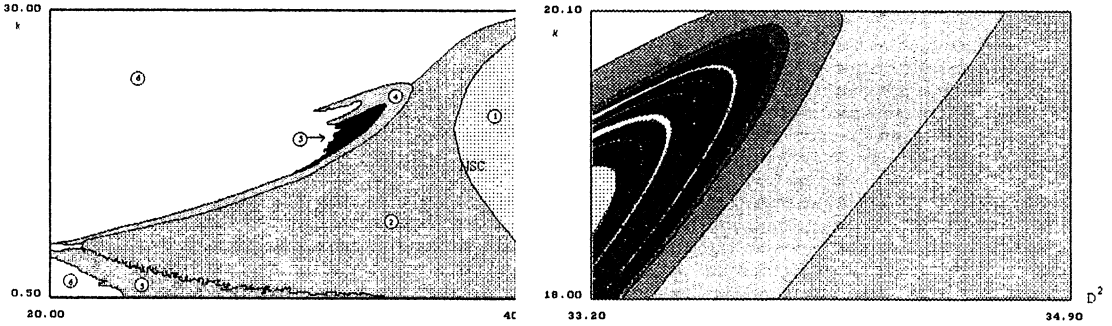

a b

Fig. 11: Left: bifurcation diagram of system (39) in parametric space (D^2, κ): 1 – stable focus; 2 – $1T$-cycle; 3 – torus; 4 – multiperiodic attractor; 5 – chaotic attractor; 6 – loss of stability. Right: enlargement of part of the left figure: 6 – $3T$-cycle.

belonging to set (38).

We start from the periodic solution that can be caught "in embryo" [7] when the linearization matrix $\hat{M}$

$$\hat{M} = \begin{pmatrix} 0 & 0 & -D \\ \gamma & \xi & Z_0 - D^2 \\ A & B & C \end{pmatrix}$$

of system (39) has one negative and two pure imaginary eigenvalues. Here

$$A = \frac{D\kappa\xi(2\xi\sigma - D^2\tau)}{Q\sigma(2\xi^2\sigma - D^2)}, \quad B = \frac{D^2(1+\xi\tau)}{Q}, \quad Q = \sigma(\chi - D^2),$$

$$C = Q^{-1}\left\{\xi\sigma\left(\chi - D^2\right) - \frac{2D^2\kappa\xi\sigma}{D^2 - 2\xi^2\sigma} + D^2\tau\left(\chi - D^2\right)\right\}.$$

The well-known Andronov-Hopf bifurcation theorem tells us that periodic solution creation can take place if one eigenvalue of matrix $\hat{M}$ is negative and the two others are purely imaginary. This is so if the following relations hold:

$$\alpha = \xi + C > 0, \tag{41}$$

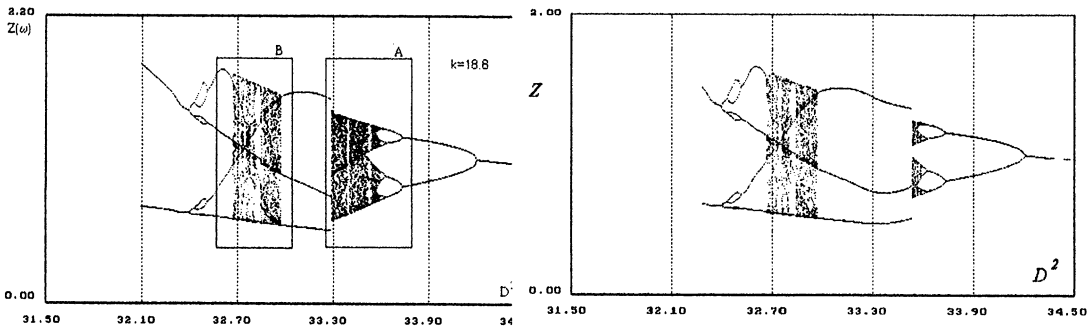

a b

Fig. 12: Bifurcation diagram of system (39) obtained at $\chi = 50$, $\xi = 1.8$, $\tau = 0.1$, $\sigma = 0.76$, $\kappa = 18.8$, decreasing D^2 (a) and increasing D^2 (b).

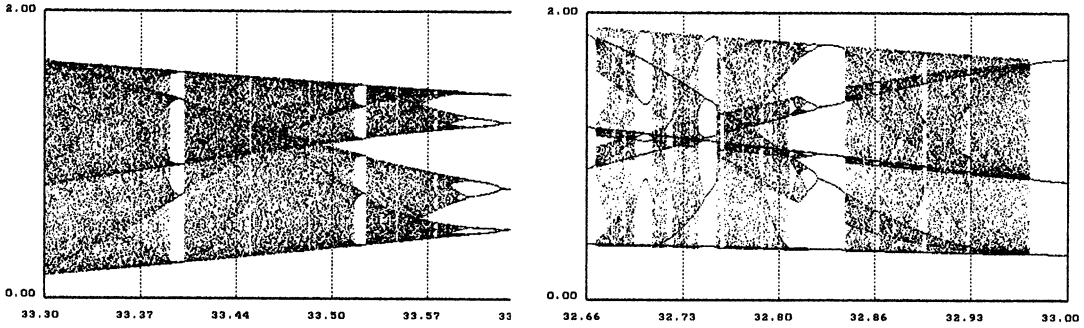

a b

Fig. 13: Enlargement of regions A and B of Fig.12.

$$\Omega^2 = AD - B\left(Z_0 - D^2\right) + \xi C > 0, \tag{42}$$

$$\alpha\Omega^2 = \xi\left(AD - Z_0 B\right) > 0. \tag{43}$$

The first two take on the form of inequalities, imposing some restrictions on the parameters. The third one determines the neutral stability curve (NSC) in space $(D^2; \kappa)$ provided that the remaining parameters are fixed. For $\sigma = 0.76, \xi = 1.8, \tau = 0.1, \chi = 50$, it looks like a parabola with branches directed from left to right, see Fig.11a.

Numerical investigations illustrated in Fig.11a show that inside the parabola, critical point (40) is a stable focus. When we cross NSC (43) from right to

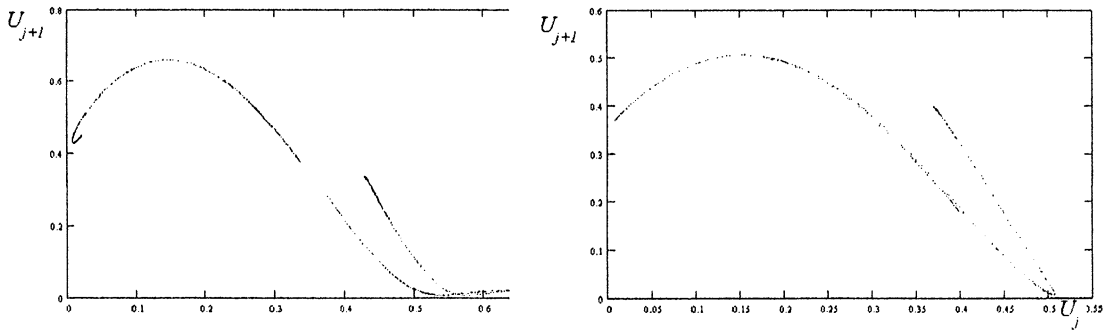

a b

Fig. 14: Hereditary maps of chaotic attractor: (a) corresponds to region B while (b) corresponds to region$A$ (see Fig.12a).

left, then the stable periodic solution softly appears. The radius of the limiting cycle grows as one moves away from the curve, until it remains stable. Future evolution of periodic regimes depends strongly on the values of parameter κ. When $\kappa > 20$ then lowering D^2 and using Poincare's section technique, one obtains the following chain of bifurcations: finite period doubling cascade (PDC)$\rightarrow$ inverse PDC $\rightarrow$ the global loss of stability.

When κ lies between 15 and 20 then PDC, appearing as the value of D^2 is lowered, leads to the strange attractor creation. The bifurcation diagram of system (39) turns out to depend on the direction of movement along the D^2 axis, as shown in Fig.12. For this range of parameter κ values, let us investigate the phase space of the dynamical system in more detail.

Building the bifurcation diagram of system (39) at $\kappa = 18.8$ and different directions of changing D^2 (Fig.12), the phenomenon of histeretic behaviour is found.

The bifurcation diagram obtained for even lower values of parameter D, see Fig.11, suggests that an infinite period doubling cascade could be present in system (39). Using the shooting method we studied period doubling bifurcation. Our calculations show that the period of the stable $2T$-cycle at $D^2 = 34.2$ (this value being a bit smaller than the critical one at which the $1T$-cycle loses its stability) is as follows: $T_s = 1.76850243$ (multipliers corresponding to this cycle take on the values $\rho_1 = 0.007799$, $\rho_2 = 1.0$,

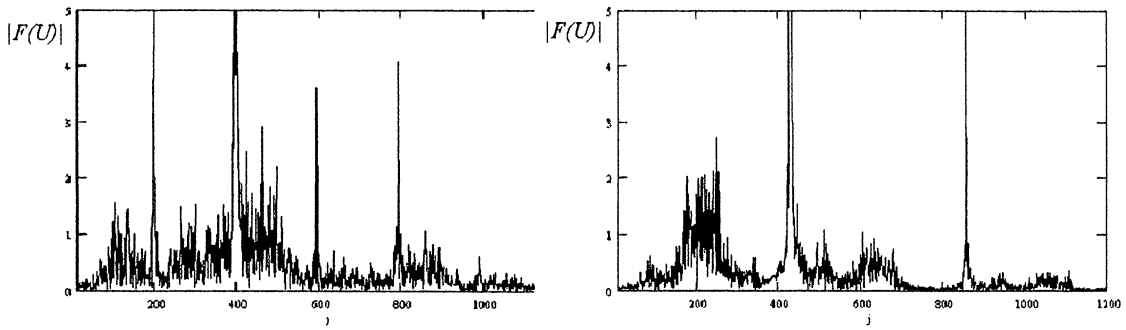

a). b).

Fig. 15: Fourier spectra of U-coordinate of chaotic attractors from regions B (left) and A (right), respectively.

$\rho_3 = 0.975490$). The period of the unstable cycle, coexisting with the previous one, is $T_u = 0.88414414$ (while multipliers are as follows $\rho_1 = -1.006123$, $\rho_2 = 1.0$, $\rho_3 = -0.086699$). So $T_s/T_u \approx 2.0$ and we observe a period doubling bifurcation. In order to find the coordinates of the bifurcation point, we used the fact that one of the multipliers of the cycle becomes equal to (-1), when the bifurcation values are attained.

Our calculations show that the values of the bifurcation point coordinates are $(34.2057, 18.8)$ (multipliers of cycle corresponding to these values are $(-1,\ 00005,\ -0.087315,\ 1.0)$). Future bifurcation values are as follows: $D^2_{4T} = 33.7349$, $D^2_{8T} = 33.62387$, $D^2_{16T} = 33.599968$. Unfortunately, the simple shooting method does not allow to find the bifurcation values corresponding to high-order period doubling series. This is due to the fact that the accuracy of the initial data is not satisfactory and iterations do not converge when one attempts to investigate multiperiodic motion.

To proceed with it, one should use, for example, the multi-shooting method, yet we did not touch upon it in this work [17]. Using the coordinates of bifurcation points available we get two elements of the sequence of scaling coefficients $\{\delta_i\} = 4.2403, 4.6452$, where

$$\delta_i = \frac{D^2_i - D^2_{i-1}}{D^2_{i+1} - D^2_i}, \qquad i = 1, 2$$

and D^2_i denote bifurcation values of the parameter (recall that δ_i describes

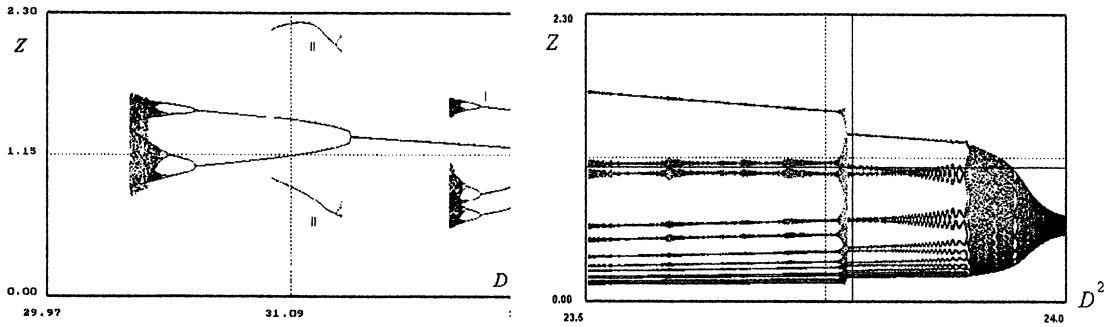

a b

Fig. 16: Bifurcation diagrams of system (39) in plane (Y, D^2), obtained for $\chi = \eta = 50$, $\xi = 1.8$, $\tau = 0.1$, $\sigma = 0.76$ and (a) $\kappa = 14$, (b) $\kappa = 1$.

Feigenbaum's phenomenon in the logistic map). So we see that the term δ_2 is very close to the Feigenbaum constant $\delta = 4.6692016091....$ This fact backs the assumption that the family of periodic solutions of system (39) constitutes the Feigenbaum cascade. In order to prove that the cascade we deal with forms a series leading to the chaotic attractor creation, let us calculate the full spectrum of Lyapunov's exponents, keeping in mind that the presence of a positive exponent in the spectrum together with the fact that the trajectories do not leave a finite volume guarantee chaotic behaviour [18].

Numerical calculations of the Lyapunov spectrum, implemented with the help of standard method [19], show that the trajectory of system (38), corresponding to the value $D^2 = 33.4$, has the following spectrum: $\lambda_1 = 0.383$, $\lambda_2 = -0.001$, $\lambda_3 = -3.201$. So the attractor appearing in system (39), is really chaotic and "strange" [18]. Its Lyapunov dimension is $D_L = 2.1193$.

The analysis of the bifurcation diagrams (Fig.13) suggests, that the phenomena of internal chaotic attractor bifurcations and folds' creation do take place. It follows from the comparison of hereditary maps (Fig.14), one-dimensional maps of maxima and the Fourier spectra (Fig.15), obtained for the values of the parameters, lying in regions A and B (see Fig.12a). Let us note, that regions A and B, manifesting chaotic behaviour, correspond to the strips adjacent to the $3T$-band presented in the two parameter bifurca-

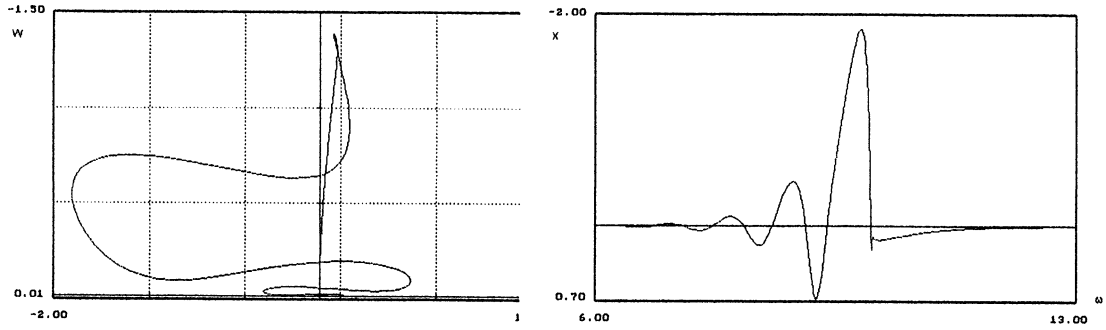

a). b).

Fig. 17: Homoclinic solution of system (39): left – projection of the phase trajectory onto the (X, W) plane; right – coordinate X versus ω.

tion diagram (Fig.11b). So, one can observe a gradual creation of internal bifurcation in the chaotic region. Internal bifurcation could be explained by the coexisting and intersection of two chaotic attractors: the first (region A Fig.12a) being created through the period doubling cascade, and the second (region B Fig.12a), perhaps, being created via the homoclinic bifurcation.

The qualitative behaviour of system (39) changes when the value of parameter κ are less than 15. Figure 16a presents the bifurcation diagram obtained for $\kappa = 14$. Chaotic oscillations, seen in the middle part of the diagram, arise as a result of periodic doubling cascade and are destroyed via a homoclinic bifurcation, taking place at $D^2 \approx 30.0$. We also succeeded in detecting an isolated regime, existing simultaneously with the main cascade and appearing as a $3T$ cycle in Fig.16a. This cycle gives rise to the period doubling cascade, followed by the creation of the strange attractor. The chaotic regime disappears at $D^2 \approx 32.1$ and continuous below the value $D^2 \approx 31.7$ as period $2T$ oscillations, coexisting with the period $2T$ mode of the main cascade and forming the outer branch in the middle part of the bifurcation diagram, separated from the main bifurcation cascade.

When $\kappa < 10$, the scenario of the development of oscillating regimes is supplied with the appearance of toroidal attractors (Fig.16b).

The variety of nonlinear oscillating solutions of system (39) presented above suggest the homoclinic trajectory with the accompanying structure

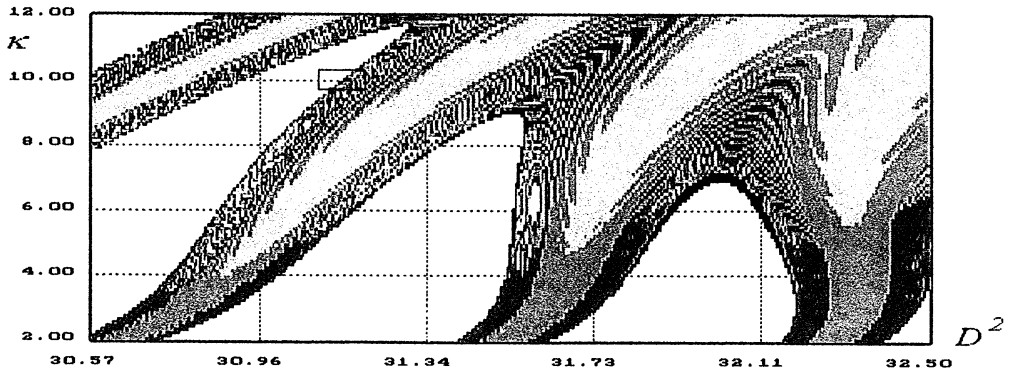

Fig. 18: A portrait of subset of parameter space (D^2, κ), corresponding to different intervals of function $f^{\Gamma}_{\min}(D^2, \kappa)$ values and following Cauchy data: $X(0) = Y(0) = 0$, $W(0) = 0.001$: $f^{\Gamma}_{\min} > 1.2$ for white colour; $0.6 < f^{\Gamma}_{\min} \leq 1.2$ for light grey; $0.3 < f^{\Gamma}_{\min} \leq 0.6$ for grey; $0.01 < f^{\Gamma}_{\min} \leq 0.3$ for deep grey; $f^{\Gamma}_{\min} \leq 0.01$ for black.

can exist in the phase space of the dynamical system and cause such complicated regimes. Since the homoclinic loop, corresponding to the soliton - like solution of the initial PDE system (37), has such great significance for applications and the understanding of the geometrical structure of the phase space of the dynamical system, we would like to pay more attention to the problem of the homoclinic loop existence.

3.2. Dynamics of the soliton - like solutions set

For the present, the question of homoclinic trajectory type Fig.17 existence in system (37) has been treated numerically.

We investigate a set of points of parameter space (D^2, κ) for which the trajectories moving out of the origin along the one-dimensional unstable invariant manifold W^u return to the origin along the two-dimensional stable invariant manifold W^s. In practice, for the given values of parameters κ, D^2, we numerically define a distance between the origin and point

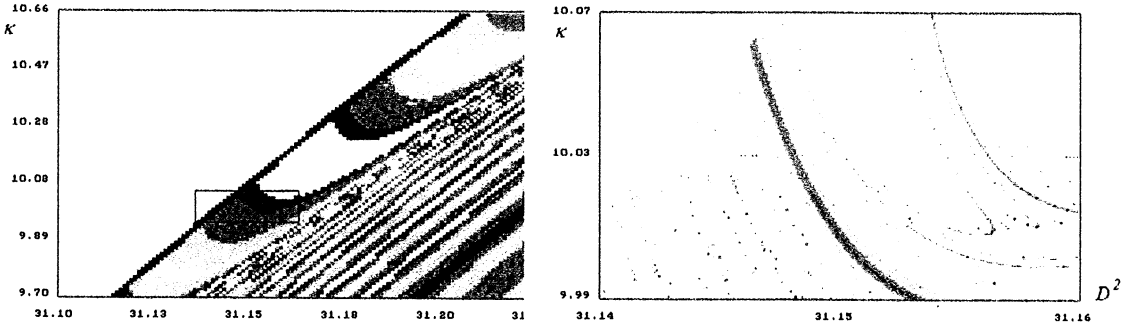

a b

Fig. 19: Enlargement (a) of the part of Fig.18 and (b) of the part of the left diagram, lying inside in the rectangle.

$(X^\Gamma(\omega), Y^\Gamma(\omega), W^\Gamma(\omega))$ of the phase trajectory $\Gamma(\cdot;\ \kappa,\ D^2)$:

$$f^\Gamma\left(\kappa,\ D^2;\ \omega\right) = \sqrt{[X^\Gamma(\omega)]^2 + [Y^\Gamma(\omega)]^2 + [W^\Gamma(\omega)]^2},$$

starting from the fixed Cauchy data $(0, 0, 0.001)$. Next we determine

$$\Phi(\kappa,\ D^2) = \min_{\omega}\{f^\Gamma\} \tag{44}$$

for the part of the trajectory which lies beyond the point at which the distance gains its first local maximum, providing that it still lies inside the ball centered at the origin and having a fixed (sufficiently large) radius (for this case $f^\Gamma(\omega) \leq 5$). The results are presented in Figs.18-19. The first is of the most rough scale among this series. Here, white color marks the values of parameters κ, D^2 for which $\Phi > 1.2$, light grey corresponds to the cases when $0.9 < \Phi < 1.2$ and so on (further explanations are given in the subsequent captions). The black coloured patches correspond to the case when $\Phi < 0.01$. Fig.19a presents the enlargement of the rectangle shown in Fig.18, whereas Fig.19b shows the enlargement of the rectangle from Fig.19a. Note that, colors in the last figure are re-scaled so that black color corresponds to the points at which $\Phi < 0.003$. Additional calculations show the independence of the qualitative structure of the presented diagram on the coordinates of the starting point of function (44).

4. Localized invariant travelling wave solutions in relaxing hydrodynamic - type model

In this section we pay attention to the problem of extracting localized travelling wave solutions associated with the homoclinic loops of a corresponding dynamical system, obtained from the initial PDE system via the group theory reduction. Presently no regular analytical method enabling to predict the appearance of a homoclinic-type solution of a multidimensional dynamical system exist yet, some information about the possibility of homoclinic bifurcation could be obtained through the analysis of Poincaré canonical form (CPF), corresponding to some type of degeneracy of the linear part of the system. Aside from the case when CPF is Hamiltonian, or close to Hamiltonian [20], this information is incomplete, therefore, answering the question on whether or not the homoclinic bifurcation takes place, one should finally resort to the numerical simulation.

We analyze this system with the help of qualitative theory methods and state the conditions assuring the existence of quasiperiodic solutions in the proximity of a fixed point. Since one of the possible scenarios of the quasiperiodic regime destruction is associated with the homoclinic bifurcation, we use the above results to localize the domain of parameter space where the homoclinic bifurcation could take place.

4.1. Soliton-like invariant solutions of relaxing hydrodynamics model

The modelling system we are going to analyze is as follows:

$$\begin{aligned} \frac{\partial \rho}{\partial t} + \chi \rho^{\sigma-1} \frac{\partial \rho}{\partial x} &= \alpha_1 (\rho - 1) + \alpha_2 (\rho - 1)^2 - q_1 \kappa \eta \\ &+ q_2 \left[\nu \eta - (\sigma - 1) \varphi (\rho - 1) - \kappa (\lambda - \lambda_0) \right], \\ \frac{\partial \lambda}{\partial t} &= -\kappa \eta, \\ \frac{\partial \eta}{\partial t} &= \nu \eta - \varphi \left(\rho^{\sigma-1} - 1 \right) + \beta (\lambda - \lambda_0)^2 - \kappa (\lambda - \lambda_0). \end{aligned} \tag{45}$$

Let us consider the ansatz

$$\rho = R(\omega), \qquad \omega = x - D t, \qquad \lambda = L(\omega), \qquad \eta = N(\omega), \tag{46}$$

which describes a family of invariant travelling wave solutions. Inserting (46) into the system (45) we obtain dynamical system

$$\begin{aligned} D\left(\chi R^{\sigma-1}-D\right)\dot{R} &= D\left[\alpha_1(R-1)+\alpha_2(R-1)^2\right]-qN\kappa \\ &\quad +p\left[\nu N-\theta(\rho-1)-\kappa(L-L_0)\right], \\ D\left(\chi R^{\sigma-1}-D\right)\dot{L} &= \kappa\left(\chi R^{\sigma-1}-D\right)N, \\ D\left(\chi R^{\sigma-1}-D\right)\dot{N} &= \left(\chi R^{\sigma-1}-D\right)\left(-\left(R^{\sigma-1}-1\right)\varphi-\nu N\right. \\ &\quad \left.-\beta(L-L_0)^2+\kappa(L-L_0)\right). \end{aligned} \tag{47}$$

where $\theta=(\sigma-1)\varphi$, $q=q_1 D$, $p=q_2 D$. It is easy to check, that the linear part of system (47) in reference frame $X=R-1$, $Y=L-L_0$, $Z=N$, centered at the critical point $A(1,\ L_0,\ 0)$, is as follows:

$$\begin{pmatrix} \dot{X} \\ \dot{Y} \\ \dot{Z} \end{pmatrix} = \begin{bmatrix} \alpha_1 D-p\theta & -p\kappa & p\nu-q\kappa \\ 0 & 0 & \kappa\Delta \\ \theta\Delta & \kappa\Delta & -\nu\Delta \end{bmatrix} \begin{pmatrix} X \\ Y \\ Z \end{pmatrix}, \tag{48}$$

where $\Delta=\chi-D$, $h=\theta/\nu$. We are going to employ the methods of local nonlinear analysis to the investigation of quasiperiodic and soliton-like solutions appearance in the vicinity of critical point $A(1,\ L_0,\ 0)$. In order for such an analysis to be effective, restrictions on the parameters should be imposed, assuring that the eigenvalues of the linearization matrix $\hat{M}$ of system (47) have the $(0,\ \pm i\,\Omega)$ degeneracy [7,21]. This leads to the following conditions:

$$\alpha_1=0, \qquad D=\chi+ph, \qquad \Omega^2=-ph^2\kappa\,(p\kappa+\nu q)>0. \tag{49}$$

In order to avoid considering the case which is obviously unstable [14], we should choose the parameters in such a way that the nonlinear wave pack velocity D be greater than the acoustic sound velocity χ. From this requirement we immediately obtain inequality

$$ph>0. \tag{50}$$

Assuming that conditions (49)–(50) are satisfied, let us construct the canonical Poincaré form corresponding to system (47). To do this we must first

make a transition to the new variables

$$\begin{pmatrix} x_1 \\ x_2 \\ x_3 \end{pmatrix} = \frac{p}{-\Omega^3 h} \begin{bmatrix} 0 & 0 & \kappa\, h^2\, (q\,\nu + \kappa p) \\ -h\,\theta\,\Omega & -\kappa\, h\,\Omega & \theta\,\Omega \\ \Omega\,\kappa\, p\, h^3 & -q\,\kappa\,\Omega h^2 & -h^2 \kappa\, p\,\Omega \end{bmatrix} \begin{pmatrix} X \\ Y \\ Z \end{pmatrix},$$

chosen in such a way that the linear part of the system is written in standard quasi-diagonal form:

$$\begin{aligned} x_1' &= -\Omega\, x_2 + \sum_{i+j=2i\le j} A_{ij} x_i x_j + \sum_{i+j+k=2i\le j\le k} A_{ijk} x_i x_j x_k + \cdots, \\ x_2' &= \Omega\, x_1 + \sum_{i+j=2i\le j} B_{ij} x_i x_j + \sum_{i+j+k=2i\le j\le k} B_{ijk} x_i x_j x_k + \cdots, \\ x_3' &= \sum_{i+j=2i\le j} C_{ij} x_i x_j + \sum_{i+j+k=2i\le j\le k} C_{ijk} x_i x_j x_k + \cdots, \end{aligned} \qquad (51)$$

where $(\cdot)' = D\,(\chi\, R^{\sigma-1} - D)\, d(\cdot)/d\omega$. Passage from representation (51) to CPF

$$r' = a\, r\, z + o\left(r^3,\ |z|^3\right), z' = b_1 r^2 + b_2 z^2 + f\, z^3 + o\left(r^3,\ |z|^3\right).$$

is based on a standard method which can be found e.g. in [7]. Connections between the coefficients of the CPF and those of system (51) prove to be as follows [22, 23]:

$$a = \frac{(A_{13} + B_{23})}{2}, \qquad b_1 = \frac{(C_{11} + C_{22})}{2}, \qquad b_2 = C_{33}. \qquad (52)$$

CPF (52) is obtained from the initial dynamical system through a series of asymptotic transformations [7], followed by the passage to the cylindric coordinates $(r,\ \varphi,\ z)$ and averaging over the "fast" angular variable φ. Therefore, the limit cycle, appearing in (52) corresponds to the quasiperiodic solution of the initial PDE system, while the homoclinic trajectory corresponds to the non-classical many-hump solitary wave pack.

As shown in [23], the stability of the periodic solution of system (52) is determined by the sign of coefficient f. The expression describing this coefficient in general case [22, 23], is too cumbersome to be of any use in

analytical treatment, but it drastically simplifies when $C_{33} = 0$. This is so when the following expression holds

$$\alpha_2 = \frac{h\,p\,\nu\,(2\,h\,\beta\,\nu - \kappa^2)}{2\,\kappa^2\,(h\,p + \chi)}. \tag{53}$$

Under this condition

$$f = C_{333} + \frac{1}{\Omega}\,(A_{33}C_{23} - B_{33}C_{13})\,. \tag{54}$$

Here and henceforth we put the calculations with $\sigma = 3$.

We must stress here that, although CPF (52) serves as a basement for the classification of regimes appearing after the removal of degeneracy, its investigation will not be of any use until coefficients (52), (54) remain unknown. This problem is rather cumbersome unless one uses some tools for symbolic calculus. Below we give the exact expressions of the CPF coefficients, obtained with the help of the program "Mathematica":

$$\begin{aligned} a &= \frac{2\,(\nu^2 h^2 p\,\beta\, - \nu\,\kappa^2\chi) - \nu\,\kappa^2 h\,p}{2\,\kappa}, \\ b_1 &= -\frac{h^4 p^2 \beta}{2\,\kappa}\left[p\left(\kappa^2 + \nu^2\right) - q\,\kappa\,\nu\right], \\ f &= \frac{h^4 p^3 \nu^2 \beta}{\Omega^2}\left(\kappa^2 - 2\,h\,\beta\,\nu\right) \end{aligned} \tag{55}$$

In order to remove the degeneracy of the linear part of system (47),a two parameter family of small perturbation is introduced:

$$F \to \alpha_1\,(R-1) + \alpha_2\,(R-1)\,, \qquad D \to \chi + h\,p + \epsilon. \tag{56}$$

This induces the following change of the CPF:

$$r' = \mu_1 r + a\,r\,z + o\left(r^3,\ |z|^3,\ |\mu_i|\right),\ z' = \mu_2 z + b_1 r^2 + b_2 z^2 + f\,z^3 + o\left(r^3,\ |z|^3,\ |\mu_i|\right),$$

where

$$\mu_1 = \frac{\nu}{2}\left(\epsilon - \frac{D h^2 p\,q\kappa}{\Omega^2}\,\alpha_1\right), \qquad \mu_2 = -\frac{D h^2 p^2 \kappa^2}{\Omega^2}\alpha_1. \tag{57}$$

As shown in our previous work [23], for sufficiently small $\mu_1\,\mu_2$ the limit cycle appears in system (57) along the manifold

$$\mu_2 + 3f\,(\mu_1/a)^2 = 0, \tag{58}$$

providing that $a\,b_1 < 0$. Here we have two possibilities:

• $f > 0$ and $\mu_1\,\mu_2 < 0$; a stable periodic regime exists if the following inequality holds

$$\mu_2 < -3f\,(\mu_1/a)^2 < 0; \tag{59}$$

• $f < 0$ and $\mu_1\,\mu_2 < 0$; an unstable periodic regime exists if the following inequality holds

$$\mu_2 > -3f\,(\mu_1/a)^2 > 0 \tag{60}$$

(note that in proximity of critical point $A(1,\,L_0,\,0)$ factor $(\chi R^{\sigma-1} - D)$ is negative and this circumstance has been taken into account when determining the stability type of the limit cycle).

Numerical simulations show that one of the scenarios of destruction of the limit cycle of system (57) is associated with the appearance of the homoclinic loop ($a = 2$ can be shown analytically [7]). These regimes correspond to the soliton-like solutions of the initial PDE system. In the first case, corresponding to formula (59), homoclinic trajectory comes out from critical point $A(1,\,L_0,\,0)$ (which is a saddle-focus) along the one-dimensional unstable invariant manifold W^u and returns to the critical point along the two-dimensional stable invariant manifold W^s. In the second case, corresponding to formula (60), the direction of movement is opposite. Analysis based on equations (55)–(60) shows that both of these cases can be observed in system (45). In the first case we obtain a soliton-like solution with oscillating front while in the second one – a localized pack with an oscillating "tail".

As mentioned above, a homoclinic bifurcation is not the only scenario leading to the destruction of quasiperiodic movement appearing in system (47). We cannot exclude other scenarios associated, for example, with a pair of tori appearance (i.e. the case when the Lyapunov indices cross the unit circle having a non-zero imaginary part). In this situation, the final answer on whether or not the soliton-like regimes appear in system can be given by the numerical experiments.

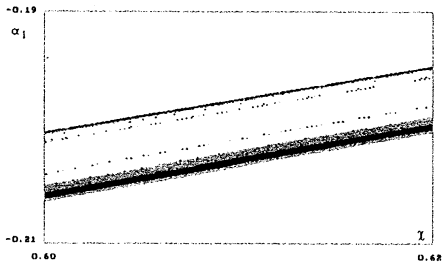

Fig. 20:

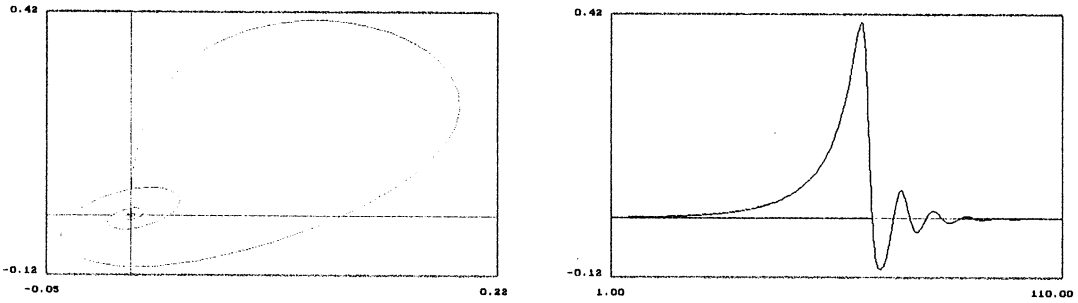

Fig. 21:

We employed the numerical procedure put forward in [21] (cf. also [24]).

This procedure enables us to find a set of points belonging to parameter plane $(\chi,\ \alpha_1)$, for which the trajectory moving out of the origin along the one-dimensional unstable invariant manifold W^u returns to the origin along the two-dimensional stable invariant manifold W^s. Having fixed the rest of the parameters as follows $\varphi = -1$, $\nu = \kappa = q = 1$, $p = -0.25$, we numerically define a distance between the origin (which coincide with critical point $A(1,\ L_0,\ 0)$) and point $X^\Gamma(\omega)$, $Y^\Gamma(\omega)$, $Z^\Gamma(\omega)$ of the phase trajectory $\Gamma(\cdot;\ \chi,\ \alpha_1)$:

$$f^\Gamma(\chi,\ \alpha_1;\omega) = \sqrt{[X^\Gamma(\omega]^2 + [Y^\Gamma(\omega]^2 + [Z^\Gamma(\omega]^2}, \tag{61}$$

starting from the fixed Cauchy data lying on the unstable manifold W^u, close to the origin. Next we determine the minimum $f^\Gamma_{\min}(\chi,\ \alpha_1)$ of function (61) for the part of the trajectory which lies beyond the point at which the

distance gains its first local maximum, providing that it remains inside the ball of a fixed (sufficiently large) radius. The results are presented in Fig.20. Here, white marks the values of parameters χ, α_1 for which $f^{\Gamma}_{\min} > 1.2$, light grey correspond to the values $0.6 < f^{\Gamma}_{\min} < 1.2$, grey - to the values $0.3 < f^{\Gamma}_{\min} < 0.6$, deep grey – to $0.01 < f^{\Gamma}_{\min} < 0.3$, black - to $f^{\Gamma}_{\min} < 0.01$. It can be seen in Fig.20, that the points corresponding to the homoclinic loop form a connected set and this is in agreement with the general statements [25]. Let us note that the employment of the same procedure for another systems gives a Cantor set instead of the connected curve [21, 24].

Numerically solving system (47) for the proper values of the parameters, one is able to obtain a soliton-like solution. Because of the numerical errors it is impossible to read the exact values of the parameters χ, α_1 corresponding to the homoclinic loop from Fig.20. Therefore, we put $\alpha_1 = -0.2$ and, using the Bolzano–Weierstrass method, varied χ until the homoclinic trajectory was attained at $\chi = 0.619803$. This approach proves to be effective because the bifurcation values of the parameters form a smooth curve in plane $(\chi,\ \alpha_1)$. Projection of the homoclinic trajectory onto the $(X,\ Z)$ plane is shown in Fig.21; while the corresponding solution $R(\omega) = R(x - D\,t)$ is shown in Fig.21(right). So, we are convinced that system (45) possesses invariant soliton-like solutions, that look like a many-hump wave pack moving with uniform speed D.

5. Invariant chaotic solutions of nonlocal models of relaxing media with spatial and temporal nonlocalities

In this section we present investigations of the generalization of the dynamical equation of state from (37), taking into account both effects of spatial and temporal non-locality. Together with balance equations for mass and momentum (3) it forms a closed system of PDE:

$$\rho\frac{du}{dt} + \frac{\partial p}{\partial x} = \gamma\rho, \qquad \frac{d\rho}{dt} + \frac{\partial u}{\partial x} = 0,$$

$$\tau\left(\dot{p}-\chi\dot{\rho}\right)=\kappa\rho-p+\sigma\left\{p_{xx}+\frac{1}{\rho}p_x\rho_x-\eta\left(\rho_{xx}-\frac{1}{\rho}\left(\rho_x\right)^2\right)\right\}-$$
$$-h\left\{\ddot{p}+\eta\left(\frac{2}{\rho}(\dot{\rho})^2-\ddot{\rho}\right)\right\}, \tag{62}$$

where parameters h and σ are associated with the temporal and spatial nonlocalities.

The model where $h=0$ (let us call it an S-model) is considered in the previous sections and the model where $\sigma=0$ (let us call it an H-model) had been investigated in section 2. Together with balance equations for mass and momentum relation (3) forms a closed system of PDE like (37). Inserting solution (38) into it one obtains the dynamical system:

$$U\frac{dU}{d\omega}=UW, \qquad U\frac{dZ}{d\omega}=\gamma U+\xi Z+W(Z-U^2),$$
$$U\frac{dW}{d\omega}=(2\gamma\xi\sigma U-\kappa U^2+\gamma h\xi U^3+\gamma\tau U^3+\eta\xi\sigma W+2\gamma\sigma UW$$
$$-2\xi\sigma U^2W+\chi\tau U^2W-h\xi U^4W-\tau U^4W+\eta\sigma W^2+ \tag{63}$$
$$\eta h(UW)^2-\sigma(UW)^2-hU^4W^2+U^2Z+h\xi^2U^2Z+$$
$$\xi\tau U^2Z)/(\eta\sigma-\eta hU^2-\sigma U^2+hU^4)$$

The critical point of the system (63) has the same coordinates (39). The linearization matrix $\hat{M}$ is

$$\hat{M}=\begin{pmatrix}0 & 0 & -D\\ \gamma & \xi & \Delta\\ A & B & C\end{pmatrix}$$

of system (39), where

$$A=\frac{D\kappa\xi(D^2h\xi-2\xi\sigma+D^2\tau)}{(-D^2+\eta)(\sigma-D^2h)(D^2-2\xi^2\sigma)}, \qquad B=\frac{D^2(1+h\xi^2+\xi\tau)}{(\eta-D^2)(\sigma-D^2h)},$$

$$C=(\eta\xi\sigma-D^4h\xi-2D^2\xi\sigma-\frac{2D^2\kappa\xi\sigma}{D^2-2\xi^2\sigma}-D^2\tau+D^2\chi\tau)/((\eta-D^2)(\sigma-D^2h)),$$

$$\Delta=z_0-D^2.$$

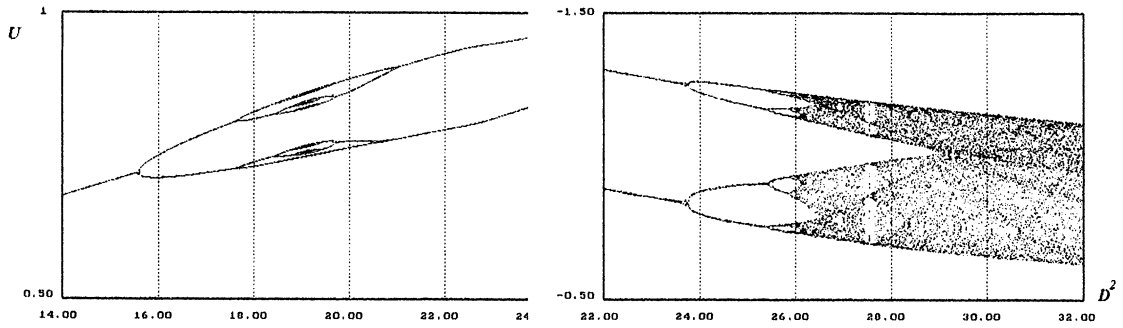

a b

Fig. 22: Bifurcation diagrams of the solutions of system (63) at $\chi = \eta = 5$, $h = 0,8$, $\xi = -1$, $\tau = 0,01$ a) $\sigma = 0$; b) $\sigma = 1$.

Let us describe the scenario of the oscillations development in system (63) in vicinity of critical point (39) when $\chi = \eta = 5$, $h = 0.8$, $\xi = -1$, $\tau = 1$. Condition (34) of the limit cycle creation on plane (D^2, κ) is described with a parabola (neutral stability curve). If parameter $\sigma = 0$ then at $\kappa = 0.3$, $D^2 = 8,8$ near NSC the limit cycle appears. The radius of the periodic orbit grows with the decreasing D^2. It loses stability giving rise to several period doubling bifurcations and complicated periodic trajectory creation. The described scenario of limiting cycle development is presented in detail in Fig.22a, where the values of U-coordinate of the intersecting point of the trajectory and section plane $W = 0$ are on the vertical axis, whereas the values of parameter D^2 are on the horizontal axis. So, at the above fixed values of the parameters, system (63) does not demonstrate a scenario of chaotic attractor creation.

Let us build the bifurcation diagram once more but at $\sigma = 1$ (Fig.22b). In this case, the phase space of system (63) contains the chaotic attractor, appearing after the period doubling cascade. A similar scenario takes place at $0 < \sigma < 1,2$.

Now, let us consider the influence of the terms with $h \neq 0$ on the trajectories of the dynamical system. If $\chi = \eta = 50$, $\xi = -1$, $\tau = 0,01$, $\sigma = 0,6$ and $h = 0$, then the limit cycle, appeared at $\kappa = 8$, $D^2 = 27.85$ near NSC, undergoes several period doubling bifurcations and it is destroyed at de-

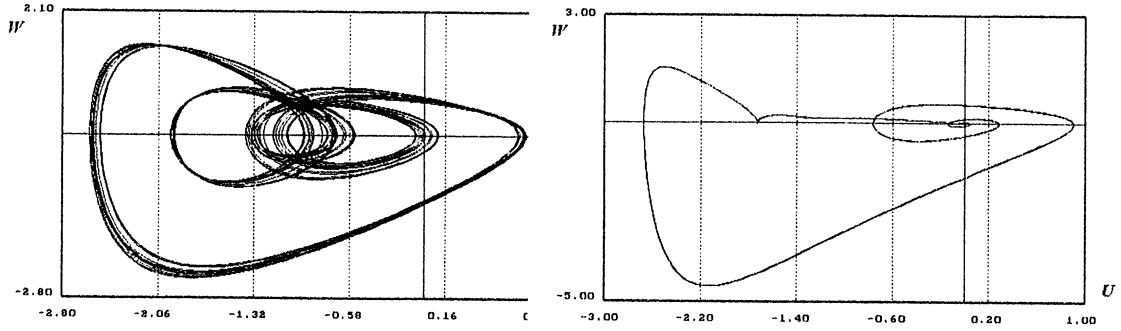

a b

Fig. 23: The phase portrait of the isolated trajectory at a) $h = 0, D^2 = 17,4$; b) $h = 0.01$, $D^2 = 16,4$.

creasing D^2. Near the main periodic orbit in interval $D^2 \in (17,4; 17,6)$ an isolated (or hidden) trajectory exists. Bifurcations of this cycle lead to the chaotic attractor creation (Fig.23a). If we add terms with $h \neq 0$, the phase space structure of system (63) changes with increasing parameter h.

Let us consider the behaviour of the solutions at $h = 0.01$ in detail. The analysis of the bifurcation diagram of Fig.24a suggests that, bifurcations of the main limit cycle, appearing near NSC, lead to chaotic attractor creation. Comparing the phase portraits of hidden trajectories, presented in Fig.23a and Fig.23, one can note the difference between their structures. There is the plausible assumption, that these regimes are the remains of the torus and homoclinic structure's existence.

Summarizing the above analysis, one can allocate the following features of the association of the S- and H-models in system (62):

1. Character of the regimes of S- and H-models save in the system (62) at the small values of h, σ, that allows us to spread the results of the submodel investigations on the generalized case.

2. One can find the values of parameters h and σ, when the additional terms begin to cooperate and cause essential changes of the phase space structure.

The important feature of H-model is the existence of the quasiperiodic

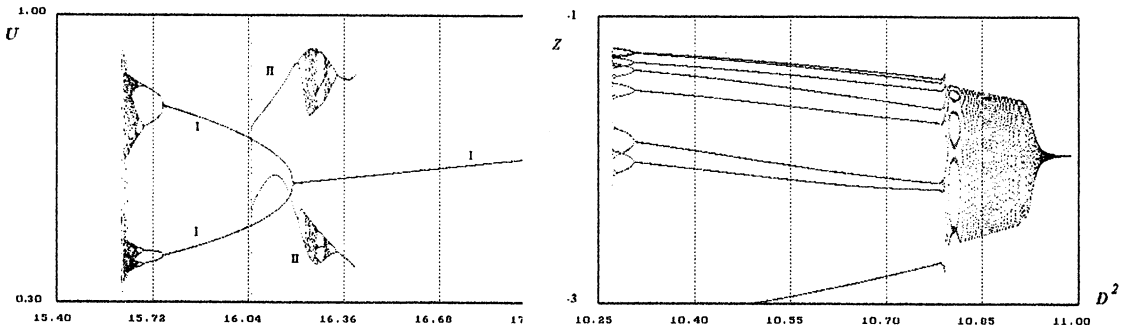

a b

Fig. 24: a). Bifurcation diagram of system (63) at $\chi = \eta = 50$, $h = 0,01$, $\xi = -1$, $\tau = 1$, $\sigma = 0,6$, $\kappa = 8$ and decreasing D^2, where I – main limit cycle, II – isolated trajectory; b). Bifurcation diagram of the torus development at $\kappa = 2$ and decreasing D^2.

solutions corresponding to the torus in the phase space of the dynamical system. The qualitative analysis of the structure of the trajectories on the torus carries out via the bifurcation diagram (Fig.24b) at the following values of parameters

$$\chi = \eta = 50,\ \xi = -1,\ \tau = 0.01,\ \sigma = 0.6,\ \kappa = 2,\ h = 0.01,\ D^2 = 11.$$

The phase portrait and its section with plane $W = 0$ are presented in Fig.25b and Fig.25b, respectively. The comparison the parameters of the torus existence with the diagram of Fig.24b suggests the coexistence of two oscillating regimes, coinciding at the smaller value of parameter D^2. The development of the quasiperiodic regimes lead to the complicated periodic orbit creation (Fig.23).

Except for the quasilinear regimes, H-model possesses the homoclinic loops, the position of which in the parametric space is shown in Fig.18. Therefore, let us introduce the temporal non-locality as a small perturbation of vector field of the H-model, putting $0 < h << 1$.

The result of calculating function (44) for singularly perturbed system is shown in Fig.26a. Comparison of figures 18 and 26a suggests about the stability of the homoclinic loop with respect to the small parameters perturbations.

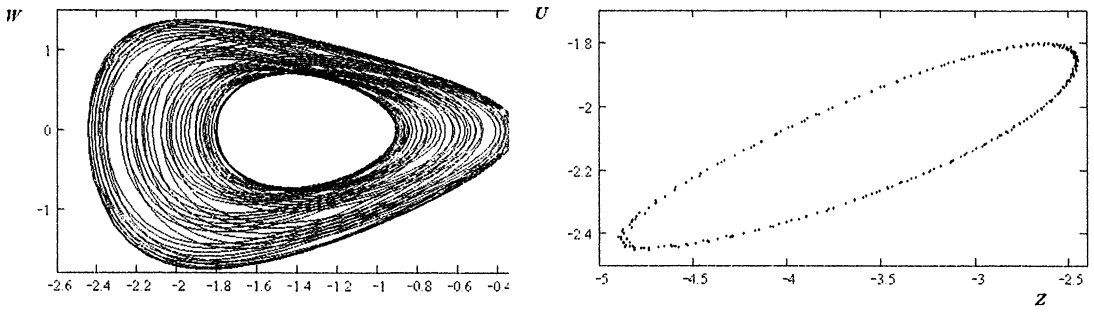

a b

Fig. 25: a) The phase portrait of the torus at $\kappa = 2$, $D^2 = 11$; b) The section of the torus with plane $W = 0$.

A set of H-model's solutions, lying close to the homoclinic loop, is found at other parameters $\chi = \eta = 50$, $h = 0.01$, $\xi = -1$, $\tau = 0.01$, $\sigma = 0.6$ with the initial data (0; 0; 0.0001). Values of function Φ (44) in the parametric space (D^2, κ) are given in Fig.26b.

6. Invariant chaotic and quasi-periodic solutions of nonlinear nonlocal models of relaxing media

Till now we dealt with models without physical nonlinearity. Generalizing the previous models in this direction we obtain the following model [26,27]:

$$\begin{array}{l} \dot{\rho} + \rho u_x = 0, \qquad \rho\dot{u} + p_x = \gamma\rho^m, \\ \sigma\chi\rho^{-2}\left[-\rho_{xx}\left(1+a\right) + \rho_x^2\rho^{-1}\left(1-na\right)\right] + h\chi\rho^{-2}[-\ddot{\rho}\left(1+a\right) + \\ 2\dot{\rho}^2\rho^{-1}\left(1-0.5a(n-1)\right) + \tau h^{-1}\dot{\rho}\left(1+a\right)] + \kappa\rho^n = p + \\ +\tau\dot{p} - h\ddot{p} - \sigma\left(p_{xx} + \rho_x p_x \rho^{-1}\right), \end{array} \tag{64}$$

where $\gamma\rho^m$ stands for the mass force ($m > 0$), parameter n characterizes physical nonlinearity of medium, components $a = \delta n\rho^{n+1}$, $\delta > 0$ relates to the temperature dependence incorporated in the equation of state.

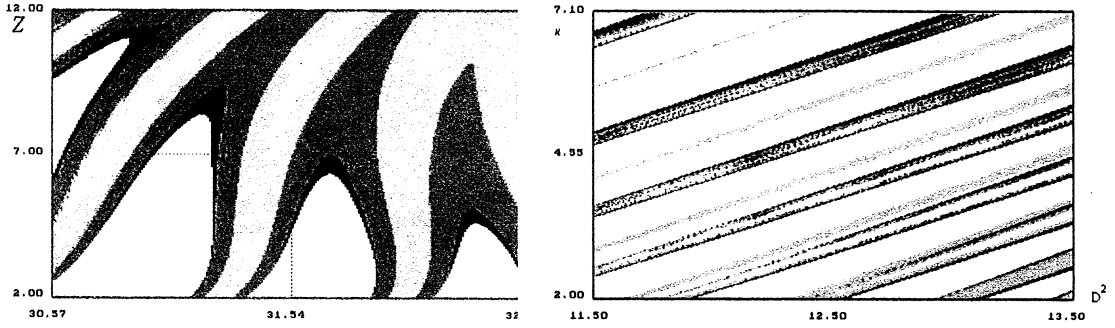

a b

Fig. 26: A portrait of subset of the parameter space (D^2, κ),corresponding to different intervals of values of function $\min f^\Gamma$, obtained for system (63) a) with $h = 0.01$ and b) with $\chi = \eta = 50, \xi = -1, \tau = 0.01, \sigma = 0.6, h = 0.01$: $\min f^\Gamma > 1.2$ for white, $0.6 < \min f^\Gamma < 1.2$ for light grey, $0.3 < \min f^\Gamma < 0.6$ for grey, $0.01 < \min f^\Gamma < 0.3$ for deep grey, $\min f^\Gamma < 0.01$ for black.

A set of properties of solutions of system (64) can be found using the symmetry of the system with respect to the Galilei group. One can be persuaded by direct verification that system (64) allows operator

$$\hat{X} = \frac{1}{2\xi}\frac{\partial}{\partial t} + t\frac{\partial}{\partial x} + \frac{\partial}{\partial u}.$$

Let us construct an anzatz with its invariants

$$\rho = R(\omega), p = P(\omega), \quad u = 2\xi t + U(\omega), \omega = x - \xi t^2, \tag{65}$$

where parameter ξ is proportional to acceleration of the wave front. While substituting (65) into the system we obtain the following quadrature:

$$UR = C = \text{const}$$

and the dynamical system

$$
\begin{aligned}
&R' = W, \quad P' = \gamma R^m - 2\xi R + \frac{C^2}{R^2} W, \\
&W' = -(\kappa R^{n+3} - PR^3 - P'R^2 C\tau - hP'C^2 W + P'R^2\sigma W + \\
&+\gamma m R^{2+m}\sigma W + \chi L\tau CW + \gamma hmR^m C^2 W + h\chi L(CWR^{-1})^2 - \\
&-2C^2\sigma W^2 + \chi M\sigma W^2 - 2C^4 hR^{-2}W^2 + \\
&+2h\chi NC^2 R^{-2}W^2 - 2R^3\sigma W\xi - 2hRC^2 W\xi)((C^2 - \chi L)R(\sigma + hC^2 R^{-2}))^{-1},
\end{aligned}
\tag{66}
$$

where $(\cdot)' = \dfrac{d}{d\omega}(\cdot)$, $L = 1+a$, $M = 1-an$, $N = 1-0.5a(n-1)$, $a = \delta n R^{n+1}$.

The studies of phase space of nonlinear system (66) can be carried out quite effectively by applying the methods of qualitative analysis [17]. Making the right parts of the equations of system (66) equal to zero, let us determine the coordinates of the single isolated equilibrium (neglecting the trivial) point:

$$
R_0 = \left(\frac{2\xi}{\gamma}\right)^{1/m - 1}, \; P_0 = \kappa R_0^n, \; W_0 = 0, \tag{67}
$$

and establish the conditions of its stability. To make further calculations easier, the origin of reference frame is put into equilibrium point (67) by the change of variables

$$
R = y_1 + R_0, \; P = y_2 + P_0, \; W = y_3
$$

and let us consider a linearized system, which looks as follows

$$
\begin{pmatrix} y_1 \\ y_2 \\ y_3 \end{pmatrix}' = \begin{pmatrix} 0 & 0 & 1 \\ a_1 & 0 & a_2 \\ a_3 & a_4 & a_5 \end{pmatrix} \begin{pmatrix} y_1 \\ y_2 \\ y_3 \end{pmatrix}, \quad i, j = 1..3. \tag{68}
$$

where

$$
\begin{aligned}
&a_1 = 2\xi(n-1), \quad a_2 = C^2 R_0^{-2}, \quad a_4 = R_0^2 \Delta^{-1}, \\
&a_3 = (2C^3 h\left[C^2 - \chi L\right]\tau\left[\gamma R_0^m - 2\xi R_0\right]R_0^{-2} + \\
&+C\chi(n+1)(L-1)\tau\Delta - C\left[C^2 - \chi L\right]\tau\Delta - \\
&-\left[C^2 - \chi L\right]\left(C^2 h R_0^{-2} + \sigma\right)\left(\kappa n R_0^{1+n} - C\tau\left(\gamma(2+m)R_0^m - 6\xi R_0\right)\right))/\Delta^2,
\end{aligned}
$$

$$a_5 = \frac{C^2\gamma h\left(nR_0^n - R_0^m\right) - C^3\tau + C\chi L\tau + R_0^2\sigma\left(\gamma\left[R_0^m + nR_0^n\right] - 4R_0\xi\right)}{R_0\Delta},$$
$$\Delta = \left(C^2 - \chi L\right)\left(C^2 h R_0^{-2} + \sigma\right).$$

Let us analyze when limit cycles can be observed in the vicinity of point (67). As is known from the Andronov-Hopf theorem [9], this can occur when the following condition takes place:

$$G\left(\xi, \sigma, n, h, \tau, \kappa, \chi\right) \equiv a_5\left(a_3 + a_2 a_4\right) + a_1 a_4 = 0. \tag{69}$$

Equation 69 gives a necessary condition for the appearance of the Andronov-Hopf bifurcation in system 66.

6.1. Studies of the effects of physical nonlinearity on the solutions of dynamical system (66)

Let us make the values of parameters fixed as follows:

$$\gamma = 1, \chi = 10, C = -2.8, \sigma = 0.2, \tau = 1.1, h = 3.2, \delta = 1.4, n = m = 3, 2.$$

A part of the graph of the neutral stability curve, which is determined by equality (69), is presented in Fig.27a.

If, for example, we make the fixed $\kappa = 0.9$, then from (69) we will numerically find that $\xi_0 = 0.157$ corresponds to birth of the limit cycle.

Choosing the value of parameter $\xi = 0.2 > \xi_0$ and applying direct numerical integration of dynamical system (66) by the Dorman-Prince method [28], one can observe the appearance of periodical vibrations, which are almost linear. We will analyze bifurcations of the revealed limit cycle using the Poincare section technique.

Let us choose plane $y_3 = 0$ as an intersecting one and find coordinates of intersection points of phase curves, which cross-sect the intersecting plane only in one direction. Plotting coordinate y_1 of the cross-section point along the vertical axis, and the value of the bifurcation parameter ξ along the horizontal one, we will obtain the bifurcation diagram (Fig.27b). From the analysis of diagram Fig.27b we can see that while parameter ξ increases the development of the limit cycle coincides with the Freihenbaum scenario, followed by the creation of a chaotic attractor.

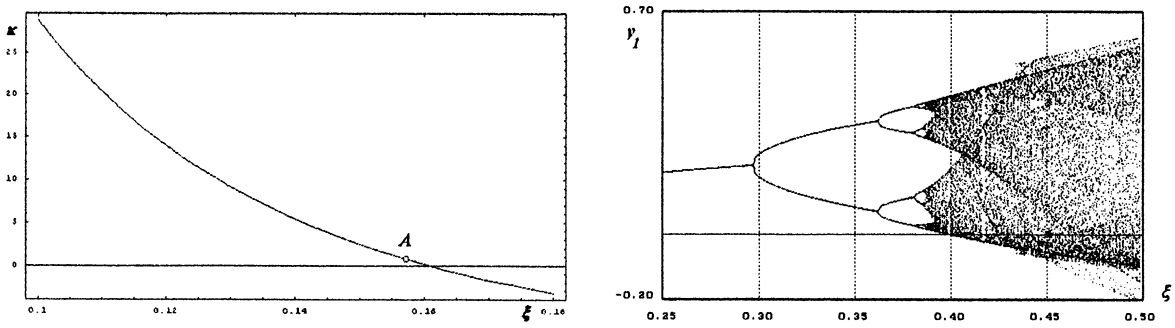

a b

Fig. 27: Fixed parameters $\gamma = 1$, $\chi = 10$, $C = -2,8$, $\tau = 1,1$, $h = 3,2$, $\delta = 1.4$, $\sigma = 0.2$, $n = m = 3,2$ a) a graph of the neutral stability curve, coordinates of point $A(0.157; 0.9)$ b) Poincare bifurcation diagram in case of increased parameters ξ, $\kappa = 0.9$.

In case of ξ close to 0.45 the structure of the chaotic attractor experiences qualitative alterations, which are evident by an abrupt change of vibration amplitude of the dynamical system solution (66).

Let us consider in more detail the influence on the revealed regimes of parameters n and δ changes, which determine nonlinearity of the medium in a dynamic equation of state. Let us make the value of parameter $\xi = 0.35$ fixed, in case of which there is a limit cycle with period $2T$ in the space of the system (Fig.27b).

For plotting a two-parametric bifurcation diagram in the plane of parameters n and δ, let us use the following practice. Let us fix the values of parameter δ from interval (0.4; 1.8). Decreasing n from 3.2 to 1.2, let us analyze the one-parametric diagram. It is convenient in this case to check a number of local maxima with different amplitudes, appearing in the graph of temporal dependence of a selected coordinate $y_1(t)$. In a temporal evolution of a periodic regime, all local maxima are equal. For a limit cycle with a $2T$ period – we have two different maxima, for a limit cycle with a $4T$ period – we have four etc.

By counting the number of local maxima with different amplitudes, one is able to distinguish different type of periodic solutions. Using this criterion, we succeeded in obtaining a two-parametric bifurcation diagram, shown in

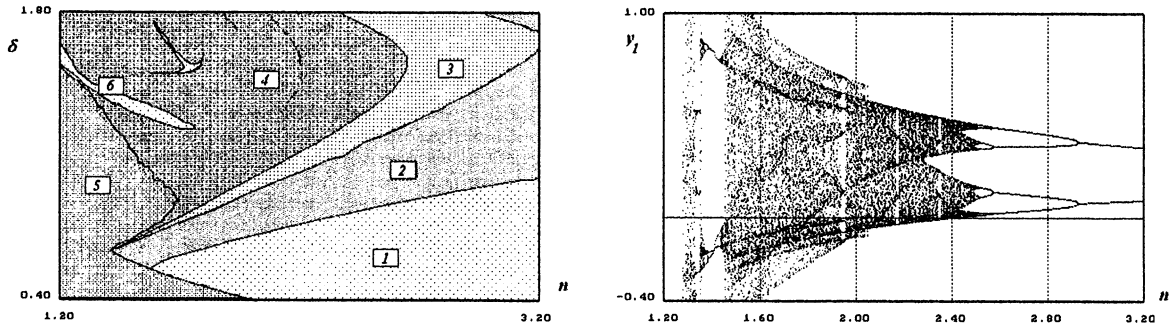

a b

Fig. 28: Fixed parameters $\gamma = 1$, $\chi = 10$, $C = -2,8$, $\tau = 1,1$, $h = 3,2$, $\sigma = 0.2$, $\kappa = 0.9$, $\xi = 0.35$, $m = 3,2$ a) two-parametric bifurcation diagram where shades of black correspond to regimes 1 – limit cycle, 2 – period doubling ($2T$-cycle), 3 – the birth of the period $4T$-cycle, 4 – chaos, 5 – exit of trajectory to infinity, 6 – complicated periodic trajectory; b) Poincaré bifurcation diagram in case of $\delta = 1.4$ and decreasing n.

Fig.28a. The diagram reveals some peculiarities of system's 66 behaviour. In particular, we would like to pay attention to the presence of a "special" point in the parameter plane, surrounded by four different types of solutions. One can also seen the "windows" of periodicity (area 6) among the chaotic area. To find out the structure of phase space in more detail near area 6 of Fig.28a, let us plot a one-parametric Poincaré diagram (Fig.28b) for $\delta = 1.4$ and a decrease of parameter n.

In case of n close to 2, abrupt reconstruction of the chaotic attractor structure can be observed, which is probably caused by the interaction of two (or more) co-existing attractors of a dynamic system. In case of $n \approx 1.4$ the chaotic trajectory is localized in a more narrow area of phase space of system (66), stipulating the appearance of a specific window of periodicity with a decrease of n. Analysis of a two-parametric bifurcation diagram for the value of parameter $\kappa = 2$ (Fig.29a) shows that the area of existence of the chaotic attractor increases and the windows of regular intervals in case of the increasing κ shift towards higher values of the nonlinearity parameter n.

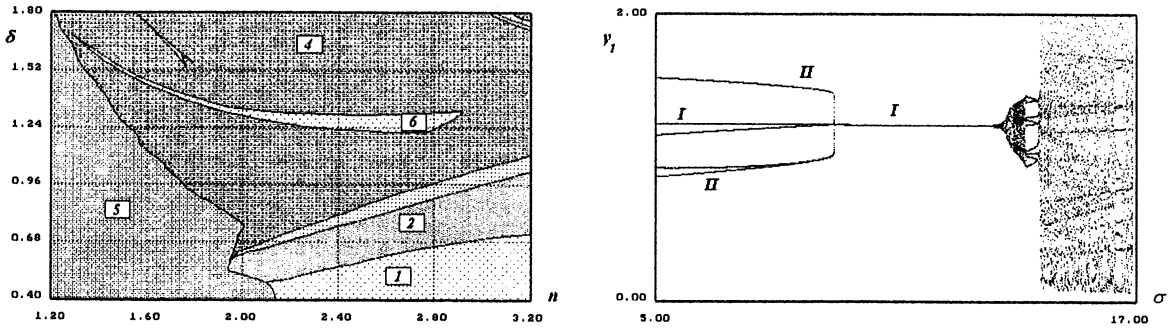

a b

Fig. 29: a) Two-parametric bifurcation diagram in case of $\kappa = 2$ (for other values of parameters and conventional symbols see Fig.28; b) Poincaré bifurcation diagram for development of the tore in case of $\gamma = 1$, $\chi = 10$, $C = -2,8$, $\tau = 1,1$, $\kappa = 0.9$, $h = 3,2$, $\delta = 0.4$, $\xi = 0.35$, $n = m = 3,2$ and increasing σ, where graph I is the basic limit cycle, graph II – complicated periodic trajectory with separated region of attraction.

6.2. Studies of the effect of spatial nonlocality on localized regimes of dynamical system (66)

A crucially different set of bifurcations is observed in case of a change of parameter σ.

Let us fix the values of parameters $\gamma = 1$, $\chi = 10$, $C = -2,8$, $\tau = 1,1$, $\kappa = 0.9$, $h = 3,2$, $\xi = 0.35$, $n = m = 3,2$ and $\delta = 0.4$. Integrating system (66) with initial data (0, 0, 0.01) and $\sigma = 5$ within phase space near the equilibrium point, in addition to the limit cycle, other periodic trajectory has been found with a separated pool of attraction (development of this regime with increasing of σ is presented in Fig.29b graph II).

The presence of such a regime leads to the thought of the existence of quasi-periodic regimes. To look for such a regime let us plot a bifurcation diagram of Poincaré for development of basic limit cycle in case of increasing parameter σ (Fig.29b graph I).

Another bifurcation, leading to the appearance of the toroidal surface, has been discovered in this system. An intersection of the toroidal attractor with the plane $y_3 = 0$ forms a closed curve, shown in Fig.30a.

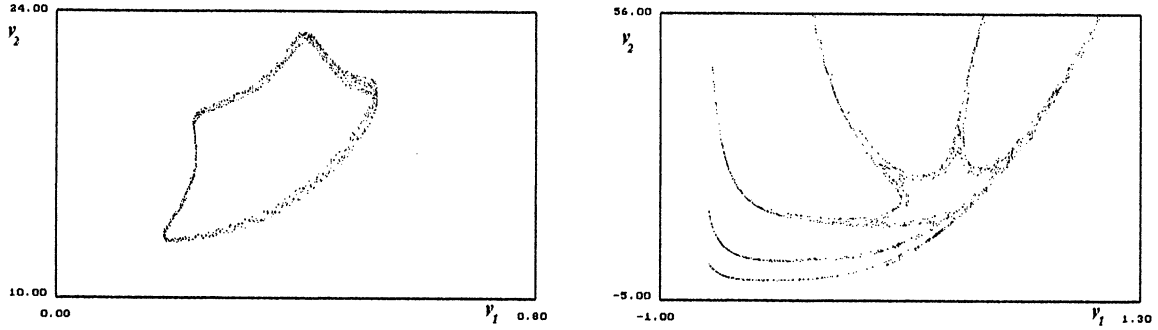

a b

Fig. 30: Fixed parameters $\gamma = 1$, $\chi = 10$, $C = -2,8$, $\tau = 1,1$, $\kappa = 0.9$, $h = 3,2$, $\delta = 0.4$, $\xi = 0.35$, $n = m = 3,2$. a) The Poincaré cross-section of the tore surface in case of $\sigma = 14$ b) The Poincaré cross-section of a chaotic attractor in case of $\sigma = 14.6$.

A further increase of parameter σ causes the synchronization of tore frequencies, and finally an abrupt increase of vibrations amplitude, which shows the creation of a crucial new dynamical behaviour. To clarify the character of the produced regime, let us analyze the Poincaré section for the case of $\sigma = 14,6$ (Fig.30b). The plotted cross-section is specific for chaotic attractor [9], which provides reasons for statements on the existence of bifurcation of a quasi-periodic regime with a producing chaotic attractor.

According to the results of the bifurcation analysis, presented in this section, dynamical system (66), which is connected to the system in partial derivatives by exact transformations has localized nontrivial attractors. Interaction of relaxation processes with nonlinearity of medium determined by dynamical equation of state 64 is one of the reasons for the appearance of such variability of regimes and bifurcation phenomena among the wave solutions: the Feigenbaum scenario, the birth of quasi-periodic regime, scenario of intermittency [26], bifurcations of chaotic attractors.

Bibliography

[1] Danylenko V.A., Danevich T.B., Makarenko O.S., Moskaliuk N. M., Skurativskiy S.I. and Vladimirov V.A., Algebra-invariant models for nonlinear nonlocal media // Algebras, Groups and Geometries, 2012. – Vol. 29, No. 3. – PP. 309–376.

[2] Danylenko V.A., Danevich T.B., Makarenko O.S., Moskaliuk S. S.(jn), Skurativskiy S.I. and Vladimirov V.A., Group analysis of reaction-diffusion-convection nonlinear equations // Algebras, Groups and Geometries, 2013. – Vol. 30, No. 3. – PP. 275–366.

[3] Danylenko V.A., Danevich T.B., Makarenko O.S., Moskaliuk V. S., Skurativskiy S.I. and Vladimirov V.A., Exact solutions and wave patterns within some non - local hydrodynamic - type model// Algebras, Groups and Geometries, 2014. – Vol. 31, No. 4. – PP. 363–436.

[4] Ovsiannikov L.V. Group analysis of differential equations, New York, Academic Press, 1982.

[5] Olver P.J. Applications of Lie groups to differential equations, Springer, New York, 1993.

[6] Hassard B.D., Kazarinoff N.D., Wan Y.-H., Theory and Applications of the Hopf Bifurcation, Springer, New York, 1981.

[7] Guckenheimer J., Holmes P. Nonlinear oscillations, dynamical systems and bifurcations of vector fields, Springer–Verlag: New York Inc, 1987.

[8] Shuster H.G. Deterministik chaos. Introduction, Weinheim, 1984.

[9] Berje P., Pomo I., Vidal K. The order in a chaos. On deterministic approach to turbulency / transl. from French, Moscow, Mir, 1991.

[10] Grebogi C.,Ott E., Yorke J.A. Chaotic attractors in crisis // Phys. Rev. Letters, 1982. – Vol.48. – P.1507.

[11] Grebogi C.,Ott E., Yorke J.A. Rises, sudden changes in chaotic attractors and transients to chaos // Physica D, 1983. – Vol.7. – P.181.

[12] Grebogi C.,Ott E., Yorke J.A. Chaotic attractors in crisis // Phys. Rev. Letters, 1982. – Vol.48. – P.1507.

[13] Grebogi C.,Ott E., Yorke J.A. Rises, sudden changes in chaotic attractors and transients to chaos // Physica D, 1983. – Vol.7. – P.181.

[14] Landau L.D., Lifshitz E.M. Hydrodynamics, Nauka, Moscow, 1986. - 736 p.

[15] Danylenko V.A., Christenyuk V.O. On the wave structures formation at the high-rate pulse load application to the relaxing geodynamical media // Reports NAS of Ukraine, 1994. – No.11. – P.112-115.

[16] Danevych T.B., Danylenko V.A. Investigations of the influence of spatial nonlocality on the waves spreading in a relaxing medium // S.I.Subbotin institute of geophusics NAS of Ukraine, preprint. – Kyiv, 1994. – 22 p.

[17] Methods of analysis of nonlinear dynamical models / S. Holodniok, A. Klich, M. Kubichek, M. Marek / Transl. from Czechish, Moscow, Mir, 1991. – 368 p.

[18] Anischenko V.S. Complicated oscillations in common systems, Moscow, 1990.

[19] Ramasubramanian K., Sriram M.S. A comparative study of computation of Lyapunov spectra with different algorithms // Physica D, 2000. – Vol.139, No.1-2. – PP.72–86.

[20] Melnikov V.K., On the stability of center for time periodic perturbations // Trans. Moscow Math. Society, 1963. – Vol.12. – PP.1–57.

[21] Vladimirov V.A., Skurativskii S.I. On invariant wave patterns in nonlocal model of structured media / in *Proceedinds of Third International Conference "Symmetry in Nonlinear Mathematical Physics"* (12–18 July, 1999, Kyiv), Editors A.G. Nikitin and V.M. Boyko, Kyiv, Institute of Mathematics, 2000, V.30, Part 1. – PP.231–238.

[22] Danylenko V.A., Vladimirov V.A. On the self-similar solutions of generalized hydrodynamics equations and non-linear wave patterns // J. Nonlin. Math. Phys., 1997. – Vol.4, No. 1–2. – PP.25–32.

[23] Vladimirov V.A. On the coefficients of canonical Poincaré form corresponding to 3-dimensional dynamical system with degenerated linear part // Gerald of Kiev National University, 2000. – No. 1. – PP.66–74.

[24] Demekhin Ye.A., Shkadov V.Ya. On the solitons in dissipative media, in *Hydrodynamics and thermal-mass transfer*, Editor G.I. Kutateladze, Novosibirsk, Insitute of Thermal Physics, 1985. – PP.32–48.

[25] Ovsyannikov I.M., Shilnikov L.P. Systems with homoclinic curve of the saddle-focus // Soviet Math. Sbornik, 1986. – Vol.130(172). – PP.552–570.

[26] Danylenko V.A., Skurativskiy S. I. Invariant periodic and chaotic solutions of a model of multicomponent medium with physical nonlinearity, spatial and temporal nonlocalities // Dop. NAS of Ukraine, 2005. – No. 8. – P. 112–115.

[27] Danylenko V.A., Skurativskyy S. I. Invariant chaotic and quasi-periodic solutions of nonlinear nonlocal models of relaxing media // Reports of mathematical physics, 2007. – Vol.59, No. 1. – PP. 45–51.

[28] Hairer E., Norsett S.P., Wanner G. Solving ordinary differential equations.I. Nonstiff problems, Springer-Verlag, 2000. - 528 p.

ALGEBRAS GROUPS AND GEOMETRIES 32 53- 134 (2015)

MATHEMATICAL MODELLING IN HYDRODYNAMICS WITH MEMORY[1]

Danylenko V.A., Danevich T.B., Makarenko O.S.[2], Skurativisky S.I. and Vladimirov V.A.
Subbotin Institute of Geophysics of the National Academy of Sciences of Ukraine
Palladin Av. 32
Kyiv, Ukraine, UA-03680
makalex@i.com.ua

Received October 30, 2014

Abstract

This article is devoted to the consideration of the mathematical aspects of solution's behavior of proposed generalized equations and their low-dimensional analogs; peculiarities of the solutions and their presumable interpretations in the theory of hydrodynamics with memory. The list of issues includes the origin of collapses in the solutions (blow-up regimes) and propagations of nonlinear wave fields in media with oscillating inclusions.

[1]Based on invited talks given by A. Makarenko at the 6th Petrov International Symposium on *High Energy Physics, Cosmology and Gravity*, Kyiv–Kosivska Poliana (Ukraine), September 5–20, 2013.

[2]On leave from the National Technical University of Ukraine (KPI), Ukraine.

Copyright © 2015 by Hadronic Press Inc., Palm Harbor, FL 34682, U.S.A

1. Collapses and selfoscillations (autowaves)

1.1. Basic equations of the relaxing media

In this we give a brief review of the types of equations used for the description of the dynamic behaviour of the strongly non-equilibrium media [1–3]. Illustrations of the basic ideas are shown for a one-dimensional equation of heat conduction (see e.g. [4–6]). As is well known, the classic heat conduction equation

$$\rho c \frac{\partial T}{\partial t} = \lambda \frac{\partial^2 T}{\partial x^2} \tag{1}$$

is derived from the energy conservation law and the Fourier law

$$q = -\lambda \frac{\partial T}{\partial x}, \tag{2}$$

where ρ is the density, c is the heat capacity, λ is the heat conduction coefficient, T is the temperature, and q is the heat flux. Equation (1) as a parabolic equation allows for physically unreal solutions which are followed by an infinitely large rate of propagation of the perturbations and infinitely large values of the fluxes in the initial instants of time. To remove this drawback, the following more precise modification to equation (2) was proposed:

$$q = \int_{-\infty}^{t} \left(\int_{-\infty}^{\infty} a\left(x, x', t, t'\right) \nabla T dx' \right) dt' \tag{3}$$

where $a(x, x', t, t')$ is the kernel of nonlocality, and (3) in its general form takes nonlocality in space and the history of the process into account.

The kernels of relation (3) are usually close to the kernels obtained under conditions near equilibrium, and the characteristic relaxation times and nonlocality scales are usually small. Under conditions in which the kernels are such that the transfer equations are partial differential equations, they turn out to have the form of parabolic equations, to which higher derivatives in time and space with small coefficients have been added (that is, they are singular perturbations of a parabolic equation). Thus, we call the analysis of self-organization processes based on generalized equations, "the

theory of singularly perturbed dissipative structures". It is clear from physical notions, that a significantly more accurate description of the transfer processes is thus obtained for problems with rapidly changing time and space variables.

Research has shown that the following approximation is most frequently obtained for kernels of a Maxwell-Cattaneo form (τ is the relaxation time)

$$a = -\frac{\lambda}{\tau} \exp\left(-\frac{t-t'}{\tau}\right) \delta(x-x') \tag{4}$$

Taking kernel (4) into account, the relation for the flow has the form

$$q = -\lambda \frac{\partial T}{\partial x} - \tau \frac{\partial q}{\partial t}. \tag{5}$$

Equation (5) was derived from within a number of different approaches - nonequilibrium thermodynamics, statistical mechanics and so on (Cattanelo, Luikov, Zubarev, McLennan, Robertson, Gurtin, Jon, Lebon). A.V. Luikov has derived his equation from within the framework of nonequilibrium phenomenological thermodynamics of irreversible approaches as a consequence of the Onsager relation between the generalized thermodynamical fluxes and forces causing these fluxes:

$$I_j = \sum_k L_{jk} X_k, \tag{6}$$

where X_k = generalized thermodynamical forces, I_j = generalized thermodynamical fluxes, and L_{ik} = phenomenological coefficients, which satisfy the condition $L_{ik} = L_{ki}$. Relations (6) are valid near the equilibrium.

For intensive processes they should be modified as follows:

$$I_j = \sum_k L_{jk} X_k + L_j^{(2)} \frac{\partial I_j}{\partial t} \tag{7}$$

where the dimension of $L_j^{(2)}$ is time-like, therefore being called the relaxation coefficients.

Thus, a hyperbolic-type equation for thermal conductivity, called the telegraph equation, is associated to the flow (5):

$$\tau \frac{\partial^2 T}{\partial t^2} + \frac{\partial T}{\partial t} = \frac{\partial^2 T}{\partial x^2} \tag{8}$$

A similar equation is obtained with the help of (5) or (7). Equation (8) is the simplest model illustrating the difference between the classical description and the description which takes memory effects into account. Note that this equation has its foundations in the Zwanzing-Mori projection formalism.

In [7], there are also equations derived for non-inertial media with memory, that is, for the extended active kinetic systems. Formalisms from [8] and the second law of thermodynamics in the form of Clausius-Dugham inequalities were used in this derivation. The final form of the equation is [7, 9, 10]

$$\begin{aligned}
&\alpha_n(0)\frac{\partial^2 z_n}{\partial t^2}(x,t) + \beta_n(0)\frac{\partial z_n}{\partial t}(x,t) + \int_0^\infty \beta_n'(s)\frac{\partial z_n(x,t-s)}{\partial t}ds = \\
&= k_n(0)\nabla^2 z_n(x,t) + \int_0^\infty k_n'(s)\nabla^2 z_n(x,t-s)\,ds + \sum_r \nu_{nr}W_r + \Phi(x,t), \\
&c_V\frac{\partial^2 T}{\partial t^2}(x,t) + \beta(0)\frac{\partial T}{\partial t}(x,t) + \int_0^\infty \beta'(s)\frac{\partial T}{\partial t}(x,t-s)\,ds = k(0)\nabla^2 T(x,t) + \\
&+ \int_0^\infty k'(s)\nabla^2 T(x,t-s)\,ds - \sum_r\sum_n \nu_{nr}H_n W_r, \\
&W_r = -\sum_{i=1}^{R}\sum_{n=1}^{N}\nu_{ni}\left[a_{ri}(0)\mu_n + \int_0^\infty a_{ri}'(s)\nabla\mu_n(x,t-s)ds\right]
\end{aligned} \tag{9}$$

Here, z_n are the reactants concentrations; μ_n are the chemical potentials; H_n are the partial molar enthalpies; W_r and Φ are the functions of internal and external sources respectively; $\beta_n'(s)$, $k_n'(s)$, $\beta'(s)$, $k'(s)$, a_{ri}' are the kinetic kernels describing the memory effects.

The kinetic kernels are time correlation functions of the fluxes with various correlation attenuation times (various memory durations). These kernels

take into account the processes approaching equilibrium faster than thermodynamical ones. In the phenomenological approach, *apriori* information upon the types of the available kernels can be obtained either from experiments, thermodynamic formalism or from the symmetry restrictions [7, 11]. The exact form of the kernels could, in principal, be obtained by means of the non-equilibrium statistical mechanics methods [12]. The appearance of integral terms in (9) is the consequence of reduced dispersion of systems on the thermodynamic level. Analogously, one can take into account the effects of non-locality by incorporating the spatially-depended kernels into the integral terms [5, 7, 11, 13]. Multicomponent media in single-velocity as well as double-velocity approximations are described in [11].

Depending on the form of the functions describing the kinetic kernels we obtain differential relations of different types. For constant values of $\beta_n(0)$, $\beta'(s)$, $k(0)$, $a_n(0)$, $\beta(0)$ and kernels $k'_n(s) = \lambda_n \times \lim_{t_0 \to 0} \delta(s - t_0)$, $k'(s) = \lambda \times \lim_{t_0 \to 0} \delta(s - t_0)$, describing an infinitely short memory, we have the parabolic equations on which the modern theory of combustion and explosion is constructed. The kernels $k'_n(s) = \lambda_n = \text{const}$, $k'(s) = \lambda = \text{const}$, describing processes with an infinite memory, lead to wave equations. In the intermediate process, with respect to memory duration described by the Maxwell – Cattaneo kernels

$$k'_n(s) = \frac{\lambda_n}{\tau'_n} \exp\left[-\frac{s}{\tau'_n}\right], k'(s) = \frac{\lambda}{\tau_n} \exp\left[-\frac{s}{\tau_n}\right],$$

one obtains the telegraph equation (8)from the system (9), taking into account the simplest form of memory – the finite substance propagation rate.

Thus, in this subsection we have introduced the general equations serving for the description of high-rate processes in multi-component media, manifesting the non-local effects. Using the different modelling kernels we get different model equations, which are the objects of these investigations.

1.2. Solutions with collapses (blow-up solutions)

Examples of the phenomena in which sharp changes occur are blow-up regimes [14]. Such regimes were initially studied using parabolic equations. Characteristic formulations of the problem involve *a regime with blow-ups*,

in which the solution of the equation grows to infinity in finite time due to a self-accelerating source, and *a boundary regime with blow-ups*, in which the value on the boundary tends to infinity in finite time. The analysis is carried out for the hyperbolic heat-conductivity equation (8), which is a singular perturbation of a parabolic equation in case of the small τ The importance of this equation resides in the fact that in many cases it is the nearest approximation, with respect to accuracy, to the generalized description, and also in the fact that so many of the important properties of these equations are revealed by the study of this example.

Lets begin the study of boundary regimes with blow-ups and consider, as an example, the heat conduction equation of the classical parabolic form and the generalized hyperbolic heat conduction equation of the second order, obtained from system (9) with the help of the source functions

$$W_r = T^i(1 - T^{m-l}) + \int_0^\infty a'_{ri}(s)T^l(s)ds, \quad r = i = 1,$$

and the kernels

$$a'_{ri}(s) = \frac{a_{ri}(0)}{\tau''_n} \exp\left(-\frac{s}{\tau''_n}\right), \; k'(s) = \frac{\lambda_n}{\tau_n} \exp\left(-\frac{s}{\tau_n}\right), \; k_n(s) = \lambda_n \lim_{t_0 \to 0} \delta(s - t_0).$$

We investigate the following problem written in a dimensionless form:

$$\tau \frac{\partial^2 T}{\partial t^2} + \frac{\partial T}{\partial t} = \frac{\partial^2 T}{\partial x^2} + f(T) \tag{10}$$

$$T(x,0) = \varphi(x) \quad \frac{\partial T}{\partial t}(x,0) = \psi(x), \quad x \in \Omega, \tag{11}$$

$$T|_{\partial\Omega} = \omega(t,x). \tag{12}$$

First of all we analyze the results of the numerical experiments (for more details see [7]). Let us consider the self-accelerating sources $f(T) = T^m$, $m > 1$ or $f(T) = \exp(T)$. These sources lead to blow-up regimes under special conditions. The results of numerical simulations, presented on fig.1 - fig.2, are obtained for the Cauchý data

$$\varphi(x) = \begin{cases} b(x - l_1)/(l_2 - l_1), & l_1 \le x \le l_2 \\ b(l_3 - x)/(l_3 - l_2), & l_2 \le x \le l_3 \\ 0, & otherwise \end{cases} \tag{13}$$

$$\psi(x) = N\varphi(x), \tag{14}$$

where $N \in \{0, 1, ..., 100\}$, $\omega(t) \equiv 0$, $b = 1$, $l_3 - l_2 = 2.8$, $l_2 - l_1 = 1.4$.

For memory duration

$$t_1 = \tau_n = \frac{[(\varphi,\varphi) + (\varphi,\psi)]^{1/2} + \left[(\varphi,\varphi) + (\varphi,\psi) + \frac{16}{m-1}(\varphi,\varphi)(\varphi,\psi)\right]^{1/2}}{10(m-1)/(l+1) + 2(\varphi,\psi) + [(\varphi,\varphi) + (\varphi,\psi)]^{1/2}},$$

$$(\varphi,\varphi) = \int_\Omega \varphi(x)\varphi(x)dx, \quad (\varphi,\psi) = \int_\Omega \varphi(x)\psi(x)dx, \quad \varphi > 0,\ \psi > 0,\ m > 1$$

the heat release in the focal explosion process is localized in a structure with a contracting half-width of the temperature profile, the development time of the thermal explosion depending on τ_n

$$t_\star = \frac{2\tau_n}{\beta_n(0)} \ln\left\{\frac{[(m-1)/4]\tau_n(\varphi,\psi) + l/4(\psi,\psi)}{[(m-1)/4]\tau_n(\varphi,\psi) - \beta_n(0)/2(\varphi,\varphi)}\right\}$$

As $\tau_n \to \infty$ the heat release in the focal explosion process is also localized in a structure with a contracting half-width of the temperature profile. The thermal explosion development time does not depend on τ_n:

$$t_\star = [4(\varphi,\varphi)/(m-1)](\varphi,\psi).$$

The memory duration also has a significant effect on the dynamics of the spread of the process beyond the explosion center. A fall in τ_n below the t_1 value leads to heat release at the initial moment taking place in a structure with an expanding half-width of the temperature profile and subsequent localization of the process on a certain length. For kernels describing an infinitely short memory the focal thermal explosion process is propagated into the surrounding reactive space from the outset. The solutions describing the propagation of solitons also depend on τ_n. The soliton solutions are contained in (9) for kernels

$$a'_{ri}(s) = \frac{a_{ri}(0)}{\tau''_n} \exp\left(-\frac{s}{\tau''_n}\right), \quad k'(s) = \frac{\lambda}{\tau_n} \exp\left(-\frac{s}{\tau_n}\right), \quad k_n(s) = \lambda_n = \lambda = \text{const}$$

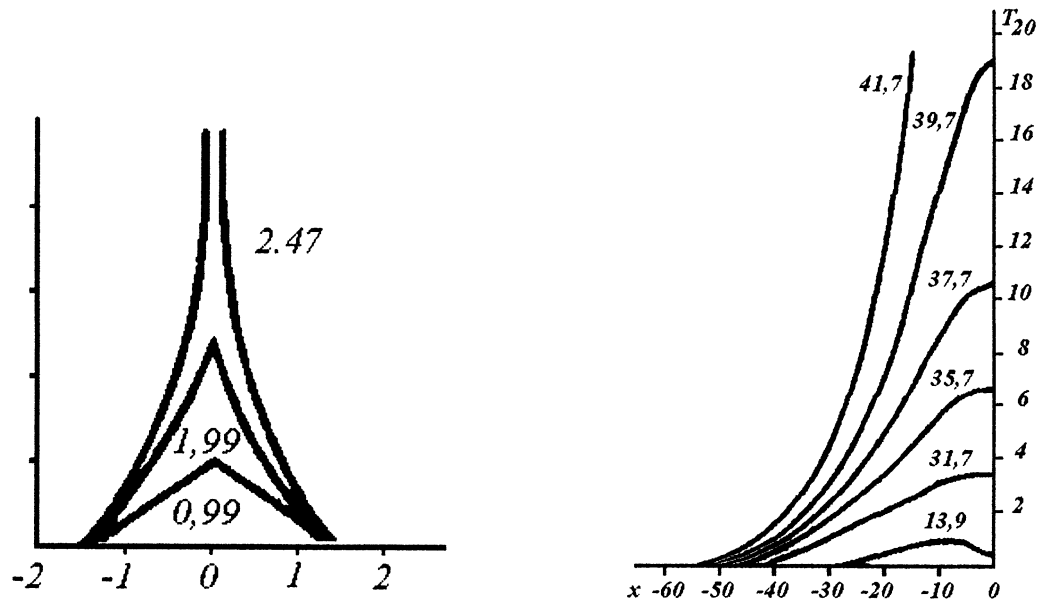

a. b.

Fig. 1: Space-time temperature distribution in focal thermal explosion resulting from a temperature fluctuation as a function of memory duration a) $\tau_n = \tau_n'' = 10^9$, $m = 7$, $l = 2$, b) $\tau_n = \tau_n'' = 10^2$, $m = l = 10$.

and source functions $W_r = \tilde{\xi} \exp(T)$,

$$W_r = T^i(1 - T^{m-l}) + \int_0^\infty a'_{ri}(s)T^l(s)ds, \quad m \geq 4, \quad l > 1.$$

The numerical results of investigating a focal thermal explosion within the model (10) for various memory durations and the boundary conditions (11), (12) are presented in figure 1. The three stages of reorganization can be easily seen: 1) the slow reconstruction of profile, 2) the slow growth of the profile, 3) the fast "blow-up" regime. In this case the blow-up time is 45.8.

Note. The description of the creation of complexity by confluence of some simple structures to one complex structure can be found in [14, 15].

The opposite process, to some extent, of the destruction of the initial pattern can be seen in figure 2. In this case, the one-humped initial dis-

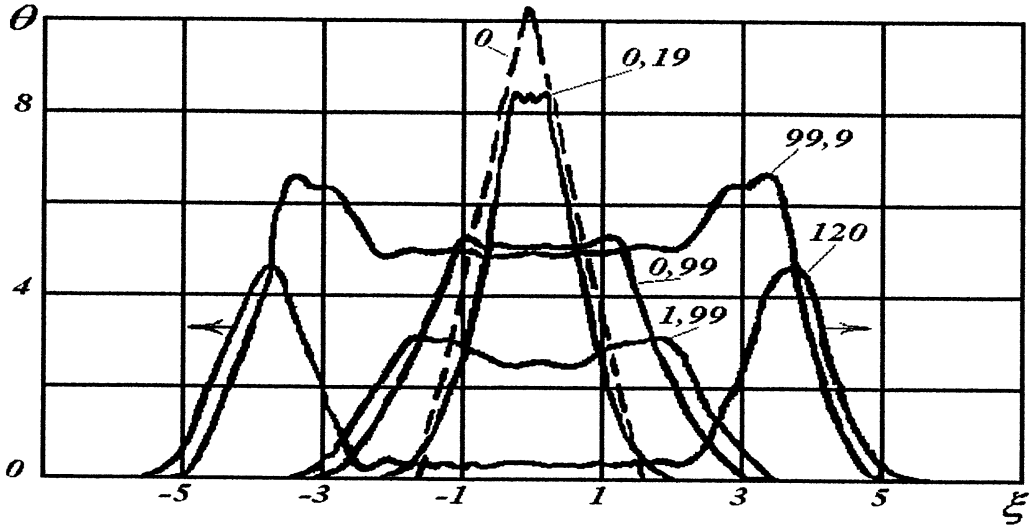

Fig. 2: Creation of two travelling waves from the initial pulse within the nonlinear hyperbolic equation. Here $\psi = N\varphi = 0$, $N = 0$, $m = l = 10$, $\tau_n = \tau_n'' = 10^3$.

tribution changes, at some stage, into two-humped distribution (see graph for $t = 13.9$). In numerical experiments $m = 10$, $\tau_1 = 10$, $\tau_2 = 100$ and with the same initial data blow-up, the times are $t_1 = 1.35$, $t_2 = 4.21$, correspondingly. For τ_i, $i = 1, 2$ we have the following relation

$$\frac{t_1}{t_2} = \frac{\sqrt{\tau_1}}{\sqrt{\tau_2}}, \tag{15}$$

which is fulfilled with 4 % accuracy. As one can see below, this is in accordance with analytical methods. The "two-humped" structure is also typical a for linear wave equation with the initial condition $\psi \equiv 0$. In this case there are two independent travelling waves moving in opposite directions. We also found the same phenomena in the nonlinear equation. The behaviour of the solution for $m = 10$, $R = 1000$ and for different moments of time is displayed in figure 2.

Dropping the initial fluctuation of the temperature on two autowaves,

moving in opposite direction, is an example of the self-organization process. In connection with this a natural question arises about the condition assuring the blow-up solutions appearance. There are many approaches to this problem. One of the most useful is connected with the nonexistence of solutions in some mathematical problems. Now we shall describe one such a theorem proved by us. Lets introduce a smooth convex function $f(T)$, $\varphi > 0$, $\psi > 0$, $\tau \equiv 1$ and ψ_0, λ are, correspondingly, the first eigenfunction and eigenvalue of the eigenvalue problem

$$\frac{\partial^2 \psi_0}{\partial x^2} + \lambda \psi_0 = 0, \ \lambda > 0, \ \psi_0 > 0, \ x \in \Omega \tag{16}$$

$$\psi_0(0) = \psi_0(1) = 0, \quad \Omega = [0,1], \tag{17}$$

ψ_0 is normed $\left(\|\psi_0\|_{L_1(\Omega)} = 1\right)$. We also introduce the following quantities:

$$\alpha_1 = \int_\Omega \varphi(x)\,\psi_0(x)\,dx, \quad \beta_1 = \int_\Omega \psi(x)\,\psi_0(x)\,dx \tag{18}$$

$$G(s) = \sqrt{2\int_{\alpha_1}^{s} \{-\lambda s + f(s)\}\,ds + (\beta_1 + \alpha_1)^2 - s}, \tag{19}$$

$$F(s) = f(s) - \lambda s \tag{20}$$

Theorem 1..1. *Let the following condition be fulfilled*

$$\alpha_1 > 1, \tag{21}$$

$$\exists\, p > 0 : F(s) > 0, \forall (s) > p, \ F - \textit{nondecreasing}, \tag{22}$$

$$G(s) > 0 \quad \forall s > \alpha_1 \quad t^* = \int_{\alpha_1}^{\infty} \frac{ds}{G(s)} < +\infty \tag{23}$$

Then the classical solution $T(x,t) \in C^{2,2}_{t,x}$ of the problem (10) – (12) cannot exist for an infinitely long time and existence time is bounded

$$\tau < t^*. \tag{24}$$

An analysis of the proof of the nonexistence theorem shows that for $\tau \to 0$ and $\phi \equiv 0$ the range of the initial data with collapses in solutions of equations with $\tau = 0$ and $\tau \neq 0$ $(\tau \to 0)$ drops together. In the case, where the problems with $\tau = 0$ and with $\tau = \varepsilon \neq 0, \varepsilon \ll 1$ has coupled blow-up solutions, blow-up times prove to coincide: $t^*_{\varepsilon \to 0} \to t^*_{\varepsilon = 0}$. In case when $\varphi \geq 0$, $\phi \geq 0$, $\tau \to \infty$ relation (15) holds and $t^* \to$ const .

1.3. Boundary blow-up regimes

To investigate the boundary blow-up regimes, we must consider the following problem in the half-space:

$$\frac{\partial T}{\partial t} = \frac{\partial^2 T}{\partial x^2}, \quad x \in (0, \infty), \quad t > 0, \tag{25}$$

$$T(x, 0) = 0, \tag{26}$$

$$T(0, t) = \mu(t), \quad t \geq 0 \tag{27}$$

We consider the monotonically increasing function $\mu(t)$ such as

$$\mu(t) \to +\infty, \quad t \to T^* < +\infty, \quad \mu(0) = 0. \tag{28}$$

It can be shown that, depending on the growth rate of $\mu(t)$, the temperature profiles evolve in regimes with diminishing, constant and growing effective width (LS, S, HS solutions, according to the terminology from [14, 15]).

For the hyperbolic heat conduction equation the problem consists of finding solutions to the equation

$$\tau \frac{\partial^2 T}{\partial t^2} + \frac{\partial T}{\partial t} = \frac{\partial^2 T}{\partial x^2}, \tag{29}$$

satisfying the conditions (26) – (28) as well as the supplementary condition

$$\frac{\partial T}{\partial t}(x, 0) = 0. \tag{30}$$

Before we begin the description of the boundary blow-up solution to equation (29), lets consider the asymptotic expansion of the bounded solution to equation

$$\varepsilon \frac{\partial^2 T}{\partial t^2} + \frac{\partial T}{\partial t} = \frac{\partial^2 T}{\partial x^2} + f(T), \quad \varepsilon \ll 1 \tag{31}$$

In [7] solution

$$T(x,t,\varepsilon) = \sum_{i=0}^{N} \varepsilon^i T_i(x,t,\varepsilon) + \sum_{i=0}^{N} \varepsilon^i v_i(x,\tilde{\mu},\varepsilon) + R_n, \tag{32}$$

was investigated by means of the Vishik-Lusternik asymptotic method. Here $\tilde{\mu} = t/\varepsilon$ is the fast time, T_i denote terms of external approximations, v_i are terms of internal approximations, R_n is the remainder. The leading term is $T_0(x,t)$ – which is the solution of the problem with $\varepsilon = 0$ and v_1, having the form

$$v_1 = \left(\frac{\partial T_0(x,0)}{\partial t} - \psi(x) \right) \exp(-\tilde{\mu}). \tag{33}$$

It must be noted that, the function $\psi(x)$ is the initial condition for the time derivative. v_1 exponentially decays till time $t \sim \varepsilon$. Thus, the hyperbolic boundary layer exists near $t = 0$. The deviation from the parabolic solution in this layer is rather significant. After $t > \varepsilon$, the solution tends to that of the parabolic equation.

With these asymptotic results in mind, lets return to the boundary blow-up solution of equation (29). The case $\tau \ll 1$ is of special interest for the theory of singularly perturbed dissipative structures. The blow-up case in principle differs from bounded case. For small time the hyperbolic boundary layer exists and then solution to (29) tends to that of the parabolic equation. However, the difference between the solutions of the parabolic model and its hyperbolic modification becomes significant again when their amplitudes grow. In case of $\tau \ll 1$ this difference concentrates on times $|t - T^*| < \tau$. Therefore, in this strip there is a new mathematical object – the second boundary layer on time (the first layer was near 0). Also, a very interesting question relates to the behaviour near the blow-up time. Lets consider the simplest case

$$\frac{\partial^2 T}{\partial t^2} = \frac{\partial^2 T}{\partial x^2} \tag{34}$$

with conditions (26) - (28), (30). Then we have the exact solution

$$T(x,t) = \begin{cases} \mu(t-x), & t \geq 0 \\ 0, & t < 0 \end{cases}. \tag{35}$$

It can be seen from (35), that $\partial T/\partial t$ increases at a fixed time. Thus, we can introduce the notion of a kernel of a solution. There are regions with significant growth of the solution. In the simplest case of boundary blow-up we can use

$$\mu(t) = \frac{1}{(T^* - t)^n} - \frac{1}{T^*}, \quad n > 0. \tag{36}$$

It can also be seen from (36), that for $n = 1$ and for $\Delta = (T^* - t) \gg x$ solution is almost constant, but for $\Delta \ll x < t$, the solution is similar to function $1/x - 1/T^*$ and $\partial T/\partial t$ has the form $1/(\Delta + x)^2$.

Thus with $\Delta \to 0$ there are strong changes in the kernel and the other part of the solution is almost "frozen". Therefore it is natural to ask the question: where does the profile of the solution tend, when $\Delta \to 0$. Since for $\Delta = 0$ the solution becomes infinitely large and is not classical, it is natural to consider the limit profile as a generalized function. For example, the solution for (36) with $n = 1$, continued in the domain $-\infty < x \leq 0$ as an odd function could be treated as a generalized function

$$\tilde{T} = P\left(\frac{1}{x}\right) - \tilde{\omega}(x),$$

where $P\left(1/x\right)$ is a generalized function corresponding to $1/x$ [16]. $\tilde{\omega}(x)$ corresponds to the function

$$\omega(x) = \begin{cases} \dfrac{1}{|x|}\operatorname{sgn} x, & |x| \geq T^* \\ \dfrac{1}{T^*}\operatorname{sgn} x, & |x| < 0 \end{cases}$$

The fact that the LS boundary blow-up regime allows for the interpretation as a generalized function, this suggests the description of the LS blow-up regimes in terms of a special generalized function. And within this class we are able to extend the blow-up solutions beyond the blow-up time.

1.4. Description of combustion

Properties, described in the previous subsection, have a large significance for general self-organization questions. The large deviations from classical

results can be found in systems which are far from equilibrium. One such a physical phenomenon is combustion. The classical combustion theory, based on parabolic transport equations [17, 18] exists here. The main source of chemical energy in this theory is the Arrhenius source

$$Q = k_0 \exp\left(-\frac{E}{R_0 T}\right). \tag{37}$$

With the help of the Frank-Kamenetzky variables, the characteristic time and space parameters in combustion problems

$$t_{ad} = \left\{\frac{Q}{c\rho}\frac{E}{R_0 T_0^2} k_0 \exp\left(-\frac{E}{R_0 T_0}\right)\right\}^{-1}, \tag{38}$$

$$\delta = \frac{Q}{\lambda}\frac{E}{R_0 T_0^2} r_0^2 k_0 \exp\left(-\frac{E}{R_0 T_0}\right) \tag{39}$$

were found here. In (37) - (39), λ is the heat conduction coefficient, c is the heat capacity, ρ is the density, E is the activation energy, Q is the heat effect of the reaction, k_0 is the pre-exponent factor, R_0 is the Avohadro constant, T_0 is the temperature of the surrounding medium, r_0 is the scale length. With these parameters we have the following dimensionless hyperbolic-type combustion equation:

$$R\frac{\partial^2\theta}{\partial t^2} + \frac{\partial\theta}{\partial t} = \frac{1}{\delta}\frac{\partial^2\theta}{\partial x^2} + \exp\left(\frac{\theta}{1+\beta\theta}\right), \quad R = \frac{\tau}{t_{ad}}, \tag{40}$$

where $\theta = E(T - T_0)/R_0 T_0^2$ is the dimensionless temperature, τ is the relaxation time. For the $\tau = 0$ equation (40), it coincides with the classical one.

It is clear, that for $R \ll 1$ solution (40) differs from the classical one in the initial boundary layer and for big θ and $\partial\theta/\partial t$ as well. But the difference can be significant for all t in the case of $R \gg 1$. In combustion this possibility ($R \gg 1$) can be realized. This is because parameter t_{ad} decreases significantly with the growth of the initial temperature. For a more detailed discussion see [19].

Next, some numerical examples illustrating the influence of relaxation on the dynamics of combustion are shown.

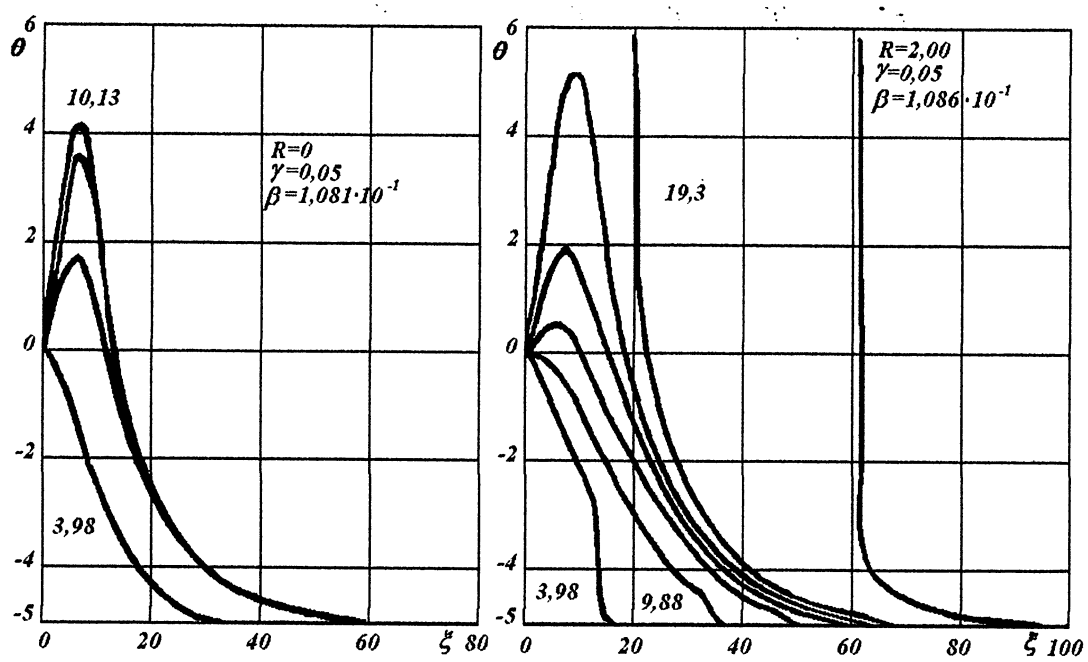

a. b.

Fig. 3: Solution for the combustion profile a) the classical case $R = 0$, $\gamma = 0.05$, $\beta = 0.1081$ and b) the hyperbolic heat equation with $R = 2.0$, $\gamma = 0.05$, $\beta = 0.1086$.

Figure 3 a was calculated from the classical theory; however, figure 3 b was computed with the help of hyperbolic heat equation for the parameters $R = 2$, $\delta = 1$, $\beta = 0,1086$, $\gamma = 0,05$. There are two distinctive features exposed by the numerical experiments. The first: solutions to hyperbolic heat equation predict the abrupt fronts' appearance. The second: relaxation causes the combustion's slow down. Figure 4 shows the evolution of the maximum temperature depending on R. From this graph we can evaluate an important combustion theory parameter, called the induction time.

In other problems of the combustion theory we investigate the heat localization near the wall of a vessel in the filter theory, stationary regimes of the combustion with large amplitude oscillations in time [13].

Further complication of the problem gives rise to burning down pro-

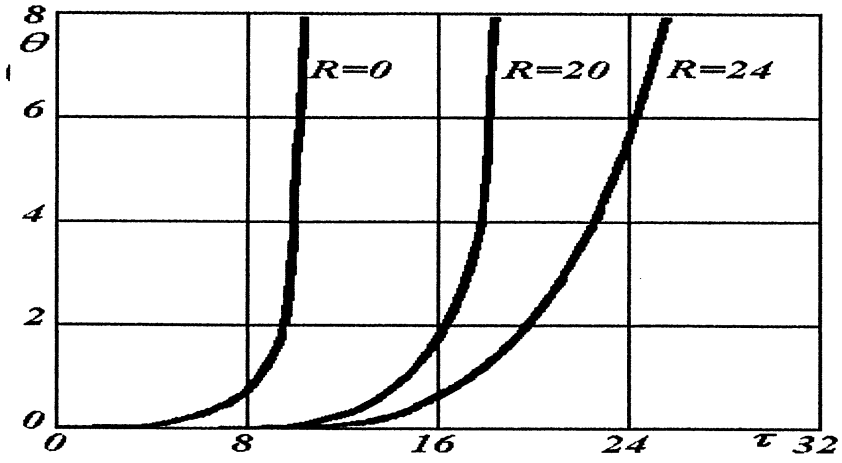

Fig. 4: Development of the maximum temperature in the combustion solutions versus relaxation time R

cesses. In the simplest case, the Arrhenius source must be modified to

$$(1-\eta)\exp\left(\frac{\theta}{1+\beta\theta}\right),$$

where parameter η is the power of burning down processes.

For η we have the following equation (the parameter γ is a constant)

$$\frac{d\eta}{dt} = \gamma\,(1-\eta)\exp\left(\frac{\theta}{1+\beta\theta}\right).$$

T and η are graphically illustrated in Fig. 5 a in the cylindrical coordinates in regimes with a travelling wave with constant speed. For other parameters, we found autowave solutions with pulsating propagation of the flame front.

In fig. 5 b, the speed of travelling wave versus space position of the wave front has been shown. It should be noted, that in [7] there are also many results of the investigations of full gas-dynamic systems with heat and stress relaxation and with chemical kinetics. In particular there are very interesting

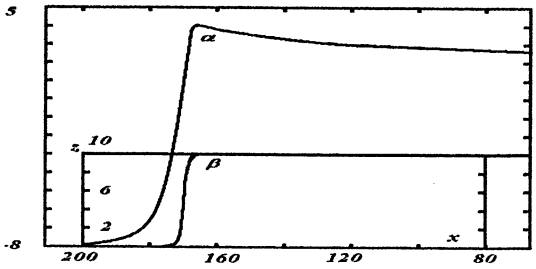

Fig. 5: a). Profiles of the space distributions of the temperature (curve a) and concentration η (curve b) in the travelling waves regime of the combustion. b). Amplitude of the travelling wave inverse speed (W^{-1}) versus the space position for the different relaxation times R in the combustion.

results on different solutions with shock and other waves [7]. Some problems with non-local effects were also considered in [13].

1.5. Solutions of the hyperbolic Burgers equation

A general theory of turbulence has still not been developed. In hydrodynamics, the viscosity is considered to be the main factor determining the dissipation of energy. The influence of collapses on the solutions of the Navier-Stokes equations was suggested by Leray. Recently, a new turbulence model was proposed, in which the random merging of solutions lying close to collapses was claimed to be the main mechanism of turbulence [20], using a nonlinear Schrödinger-type equation.

The possibility of such phenomena also occurs in model equations of so-called generalized hydrodynamics. Generalized hydrodynamics takes into account memory and nonlinearity effects far from equilibrium. For noncompressible viscous fluids such equations are a generalization of the Navier-Stokes equation. In this subsection we consider the the hyperbolic modification of the Burgers equation serving as the model equation for such effects, and study the properties of its solutions, especially the collapsing solutions.

For convenience we give a brief description of some general principles

in modelling hydrodynamics and of the choice of model equations. The standard object in mathematical investigations of turbulence in fluid is the Navier-Stokes system [21]. As is well-known, such systems formally possess the property of an infinite speed of signal propagation. Also, in some cases there are paradoxical solutions, for example, in the fluid motion between the parallel plates, where an infinite tangent stress on the plates at the initial moment formally exists. This raises questions about the restricted applicability of the Navier-Stokes system to turbulence. The great number of results obtained in hydrodynamics, turbulence and statistical physics enables one to also find the right position of the Navier- Stokes system in the hierarchy of continuous media models. Thus, the Navier-Stokes system is connected with the reduced description chain of Bogolubov, Born, Kirkwood, Green and Ivon.

The Navier-Stokes system is usually obtained in the following way. The equation of motion for a non-compressible fluid has the form

$$\frac{\partial \overline{V}}{\partial t} + V_k \frac{\partial \overline{V}}{\partial x_k} + \operatorname{grad} P = \operatorname{div} \sigma + f, \quad \operatorname{div} \overline{V} = 0. \tag{41}$$

These equations are closed by an equation which connects the stress and strain in a Newton fluid [21]

$$\sigma = 2\nu D, \quad D_{ik} = \frac{1}{2}\left(V_{i,x_k} + V_{k,x_i}\right) \tag{42}$$

where ν is the viscosity coefficient, P the pressure, σ the stress tensor, V the velocity, f the external forces, and D the strain tensor.

There are some studies on the derivation of fluid motion equations from the basic principles where the hydrodynamics level of description is still valid. In general, there are five groups of basic variables at this level: stress, velocity vector and temperature. It is known that in a state far from equilibrium, the equation of motion (41) preserves its form and the constitutive equation (42) takes a more general form, which in the one- dimensional case is [22–24]

$$\sigma(r,t) = -\int_{-\infty}^{t} dt \int dr K(r,t;r',t') \frac{\partial V}{\partial x}(r',t'). \tag{43}$$

Expressions like (43) take into account the influence of the prehistory of the processes. These are also called memory effects (or relaxation, or, in some cases, time dispersion). This equation also takes into account the nonlinearity and space nonlocality. In the first case, the values at various points in space depend on the values in a certain vicinity of the point taken.

From another point of view, expressions like (43) are postulated in some other well-defined theories, like rational thermodynamics or phenomenological thermodynamics of media with memory [8]. It can also be mentioned that similar expressions often occur in experiments in many fields of science and technology, for example in neutron scattering in liquids, in turbulence [25], in the motion of viscous-elastic fluid.

It can be seen from (43) that memory, nonlocality and nonlinearity effects are defined by the type of kernel $K(\cdot)$. Inserting (43) into (41) gives in general non- linear integral-differential equations. Particular forms of $K(\cdot)$ give particular forms of hydrodynamics equations, including (41).

In general cases, equations with a general form of expression (43), can hardly be studied, especially in connection with experimental hydrodynamics. Therefore, it may be useful to consider the simple consequences of (41), (43) which, for the above-mentioned reasons, could be more precise than the Navier-Stokes models. One such model can be obtained for linear cases with memory effects described by the exponential-type kernels

$$K(\cdot) = \text{const} \times \exp\left(-\frac{t-t'}{\tau}\right)\delta\left(x-x'\right), \tag{44}$$

where τ is the relaxation time. It can easily be seen that for this example, equation (43) gives, in the one-dimensional case, the constitutive equation

$$\sigma + \tau\frac{\partial\sigma}{\partial t} = \nu\frac{\partial V}{\partial x}. \tag{45}$$

Expressions (45) with (41) give systems of equations that are similar to the linear model of viscous-elastic media taking the form of Maxwell media

[26, 27]

$$\frac{\partial \overline{V}}{\partial t} + V_k \frac{\partial \overline{V}}{\partial x_k} + \tau \left(\frac{\partial^2 \overline{V}}{\partial t^2} + \frac{\partial V_k}{\partial t} \frac{\partial \overline{V}}{\partial x_k} + V_k \frac{\partial^2 \overline{V}}{\partial t \partial x_k} \right)$$
$$-\nu \triangle \overline{V} = -\left(1 + \tau \frac{\partial}{\partial t}\right) \operatorname{grad} P + f, \tag{46}$$
$$\operatorname{div} \overline{V} = 0$$

Although this model does not take into account some nonequilibrium effects, it is more accurate than the Navier-Stokes model. It is reasonable to consider this model as the next step in the hierarchy of more precise models. A particularly interesting aspect of such models is the problem of chaotic behaviour in such models. Considering the space nonlocality effects in (43), the simplest case gives some modifications of (46). This will be briefly discussed later.

It can also be mentioned that with the help of the exponential kernels for the heat flux in expressions like (43), the telegraph equation (8) is given.

Of course, we can expect a large difference between the results obtained with the usual and generalized equations in cases when the relaxation time T is greater than the intrinsic time of the process in the system, and if the characteristic scales of flows are smaller than the parameter of nonlocality l [25, 28, 29]. In the general theory, the parameters τ, l are connected with corresponding correlation functions by complicated formulas [22–24]. There are many experimental, phenomenological and qualitative studies on the manifestation of memory and nonlocality effects in different media: gas, fluids, solids, plasma. These results show that under normal conditions of slow processes τ is sufficiently small: $\sim 10^{-9}$ sec in gases, less than $10^{-8} - 10^{-9}$ sec in fluids, less than 10^{-12} sec in solids. The nonlocality parameter l is usually small as well. Thus, for instance, for laminar flows of common fluids the difference in description may be found only at a microscale level. However, for viscoelastic fluids, the memory effects may be essential: in polymers τ may achieve minutes [30] or years in geotectonic flows [29, 30]. It is very important that for turbulent flows of common fluids, the tension relaxation time reaches $10^{-3} - 10^{3}$ s [25]. Under these conditions the nonlocality parameter l may also reach values of millimeters. This is because the turbulence is described by the hydrodynamic equations with some effective parameters.

Though the problem of calculation of effective parameters is under intensive study, it is still far from a complete solution, and different empirical relations and phenomenological approaches are used. Among those, most frequently used are the various modifications of Prandtl's mixing length theory, which estimates integral time and length scales in turbulent flows.

The many methods of investigations of systems (41), (43) and their consequences (functional analysis, asymptotic methods, low-dimensional dynamic systems and so on) are all complex. Thus, for a better understanding of their possible properties, it is also useful to study the extraction of the model equations. Usually such equations are the simplification of original systems, and, at the same time, they may take into account some of the main mechanisms. In this subsection we present such a study. It is well known that in many cases a valid model equation for hydrodynamics is the Burgers equation [31–35]

$$\frac{\partial u}{\partial t} + u\frac{\partial u}{\partial x} = c\frac{\partial^2 u}{\partial x^2} \tag{47}$$

This equation was proposed in [31] to take into account the dissipation effects (viscosity) and nonlinearity in flows. This was done by introducing the terms $\nu\partial^2 u/\partial x^2$ and $u\partial u/\partial x$. Its connection with the form of the first equation of the Navier-Stokes system is obvious. The Burgers equation (47) was later derived by asymptotic methods for media with weak dispersion for the evolution of unique travelling waves [32,33]. Eq. (47) is a model equation, but it efficiently approximates many features of the solutions of the original equation. In a more general case, with exponential memory kernels and resulting hydrodynamic system (46)) the basis for the model equation may be the same as for (47). There must also be terms which take dissipation effects and nonlinearity of flows into account. Moreover, there should be a term accounting for the memory (relaxation) effects. From equation (45) we can see that such a term in (45) is $\tau\partial\sigma/\partial t$, which, being inserted in (41), gives the terms in (46) with factor τ. In a one-dimensional case, assuming that the nonlinear product in parentheses with τ in the second and third terms are small compared with $\tau\partial^2 V/\partial t^2$, we get a model equation which is a hyperbolic modification of the Burgers equation [34–36]

$$\mu\frac{\partial^2 u}{\partial t^2} + \frac{\partial u}{\partial t} + u\frac{\partial u}{\partial x} = \nu\frac{\partial^2 u}{\partial x^2} \tag{48}$$

This equation was proposed as a model equation in Ref. [35]. Note that in [37] there are also more general nonlinear hydrodynamic equations. The second-order term may also follow from the consideration of the amplitude equations in media with two complex-conjugate roots of the dispersion equation in the original equation (see [33], Ch.9). Equation (48) can be obtained as an amplitude equation by asymptotic methods for systems with memory effects when two interacting waves travelling in different directions are considered. Equation (48) is probably the simplest equation taking into account effects of different flow velocities and characteristic speeds of small perturbations of a wave operator. We will focus our attention now on the properties of the solutions of (48). In [35, 36] it is shown that, under some conditions, (48) has blow-up (collapsing) solutions. We will give possible interpretations of such solutions in the study of turbulence.

The basic feature of the model equation is that solutions of (48) can be different from the solutions of the Burgers equation ($\mu = 0$). Lets consider the linearized equation (48) with constant coefficients

$$\mu \frac{\partial^2 u}{\partial t^2} + \frac{\partial u}{\partial t} + a \frac{\partial u}{\partial x} = \nu \frac{\partial^2 u}{\partial x^2}, \quad a = \text{const}. \tag{49}$$

We can define $M = |a|/c$, $c = \sqrt{\nu/\mu}$ as a Mach number. Then, the harmonic analysis shows that when $M < 1$, equation (49) does not have growing solutions. However, when $M > 1$ there is a branch of harmonics with exponential growth. Equation (49) also has an exact solution in terms of Bessel functions J_0, J_1. This solution gives a lot of information about equation (49). Lets consider the simplest case for the illustration. The initial value problem for equation (49) with the initial conditions $u(x;0) = 0$, $\partial u/\partial t = \delta(x)$ has the solution

$$U(x,t) = \begin{cases} \frac{1}{2} \exp\left(-\frac{pct}{2}\right) \exp\left(-\frac{bx}{2}\right) J_0\left(\sqrt{c_1}\sqrt{x^2 - ct^2}\right), & x^2 - ct^2 \le 0 \\ 0, & x^2 - ct^2 > 0 \end{cases}, \tag{50}$$

where

$$c_1 = \frac{1}{\mu}\left(\frac{1}{4\mu} - \frac{a^2}{4\nu}\right), \quad p = -\frac{1}{\mu}, \quad b = -\frac{a}{\mu}.$$

From (50) it is clear that when $M > 1$ ($c < 1$) there is growth in the range of $\{pct - bx > 0\} \cap \{x^2 - ct^2\}$. The growth rate is proportional to $\sqrt{\mu}$. The

solution in this case has an oscillation of a packet type. The form of this solution follows from the properties of the Bessel function. The characteristic length of the oscillations is determined by the zeros of the Bessel functions and is equal to

$$\lambda \approx 2.5c/\sqrt{c_1} \quad \text{for} \quad c_1 < 0, \tag{51}$$

It can be seen from (51) that when $c_1 \to -\infty$ the number of oscillations per unit length increases. This can be called the decrease or nucleation of the length scale of the solution. The exact solution of equation (48) shows a similar behaviour when the analog of $M > 1$ is satisfied. The behaviour of harmonics and the analysis of the exact solution of the linearized equation indicates the possibility of blow-up solutions for the nonlinear equation.

Important features of solutions of the nonlinear equation (48) can be found when studying a set of travelling wave solutions

$$u(x,t) = u(\xi),\ \xi = x - Dt. \tag{52}$$

Using the transformation

$$u = \overline{u}\sqrt{\frac{c}{\mu}},\ t = \overline{t}\mu,\ x = \overline{x}\sqrt{c\mu}$$

equation (48) can be presented as follows:

$$\frac{\partial^2 u}{\partial t^2} + \frac{\partial u}{\partial t} + u\frac{\partial u}{\partial x} = \frac{\partial^2 u}{\partial x^2}. \tag{53}$$

Inserting (52) into (53) we get the equation

$$u_{\xi\xi}\left(1 - D^2\right) + u_\xi(D - u) = 0. \tag{54}$$

Integrating it we obtain the quadrature

$$u_\xi\left(1 - D^2\right) - \frac{1}{2}(D - u)^2 = K = \text{const}.$$

Further considerations depend on the sign of parameter K. There are three possibilities:

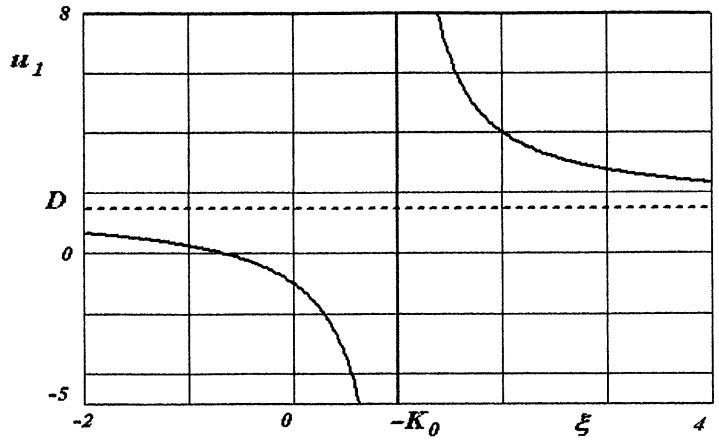

Fig. 6: The graph of the self-similar solution $u_1(\xi)$ of equation (53).

1. if $K = 0$, then $u_1(\xi) = D + \dfrac{2(D^2-1)}{(\xi + K_0)}$,

2. if $K = -2K_1^2$, then $u_2(\xi) = D + 2K_1 \dfrac{1 - \exp\{\alpha(\xi + K_0)\}}{1 + \exp\{\alpha(\xi + K_0)\}}$, $\alpha = \dfrac{2K_1}{1 - D^2}$,

3. if $K = 2K_1^2$, then $u_3(\xi) = D + 2K_1 \tan \dfrac{K_1(\xi + K_0)}{1 - D^2}$.

Here $K_{0,1}$ are constants. An analysis of the solution corresponding to case 1 (Fig.6) with $D > 1$ in the characteristic triangle, placed on the right from line $\xi = -K_0$ but closely to it, shows that the solution tends to infinity in finite "time", hence there does not exist the global solution in the classical sense. The solution in this case corresponds to the blow-up regime of the LS-type. Thus, the existence of the traveling waves u_1 testifies that equation (53) can possess solutions with collapses in the absence of a source term.

Equation (53) is a particular case of the $u_{xt} = f(u, u_x, u_t)$. In some cases it is possible to use the methods widely used for parabolic equations and based on the employment of comparison theorems for this equation. Generally speaking, comparison theorems (or the principle of maximum) are

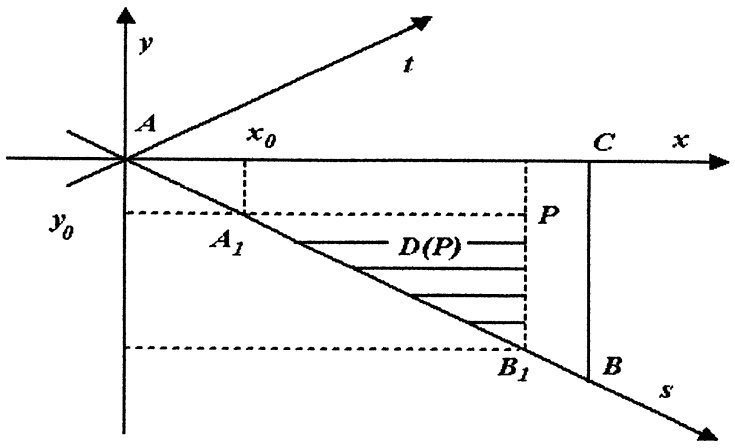

Fig. 7: The characteristic triangle.

the standard methods for investigating the parabolic and elliptic equations, but not the hyperbolic ones. Yet, with some additional assumptions the principle of maximum can still be valid for the hyperbolic problems.

Lets prove the comparison theorem for our equations.

Let G denote the given triangle region (Fig.7), A, B, C are the vertices of the triangle and $Q = AB$ is its base. Consider the following problem in region G for the equation

$$u_{sy} = f(s, y, z_1, ..., z_k), \; z_i = g_i(u, u_s, u_y), \; i = 1, ..., k \tag{55}$$

with initial conditions in Q:

$$u\Big|_{s,y\in Q} = \varphi(s, y), \; u_s\Big|_{s,y\in Q} = \psi(s, y), \; u_y\Big|_{s,y\in Q} = \omega(s, y). \tag{56}$$

Lets suppose the existence of a solution to the problem (55)-(56) in region G, belonging to class $C^{2,2}_{s,y}$. Additionally let the function f be a monotonically increasing function of variables $z_1, ..., z_k$ and functions f, g_i are infinitely differentiable functions of their variables.

Together with the problems (55)-(56), we can consider another problem in G:

$$v_{sy} = f(s, y, z_1, ..., z_k), \; z_i = g_i(v, v_s, v_y), \; i = 1, ..., k \tag{57}$$

with the following initial conditions posed on Q:

$$v\Big|_{s,y\in Q} = \varphi_1(s,y), v_s\Big|_{s,y\in Q} = \psi_1(s,y), v_y\Big|_{s,y\in Q} = \omega_1(s,y). \qquad (58)$$

We assume that the solution to problems (57)-(58) belongs to class $C^{2,2}_{s,y}$ as well.

Theorem 1..2. *Let the following relations hold*

$$\varphi_1 < \varphi,\ \psi_1 < \psi,\ \omega_1 < \omega \qquad (59)$$

under the above restrictions for functions f, g_i. Then for the solutions u and v of the problems (55)-(56) and (57)-(58) the inequalities

$$v(s,y) < u(s,y),\ v_s(s,y) < u_s(s,y),\ v_y(s,y) < u_y(s,y) \qquad (60)$$

are held throughout region G.

Proof. By integrating equation (55) over the variable s from point $A_1 \in Q$ to point $P = (s_0, y_0) \in G$, we come up with the following integral equation

$$\frac{\partial u}{\partial y}(P) = \frac{\partial u}{\partial y}(A_1) + \int_{A_1}^{P} f(r, y_0, u, u_s, u_y)\, dr$$

By analogy,

$$\frac{\partial u}{\partial s}(P) = \frac{\partial u}{\partial s}(B_1) + \int_{B_1}^{P} f(s_0, r, u, u_s, u_y)\, dr \qquad (61)$$

Integrating equation (61) over the variable y once more we get

$$u(s,y) = u(B_1) + \int_{B_1}^{A_1} \frac{\partial u(s)}{\partial y}\Big|_{s\in[B_1,A_1]} ds + \int\int_{D(P)} f\,dr\,dy, \qquad (62)$$

where $D(P)$ is the shaded region in figure 7. The validity of the inequality (60) in G can be shown by contradiction. Namely, suppose that R is a set of points from G, for which at least one of the following equalities is valid:

$$u = v,\ u_s = v_s,\ u_y = v_y \qquad (63)$$

i.e.

$$R = R_1 \cup R_2 \cup R_3,$$

where $R_1 = \{s, y \in G \Big| u = v\}$, $R_2 = \{s, y \in G \Big| u_s = v_s\}$,$R_3 = \{s, y \in G \Big| u_y = v_y\}$. Lets show that R is empty. Since the functions u and v are of the $C^{2,2}_{x,t}$ class, then set R is closed. Denote $\ell(s, y)$ the distance from a point $(s, y) \in R$ to the base Q of the triangle ΔABC. The function $\ell(s, y)$ is continuous. Since the closed set R is contained in G, then it is compact and therefore the continuous function ℓ reaches a minimum ℓ^* in R in accordance with the Weierstrass's theorem. Relation $Q \overline{\in} R$, implies the existence of a strip of width ℓ^*, adjacent to Q, so that none of the inequalities (63) is valid in its vicinity.

A set of points from R, placed at the distance of ℓ^* from Q are denoted by the symbol M. Suppose, that a point $\overline{p} = (\overline{s}, \overline{y}) \in M$ exists, for which

$$v < u, \; v_s < u_s \tag{64}$$

(the case with $v_y = u_y$ is proved by analogy). From the integral representation of the type (61) for v_s we have

$$\frac{\partial v}{\partial s}(\overline{p}) = \frac{\partial v}{\partial s}(B_1) + \int_{B_1}^{\overline{p}} f(\overline{s}, r, v, v_s, v_y)\, dr \tag{65}$$

Due to the second condition (59), from the relation (65) the following inequality takes place:

$$v_s(\overline{s}, \overline{y}) < u_s(\overline{s}, \overline{y}).$$

The obtained contradiction proves, that a point $\overline{p} \in M$ with the property (64) does not exist. The properties concerning the values v_y, u_y are checked out in the same way.

Suppose now, that point $\overline{p} \in M$ exists:

$$v(\overline{p}) = u(\overline{p}), \; v_y(\overline{p}) > u_y(\overline{p}). \tag{66}$$

From the integral representation (62) together with (59) and (60) it follows that $v(\overline{p}) < u(\overline{p})$. The obtained contradiction proves, that the point with such properties does not exist in M. Other possible cases are examined

by an analogy. Thus set R is proved to be empty. Since M is a part of a boundary of closed set R, then set R is empty as well. As a result, property (60) is fulfilled everywhere in G and the theorem is proved. ■

Lets consider the application of theorem 1..2 to equation (53) with initial conditions

$$u(x,0) = \varphi(x,0),\ \frac{\partial u}{\partial t}(x,0) = \psi(x). \tag{67}$$

We begin with the following change of variables

$$t + x = s,\ t - x = y$$

for which

$$\frac{\partial u}{\partial t} = u_s + u_y,\ \frac{\partial u}{\partial x} = u_s - u_y. \tag{68}$$

Thus, equation (53) will take the following form

$$u_{sy} = -u_s - u_y + u\,(u_y - u_s) \equiv f\,(u,\ u_s,\ u_y)\,.$$

The initial data from (67), together with (68), give rise to the following conditions in base Q of the triangle G, corresponding to the value of $t = (s+y)/2 = 0$:

$$\frac{\partial u}{\partial s} = \frac{1}{2}\left(\frac{\partial u}{\partial t} + \frac{\partial u}{\partial x}\right) = \frac{1}{2}\,(\psi + \varphi_x)\Big|_{s+y=0}$$

and

$$\frac{\partial u}{\partial y} = \frac{1}{2}\left(\frac{\partial u}{\partial t} - \frac{\partial u}{\partial x}\right) = \frac{1}{2}\,(\psi - \varphi_x)\Big|_{s+y=0}.$$

Thus as a consequence of theorem 1..2 we get the following assertion.

Conclusion. *Let the solution u_1 of the initial-value problem (53) - (67) exist in G with such values of parameters c_0, s_0, D that*

$$D > 1,\ T_\star = \frac{|s_0|}{D} < T^* = L, \tag{69}$$

where L is a length of side of the characteristic triangle G and

$$\varphi > u_1,\ u_s > u_{1s},\ u_y > u_{1y} \tag{70}$$

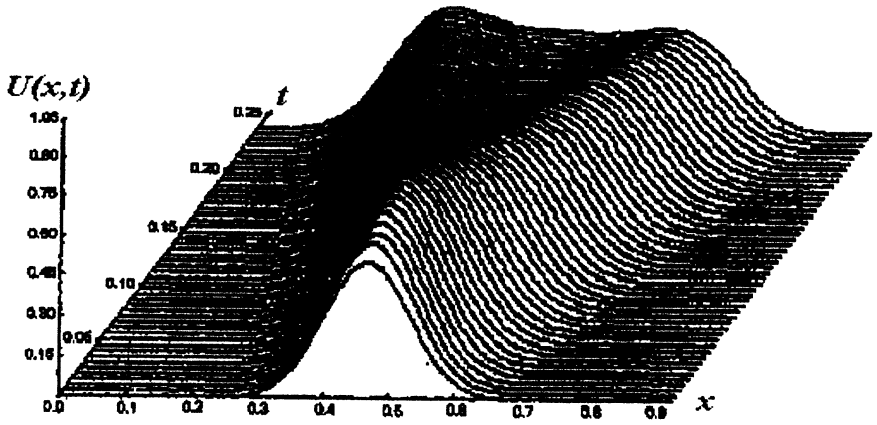

Fig. 8: Solution without growth. Parameters: $\mu = \nu = 0.3$, space step $h = 0.01$, time step $\tau = 0.005$. Initial conditions: $u(x,0) = A\exp[-\sigma(x-x_0)^2]$, $\sigma = 100$, $A = x_0 = 0.5$ [38].

in segment Q while

$$f(u_1, u_{1s}, u_{1y}) < f(u, u_s, u_y) \tag{71}$$

for all $t < T^*$. Then the classical solution $u \in C^{2,2}_{x,t}$ does not exist in all of set G and time of existence of the solution is bounded from above by the value of T^*.

Here, the self-similar solution $u_1(\xi)$, serving as "low solutions" in comparison theorems, leads to blow-up regime (or collapse) and assures the infinite growth of solution $u(s,\ y)$ in G as $t \to T^*$ from below. This conclusion was confirmed by numerical calculations with initial hump-type data. Fig. 8 shows the numerical solution when $M < 1$ under the condition $\partial u/\partial t|_{t=0} = 0$. Fig. 9 gives the solution when $M > 1$. Here we can see the self-accelerating increase of peaks and a decrease of characteristic length.

Conditions (69) ensure the singularity of solution u_1 within the characteristic triangle G. Assuming the existence of the classical solution $u(s,y)$ for $t < T^*$, we conclude that $u(s,y)$ allows for unbounded values on side Q, i.e. it is a true blow-up regime. Thus, the conditions formulated in the conclusion to theorem 1..2 assure the existence of the blow-up regime. No-

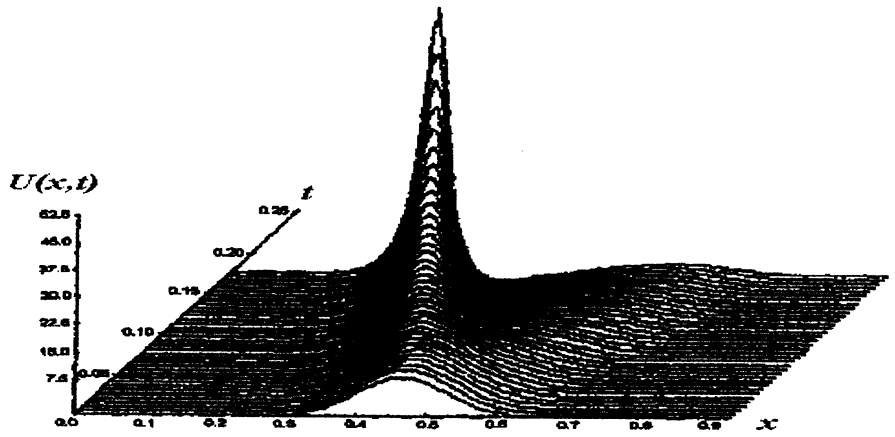

Fig. 9: Solution with collapse. Parameters:$\mu = \nu = 0.3$, space step $h = 0.01$, time step $\tau = 0.005$. Initial conditions: $u(x,0) = A\exp[-\sigma(x-x_0)^2]$, $\sigma = 100$, $A = 10$, $x_0 = 0.5$ [38].

tice that the existence of a classical solution for $t < T^*$ is a consequence of the existence of the u_1-type solution, being the "upper solution" for $u(x,y)$ with the same value of T^*.

To check the conditions of the above conclusion, we restrict our consideration to that part of the profile of u_1, which is placed to the right from singularity and moves from left to right ($K_0 > D$, $D > 0$). For this part of u_1

$$\frac{\partial u_1}{\partial s} = \frac{(D-1)(D^2-1)}{(x-Dt+K_0)^2} > 0, \quad \frac{\partial u_1}{\partial y} = \frac{(D+1)(D^2-1)}{(x-Dt+K_0)^2} > 0 \text{ at } D > 1,$$

and

$$f(u_1, u_{1s}, u_{1y}) > 0.$$

Therefore the inequalities (70) - (71) together with the last relations and (67) imply

$$\varphi > 1, \ \psi - \varphi_x > 0, \ -\varphi_x(2\varphi+1) - \psi > 0.$$

As shown above, model (53) has some interesting solutions. Here, we will discuss their possible hydrodynamic interpretations. To begin with, we

must note that in classical hydrodynamics the analog of (54) is obtained in the case of negative effective viscosity [39]. Next, let us note that the blow-up solutions appear as a rule as a result of some kind of idealization, and in reality some mechanisms of limitations exist for great amplitudes. For example, in plasma there is the Landau damping. In generalized hydrodynamics, the natural limiting mechanisms also exist. The spatial nonlocality (space dispersion) may serve as such a mechanism. Expressions of type (50) may in principle explain the influence of nonlocality, but the search for an adequate model equation is very complicated. One of the simplest models which takes such effects into account, leads to the complementary term $\chi\frac{\partial^3 u}{\partial x^2 \partial t}$ in (46). Remarkably, terms of such type may appear in equations obtained within the different approaches e.g. within the kinetic theory [26], or when considering the transport phenomena in heterogeneous media with nonlocality [40]. Nonlocality also occurs in the critical region and in the phase transition. In [41] such a term appears as the consequence of basic postulates. Similar terms appear in the continuum limits in the consideration of random walks [42]. Moreover, from an analogy with the hyperbolic modification of the Burgers equation, the model equation may take the form

$$\mu\frac{\partial^2 u}{\partial t^2} + \frac{\partial u}{\partial t} + u\frac{\partial u}{\partial x} = \nu\frac{\partial^2 u}{\partial x^2} + \chi\frac{\partial^3 u}{\partial x^2 \partial t} \tag{72}$$

The case of $\chi \ll 1$ is of particular interest. Our investigations show that in this case the solution of (72) initially has a growth similar to the solutions of (48) in the blow-up regimes if equation (48) has a collapse. But the nonlocal term may destroy the collapse, causing the global existence of solutions, as claimed in [43], Ch. 4. Thus, equation (72) inherently has two mechanisms of the turbulence proposed in [20]: the blow-up property (or homoclinic excursion) and the collapse-limiting mechanism. We should note also that another collapse-limiting mechanism exists, namely, the nonlinearity of the diffusion coefficients [36].

All pictures of turbulence in [20] (for instance the random appearance of structures) can be transferred to our case. Because of the threshold dependence of our model on M, it is clear that fluctuations have a different behaviour depending on M. For $M < 1$ this behaviour is close to the behaviuor of the solution in case when $\mu = 0$ (for example, for smooth initial

data). However, if $M > 1$, there are oscillations with decreasing scales, and for fixed m and n the length of oscillations decreases when u increases. It may be suggested that a similar behaviour of solutions with different M exists in full generalized hydrodynamics. In this case we may take as M the quantity u/c_{eff}, where c_{eff} is the effective speed of sound. Then if Re is relatively small, the transition to turbulence is similar to the transition to turbulence from low-dimensional stochasticity, for example, in the Navier-Stokes equations.

When turbulence is strong, Re is high, and $M > 1$. In this case we may have turbulence behaviour of another type. The elements of this behaviour are the solutions with collapses and oscillations shown in this work. Possibly the $M > 1$-type criterion is related to the separation of turbulence on "soft" and "hard" [44]. The characteristic length of oscillations may be associated with the Kolmogorov length of viscous dissipation in turbulence.

The simplest two-dimensional models of generalized hydrodynamics have also been investigated. For $M > 1$, solutions with collapse and with vorticity growth were also found in [34]. Some features were also confirmed in numerical solutions of finite-dimensional dynamical systems. These results will be the subject of our further investigations.

1.6. Quasilinear model equation of generalized hydrodynamics

In this subsection we consider quasilinear hyperbolic modification of the Burgers equation

$$\mu \frac{\partial^2 u}{\partial t^2} + \frac{\partial u}{\partial t} + u \frac{\partial u}{\partial x} = \nu(u) \frac{\partial^2 u}{\partial x^2} \tag{73}$$

Lets suppose that $\nu(u) > 0$ for any u and introduce the quantity

$$M = \frac{|u(x,t)|}{\sqrt{\nu(u)/\mu}}$$

known as the local Mach number. Lets investigate (73) numerically particularly in

$$\nu(u) = \left(a + bu^2\right)^2, \quad b = (1-a)\,\alpha, \quad a > 0, \quad b > 0. \tag{74}$$

We apply the finite difference scheme

$$\mu y_{t\bar{t}} + y_{\hat{t}} + y y_{\hat{x}} = v(y)\, y_{x\hat{x}}$$

with initial data of the type

$$u(x,0) = \begin{cases} A\left(R^2 - (x-x_0)^2\right) & \text{if } x_0 - R \le x \le x_0 + R \\ 0 & \text{otherwise} \end{cases} \qquad \frac{\partial u}{\partial t} = 0. \tag{75}$$

In calculations we used the following values of the parameters: $\mu = 1$, $a = 0,01$, $\alpha = 10^{-4}$, $A = 3,0$, $x_0 = 0,5$, $R = 0,2$, $h = 0.01$, $\tau = 5 \cdot 10^{-4}$. Fig. 10 a corresponds to $t = 0.65$ while Fig. 10 b corresponds to $t = 2.0$. A comparison of Fig. 10 b with the results from the previous subsections shows, that solutions of (73) at the initial moments of time behave as the blow-up solutions of equations with the fixed coefficients at the highest derivative. This means that at this stage, an influence of the term bu^2 is negligible. The difference in (Fig. 10 b) is evident. In Fig. 10 b the development of irregular oscillations is seen.

Another type of solution is shown in Fig. 11. The value of parameters are $\mu = 1$, $a = 0,01$, $\alpha = 1$, $A = 10$, $z = 0,5$, $R = 0,2$, $h = 0,04$, $\tau = 0.02$. In Fig. 11 a there is the initial graph and in Fig.11 b the graph is placed at time $t = 2.5$. Calculations for further times exposed stationarity of this wave packet solution. An analysis of Fig. 10 - 11 and results of the previous subsections allows us to make some conclusion about the solution of (73).

Firstly, for nonlinear coefficient $\nu(u)$ with $u > \sqrt{\nu(u)/\mu}$ for $u > p$, $p = const$, solutions under certain conditions (one of them taking the form $\max M|_{t=0} > 1$) can evolve in the blow-up regime.

Secondly, if $u > \sqrt{\nu(u)/\mu}$ for $u \in [c_1; +\infty)$ and $u \in (-\infty; c_0]$, $c_{0,1}$ are constants, then solution with $\max M|_{t=0} > 1$ can evolve with drop of the space characteristic length. We may suppose that analogous properties apply for solutions to more general equations, for example of the

$$D\left(\frac{\partial^2 u}{\partial t^2}, \frac{\partial^2 u}{\partial x^2}, u\right) + B\left(\frac{\partial u}{\partial t}, \frac{\partial u}{\partial x}, u\right) = 0,$$

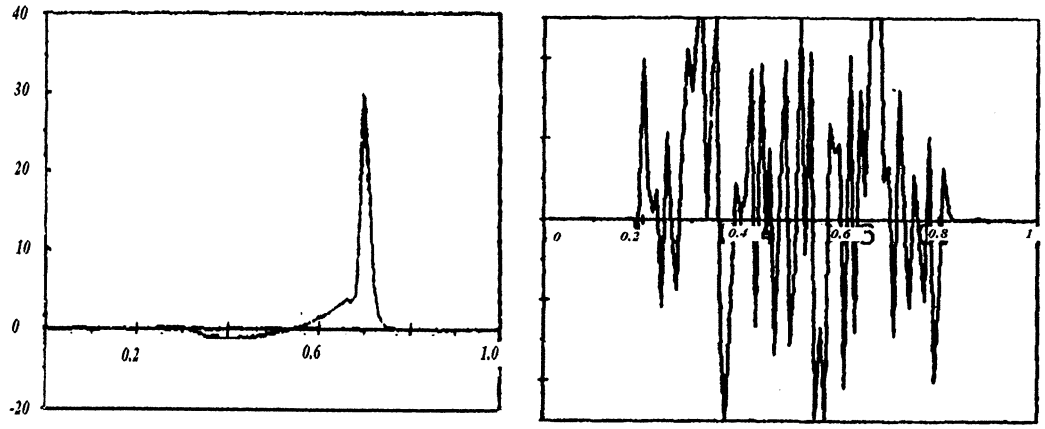

Fig. 10: Solutions of equation (73) with initial conditions (75) at a) $t = 0.65$ b) $t = 2.0$.

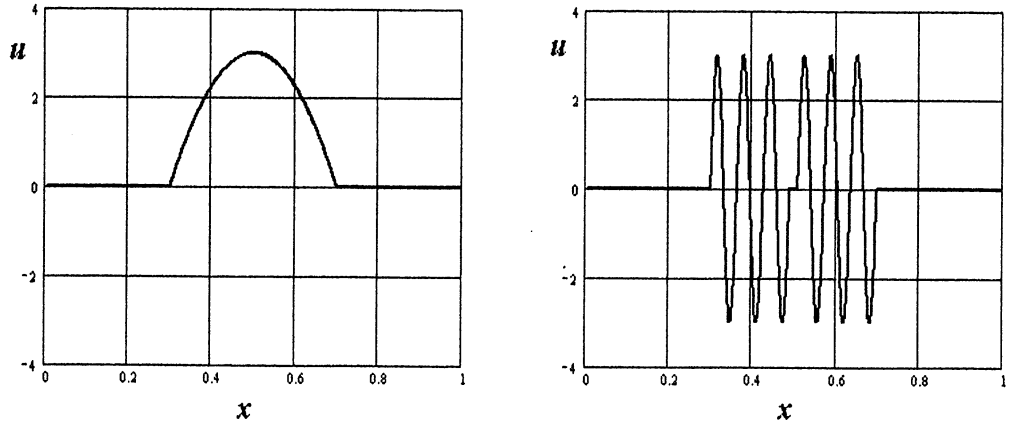

Fig. 11: Solutions of equation (73) with initial conditions (75) at a) $t = 0.0$ b) $t = 2.5$.

type where D and B are hyperbolic operators of the second and the first order with nonlinear coefficients. The local Mach number $M = V(u)/U(u)$ plays a crucial role, where $V(u)$, $U(u)$ are characteristic speeds of operators D and B. Oscillating solutions were found earlier within the models containing merely the first order derivatives with respect to temporal variable [43] in case of the negative viscosity coefficient. In our case this requirement is not supposed. Such oscillations are similar (at least visually) to those encountered in the "dry" turbulence model [45]. An intriguing problem would be to find out nonlinear coefficients, causing these types of solutions.

2. Numerical results on the two-dimensional model

The simplest two-dimensional generalization of equation (10) has the form

$$\mu\frac{\partial^2 u}{\partial t^2} + \frac{\partial u}{\partial t} = c^2\left(\frac{\partial^2 u}{\partial x^2} + \frac{\partial^2 u}{\partial y^2}\right) + u\frac{\partial u}{\partial x} + u\frac{\partial u}{\partial y} \tag{76}$$

Numerical experiments expose the role of condition $M > 1$ analogous to that of the one-dimensional case. In our computations we have also found a solution with four peaks, which corresponds to one-peak initial data.

A more complicated two-dimensional model equation of generalized hydrodynamics also exists:

$$\mu\frac{\partial^2 u}{\partial t^2} + \frac{\partial u}{\partial t} = c^2\left(\frac{\partial^2 u}{\partial x^2} + \frac{\partial^2 u}{\partial y^2}\right) + u\frac{\partial u}{\partial x} + v\frac{\partial u}{\partial y}, \tag{77}$$

$$\mu\frac{\partial^2 v}{\partial t^2} + \frac{\partial v}{\partial t} = c^2\left(\frac{\partial^2 v}{\partial x^2} + \frac{\partial^2 v}{\partial y^2}\right) + u\frac{\partial v}{\partial x} + v\frac{\partial v}{\partial y}. \tag{78}$$

Quantities u, v can be interpreted as flow velocity components along the axis OX and OY. In numerical experiments performed for system (77) –

(78) we used the initial data of the following form:

$$
\begin{aligned}
u(x,y,0) &= \begin{cases} \frac{A}{4r_0^2}(r-r_0)(x-x_0), & r=\sqrt{x^2+y^2}\le r_0, \\ 0, & r>r_0, \end{cases} \\
v(x,y,0) &= \begin{cases} \frac{A}{4r_0^2}(r-r_0)(y-y_0), & r=\sqrt{x^2+y^2}\le r_0, \\ 0, & r>r_0, \end{cases} \\
\frac{\partial u}{\partial t} &= \frac{\partial v}{\partial t} = 0 \quad \text{for} \quad t=0.
\end{aligned}
\tag{79}
$$

This data has finite support.

Initial data (79) corresponds to the vortex with the rotation center placed in point $(x_0; y_0)$ with clockwise rotation. As in previous cases, the evolution depends in an essential way upon the flow speed amplitudes. It can be easily seen when analyzing the results of calculations performed with $h_x = h_y = 0.04$, $\mu = 0.02$, $c^2 = 0.03$, $x_0 = y_0 = 0$, $r_0 = 0.2$ [36]. In this case the solution decays with time and the following peculiarities of its dynamics should be noted: 1) the solution grows in time, 2) the characteristic length drops. Finally, the evolution of the initial data leads to new vortices generation with scales smaller, than the scale of the initial vortex.

Thus, we have presented new interesting properties of the model equations for generalized hydrodynamics in this section, namely, the possibility of growth in flow with convection and the possibility of scale dropping in time. Obtained solutions may be used as a basis for the construction of so called "wavelet" solutions.

3. Modelling self - origin of collapses in hydrodynamics with memory

Generalization and consideration of the three-dimensional version of (47) became an interesting and logical extension of research [46]:

$$
\tau\frac{\partial^2\vec{V}}{\partial t^2} + \frac{\partial\vec{V}}{\partial t} + \left(\vec{V}\nabla\right)\vec{V} = \nu\Delta\vec{V}, \tag{80}
$$

where $\vec{V}\nabla = \sum_{i=1}^{3} V_i\frac{\partial}{\partial x_i}$.

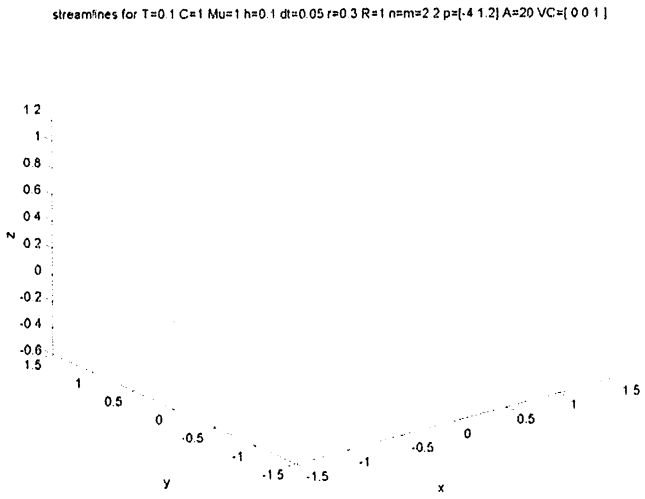

Fig. 12: Streamlines of initial disturbance.

Let us consider the problem of behaviour exploration of solutions for three-dimensional generalization of modified Burger's equations. Taking into consideration the complexity of the analytical study of system (80), a numeric experiment was conducted for the main exploration method, and therefore it was necessary to formulate a new problem definition, which would include initial and boundary conditions as well as spatial area of exploration.

It was proposed to take toroidal vortex in laminar fluid flow as initial conditions for the task. The following toroidal disturbance had been chosen:

1. Torus is a typical initial setting in hydrodynamics tasks, such types of turbulence are analyzed when it comes to description of turbulence, because in reality turbulence happens on torus' boundaries;

2. Phenomena, appearing in real fluids during the movement of toroidal vortex are experimentally researched;

3. It is appearing for problems in plasma physics.

Therefore, due to "typicalness" and the results for classic equations, the choice of toroidal disturbance for initial conditions allows to compare the obtained results with known and natural phenomena, to speculate about

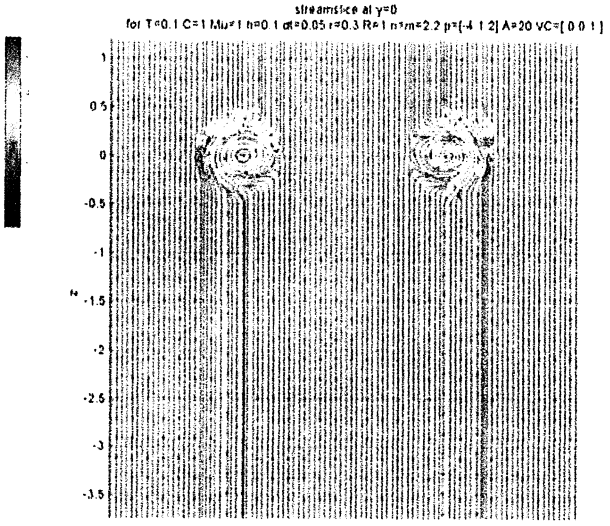

Fig. 13: Streamlines of initial disturbance by OZX plane.

the adequacy and inadequacy of description and to prognosis new types of phenomena. For the convenience of analysis, torus' center was placed in the coordinate origin, and laminar flow was directed along the OZ axis. Area of modeling is an parallelepiped. Such dimensions of the modeling area were chosen that during computation time, the disturbance did not spread past the area borders, and therefore values of vector field on the borders of area remained equal to the initial laminar flow.

The following is a formal problem definition:

$$\tau\frac{\partial^2\vec{V}}{\partial t^2}+\frac{\partial\vec{V}}{\partial t}+\left(\vec{V}\nabla\right)\vec{V}=\nu\Delta\vec{V},\quad \frac{\partial\vec{V}}{\partial t}(\vec{x},0)=\vec{0},$$

$$\vec{V}(\vec{x},0)=\begin{cases}-\alpha\varphi(x)\begin{pmatrix}\frac{xz}{\sqrt{x^2+y^2}}\\ \frac{yz}{\sqrt{x^2+y^2}}\\ R-\sqrt{x^2+y^2}\end{pmatrix}+\vec{V}_C & \text{when } x\in T(\vec{0},R,r)\\ \vec{V}_C & \text{when } x\notin T(\vec{0},R,r)\end{cases} \tag{81}$$

$\vec{V}(\vec{x}, 0) = \vec{V_C}$ when $\vec{x} \in \Omega(D)$, where $D = [a_1, b_1] \times [a_2, b_2] \times [a_3, b_3]$. Here α is a coefficient defining the value of the initial amplitude of toroidal disturbance, it is a variable system parameter and is specified by researcher; $T(\vec{0}, R, r)$ is the toroidal vortex with the center in point $\vec{x} = \vec{0}$ and greater and lesser radiuses R and r accordingly, $\vec{V_C}$ is the velocity of laminar flow, $\varphi(x)$ is the fitting function for removal of interruptions of vector field between laminar flow and toroidal vortex, $\Omega(D)$ edge of region D. The problem is analysis of system's solutions behaviour, depending on parameters τ, ν, $\vec{V_C}$, α.

3.1. Numerical computation scheme

As the numerical experiment was the main exploration method, the next researcher problem became the choice of numeric modeling algorithm. Based on the experience of previous research and on the widely used practice of modeling hydrodynamics problems, the approach based on building discrete analog using difference scheme was chosen.

Considering the fact, that the so-called "cross" scheme [47] is known as a good method for hyperbolic equations solution, and keeping in mind the previous numeric research of one- and two-dimensional systems which had been performed using this scheme, it was decided to continue the research without altering the approach (scheme).

The following criteria were most important when choosing the scheme:

- simplicity of implementation, as it is an explicit scheme;
- an explicit scheme is less demanding compared to an implicit one for the resources of CPU time and memory; considering that the problem is three-dimensional, this aspect was critical;
- particularities of this scheme were researched many times using different kinds of gas dynamics hyperbolic equations [48, 49], that allow to separate scheme features from specific equation's solution features.

Moreover, there were additional research problems related to the behaviour of the scheme at the rapidly growing solutions, and based on the

results of the research, recommendations regarding the choice of time and space step values, and detection of so called sharpening modes.

The complexity of checking scheme and scheme's program implementation's correctness is explained by the absence of an analytical solution for both model equations and source system. To solve the two problems at once, the authors have chosen two ways of verification:

1. scheme verification at the known solutions by modifying the right part of equation;

2. verification of computation stabilization when decreasing the spatial and time steps.

First of the methods has the following algorithm:

1. specify any desired system's solution, i.e. provide a view of vector field $\vec{V}(\vec{x}, t)$;

2. instead of the initial system we are considering the modified system with an extra term in the right-hand side:

$$\tau \frac{\partial^2 \vec{V}}{\partial t^2} + \frac{\partial \vec{V}}{\partial t} + \left(\vec{V}\nabla\right)\vec{V} - \nu\Delta\vec{V} = \vec{f}(\vec{x}, t) \tag{82}$$

3. substituting the values of chosen $\vec{V}(\vec{x}, t)$ in the system we find the function $f_k(\vec{x}, t)$ where $k = 1...3$

4. we analyze the behaviour of numeric solution of modified system (82), having an analytical solution, given in the item 1 for comparison.

The second method (computation stabilization) is the analysis of change of structure of resulting system's solution when decreasing the spatial and time steps. It was essential for this research to ensure that the solution does not change its structure (does not break up) when the grid scale is changed.

During the verification it was found that the scheme provides adequate results for the solutions, in which the absolute value of velocity module is not greater than given value V_{crit}.

When this value is exceeded ($\exists \vec{x} : \|\vec{V}(\vec{x},t)\| > V_{crit}$), discrepancy grows quickly and exceeds the solution values, therefore such solution should not be considered. Taking this into account, it was decided that when rapidly growing solutions emerge, the modelling shall be performed to the instance $\|\vec{V}(\vec{x},t)\| > V_{crit}$. Experimentally derived value $V_{crit} \sim 10^4$.

3.2. Discussion of numerical results

General conclusions:

- depending on system parameters, the process evolves by one of three possible scenarios, two of which can be interpreted as sharpening modes;
- relation $M = \frac{\vec{V}(\vec{x},0)}{\sqrt{\nu/\mu}}$ is definitive for the evolution of the sharpening mode. While for the one-dimensional problem set-up 1 was the threshold value, for the three-dimensional set-up and this type of initial conditions the value is one order greater;
- sharpening always has a local spatial nature and gets narrower with time;
- in the sharpening area oppositely directed flows with big velocity values can exist; this can be interpreted as disruption of vector field;
- simultaneously with the emergence of sharpening modes, the mergence of numerous vortices with small radius is observed, which can be interpreted as the process of decreasing of significant scale;
- it was stated that the numeric solutions at some parameter values are similar to the experimental shots of fluid flows.

System evolution scenarios. During system modelling, the picture of evolution of maximal velocity absolute value was considered at first. When evolution starts, all graphics have a similar structure independent of parameter values. When starting with some parameter values the velocity slowly decreases to the stationary value, with another values velocity jumps up

and grows steadily. It is considered that the system is in a numerically observable sharpening mode, when the mentioned growth of absolute velocity to 4 and higher is present on the graphic.

The following pictures show the examples of the described graphs:

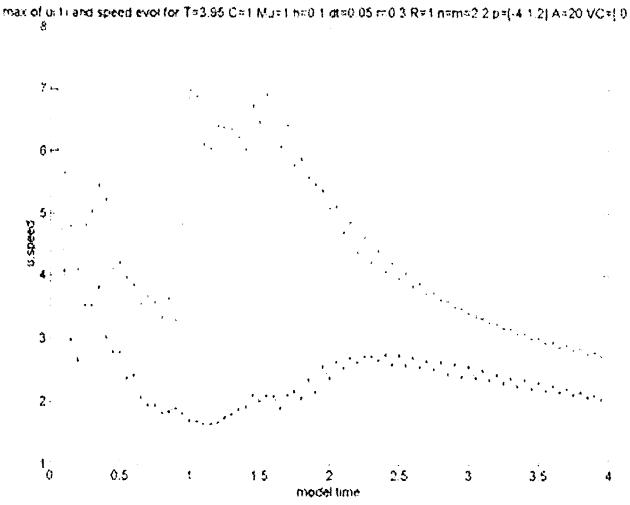

Fig. 14: Graphic of maximal absolute velocity during dissipation of disturbance.

Due to big values during the final periods of analysis, the initial oscillations on the graph are flattened. To illustrate the aforementioned similarity of velocity evolution graphs, no matter of sharpenings evolve or not, we will consider the graph from Fig. 3.2. to the moment of time $t = 1.3$, and compare it to Fig. 14.

To explain the obtained results we shall consider the most featured and characteristic representatives of every scenario in detail, paying additional attention to the appearance of specific effects.

Having fixed values of parameters which correspond to viscosity and time of relaxation, we shall examine the dependency of solutions' behaviour upon the amplitude of initial disturbances. When the velocity of initial disturbances is low, dissipation of the toroidal vortex is observed. The dissipation happens according to the following sequence:

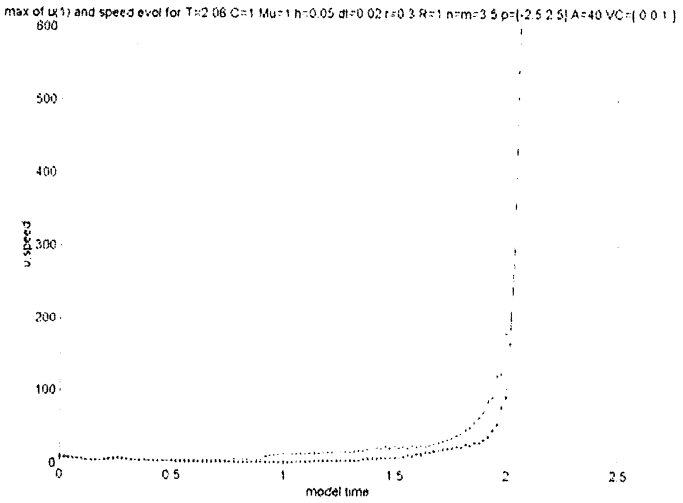

Fig. 15: Graphic of maximal absolute velocity during sharpening emergence.

1. Gradual expansion of torus area. It is clearly seen when comparing Fig. 17 and Fig. 18, where a smaller torus radius expands. Here, under the torus area we understand a part (area) of the vector field, in which the vector direction and amplitude significantly differ from a stationary laminar flow. In the initial moment (see Fig. 13) the torus area is clearly seen on the shear of flow lines and corresponds to two symmetric circles.

2. Section of torus by Oz axis. The section leads to the emergence of so called "maximal velocities area" (m.v.a) - localized area in space, where absolute velocity value is considerably bigger than the amplitudes in all other areas in space. Moreover, below the area of maximum velocity along OZ axis an area appears, in which the vector field has direction opposite to the main flow, which causes the emergence of numerous vortices system in the area.

3. The vortices divide, become smaller and eventually dissipate, while moving along the flow

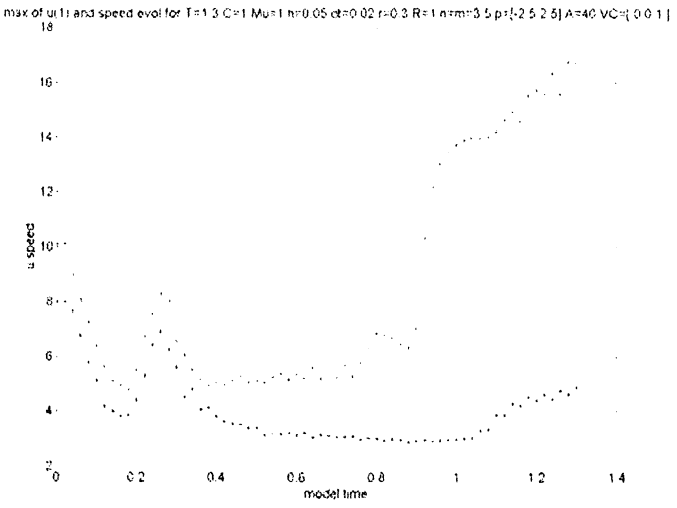

Fig. 16: Evolution of maximal absolute velocity before emergence of sharpening.

4. Eventually the flow becomes laminar, i.e. all disturbances and vortices disappear.

The following increase of amplitude of initial disturbances leads to the emergence of additional vortices at the crossing of torus on the OZ axis. New vortices are located symmetrically in the octants of Cartesian coordinates, but they do not always retain the torus form. Some of these vortices are shown in detail in Fig. 20, Fig. 21.

An increase of initial turbulence amplitude leads to an increase of value of the definitive parameter M and sharpening emerges in the system. Like for the case of turbulence dissipation, the torus area slowly expands, and upon the crossing the OZ axis a system of vortices and the area of maximal velocities emerges. Next, the velocities in the sharpening area quickly increase. Substantial velocity difference between the sharpening area and the surrounding field leads to the deformation of flow lines, which can be interpreted as interruption or breakage. Structure of field at the moment of sharpening is shown in the following pictures:

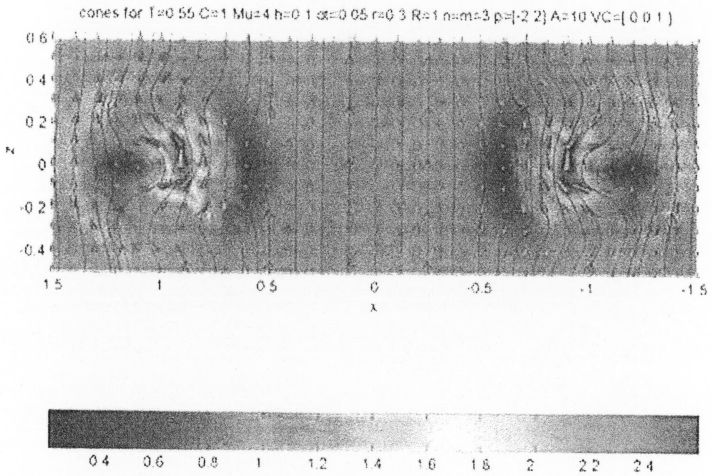

Fig. 17: Field from ZX perspective with $t = 0.55$.

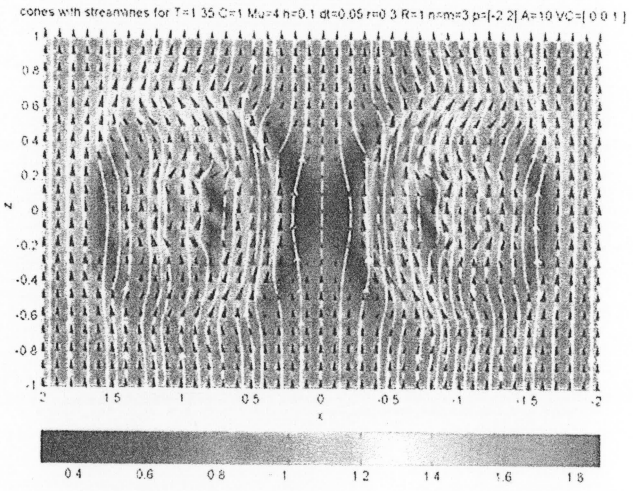

Fig. 18: Field from ZX perspective with $t = 1.35$.

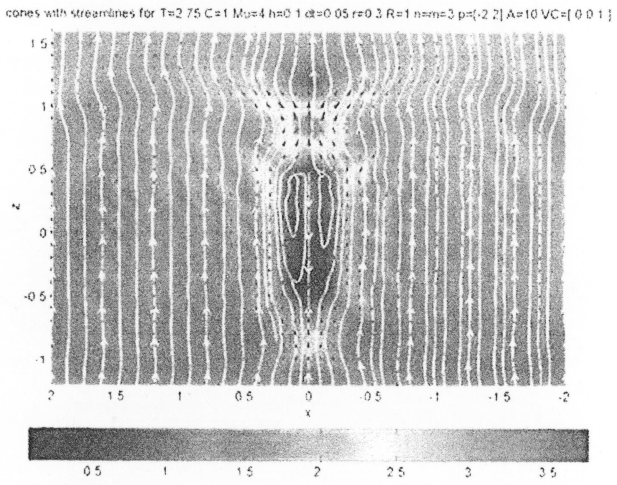

Fig. 19: Field structure at the moment $t = 2.75$, area of maximum velocity is at the level $Z = 0.9$ and is marked black

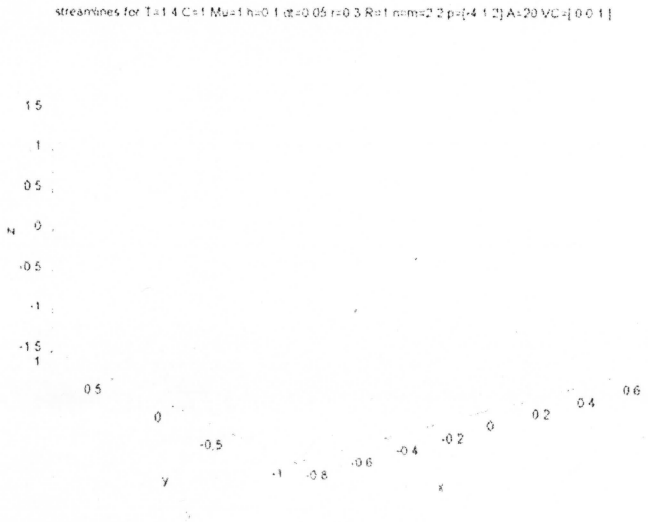

Fig. 20: Emergence of vortices at the crossing of the torus area on the OZ axis.

Fig. 21: Emergence of the vortex system at the crossing of the torus area on the OZ axis. 3-D lines of flow are shown, detailing vortex areas from Fig. 20.

The sequence of field evolution in this scenario can be described as follows:

1. expansion of the torus area
2. crossing of the torus area, creation of upper and lower vortices and emergence of area of maximum velocity
3. emergence of turbulence in the central area, which evolves to a new toroid vortex
4. dissipation of central vortex which divides into smaller vortex-rings along the OZ axis, simultaneously moving along the flow
5. disappearance of upper and lower vortices
6. growth of velocity in the maximal velocity area to the highest allowable values and its movement along the flow. In the m.v.a nearest field

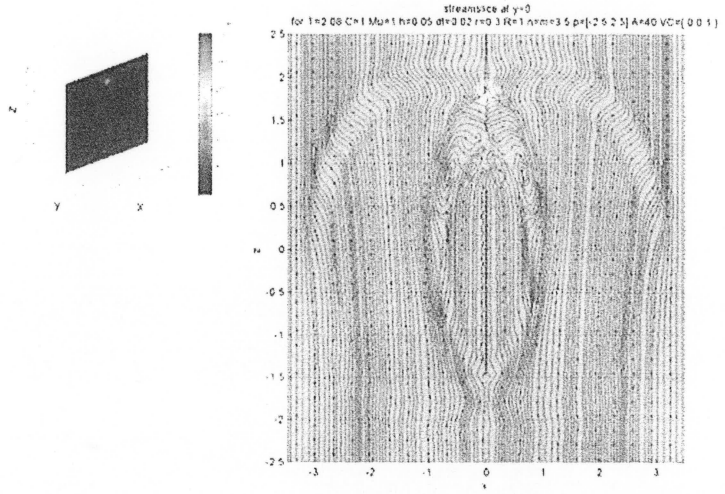

Fig. 22: Sections of flow lines at the moment of sharpening emergency. The sharpening area is shown in red and yellow and is located at the height $Z = 1.8$.

layers have opposite directions, which causes severance of flow lines. Moreover, new smaller turbulence areas appear, to which a lot of lines converge, in places where two flows meet (one directed along the stationary flow and another - created by big velocities in m.v.a). One of such places is the small vortex at level $Z = 1.4$, shown in Fig. 24. M.v.a. decreases with time, but simultaneously the border between m.v.a. and the main flow becomes more distinctive and expressed.

It is interesting to consider the case with big values of both, the initial disturbance and the laminar flow, which bypass the vortex. It illustrates that vortices existence is not necessary for sharpening emergence.

Due to the growth of the velocity value of stationary flow in the initial moment of time the vortex does not exists (by general definition), and even the toroidal structure of vector field does not exist, as it is being diffused by the flow (see Fig. 25, where the image of the vector field is shown by cones in plane Ozh against a background of secant plane of velocity absolute value: As in previous cases, we see a "bump" on the velocity evolution graph

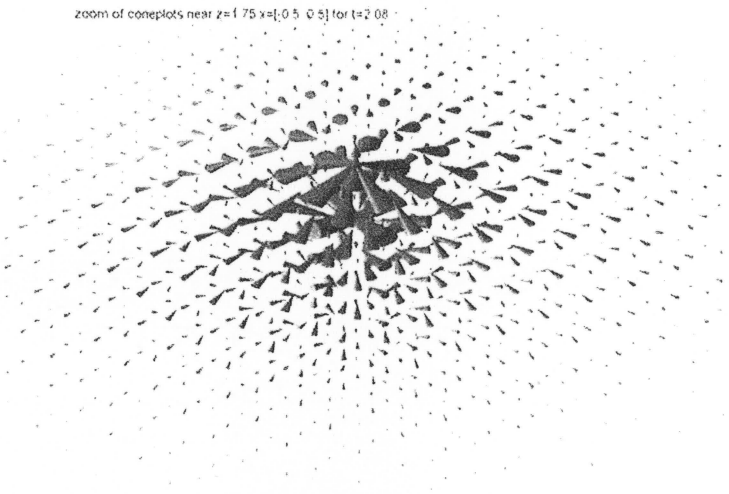

Fig. 23: View of the vector field in the sharpening area. Cones and their sizes represent velocity values and directions. It can be seen that nearby located field layers have opposite directions.

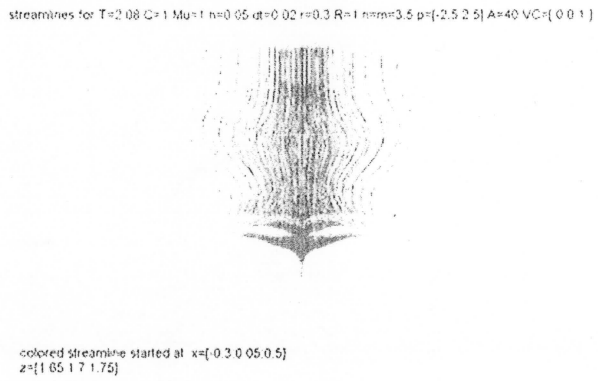

Fig. 24: Lines of flow in the sharpening area. Small shift of initial flow lines causes sharp change of line direction.

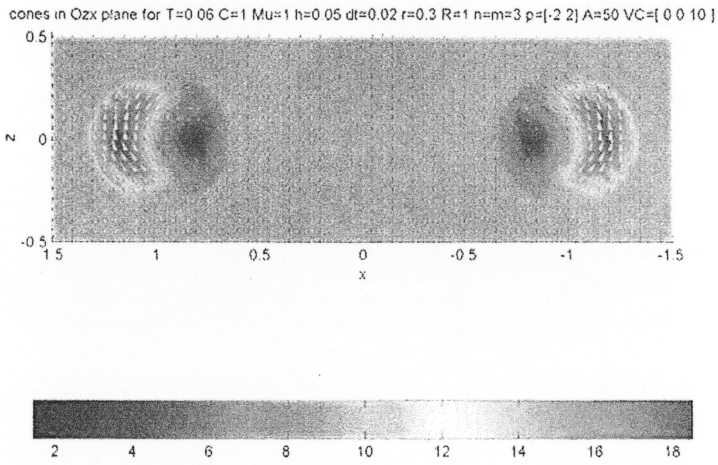

Fig. 25: Vector field in plane OZX, evolution begins.

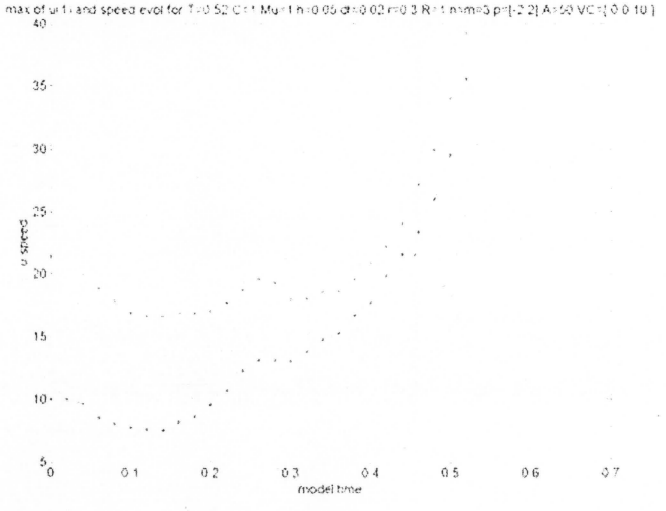

Fig. 26: Evolution of maximum absolute velocity.

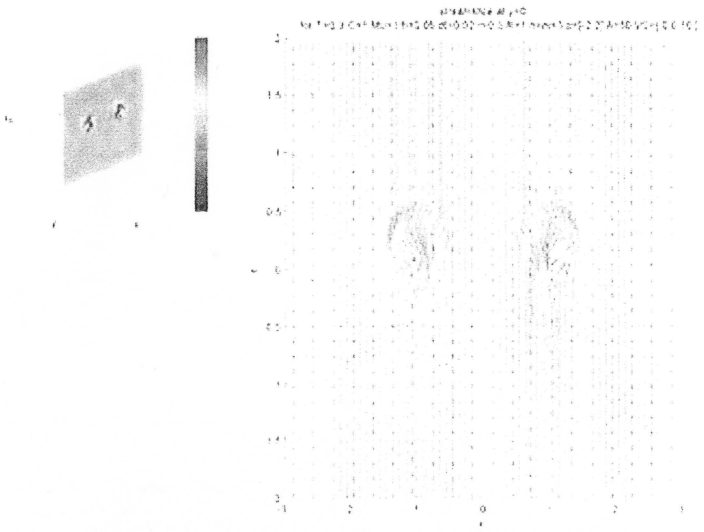

Fig. 27: Section of flow lines in OZX plane at the moment $t = 0.3$.

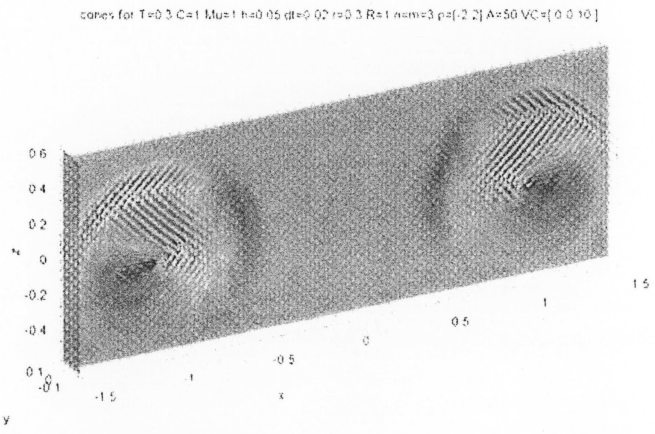

Fig. 28: Vector field near OZX plane at $t = 0.3$.

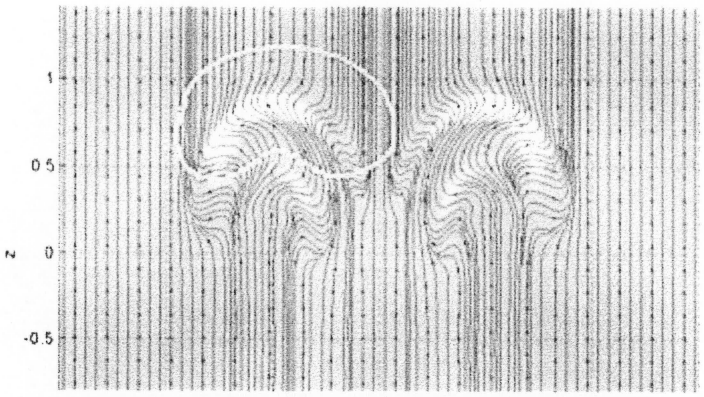

Fig. 29: Flow lines in OZX plane at $t = 0.7$.

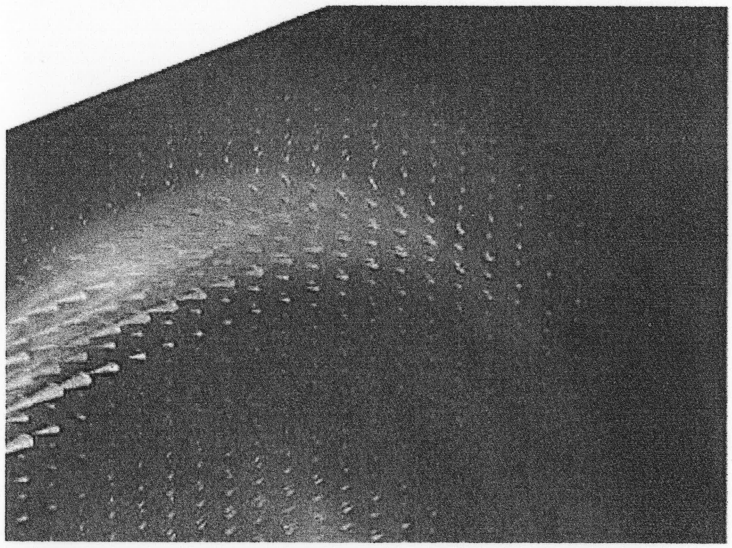

Fig. 30: Zoomed image of selected area of Fig.18.

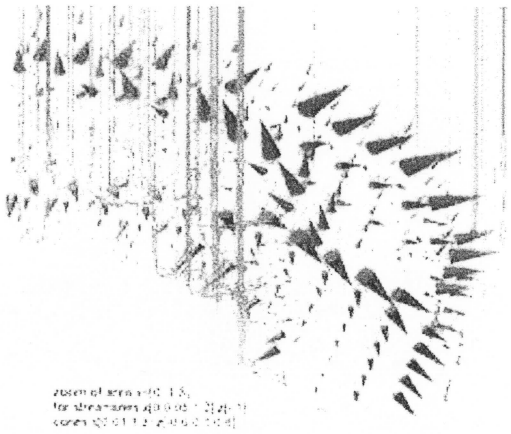

Fig. 31: Sharp changes of the vector field, leading to flow line deformation.

Fig. 26 and an eventual expansion of the torus area. The first bump on the graph corresponds to m.v.a transition to the outer ring of the torus area, the second sharp increase of m.v.a before intensive growth is not observed there. At the moment $t = 0.3$, before the start of intensive velocity growth, the field changes its configuration like shown in Fig. 28.

The area of maximal velocities is marked in red, as before, and it is seen that the torus area expands significantly, and flexure of the vector field in the m.v.a area is seen, but turbulences are absent, it is proven by flow lines in Fig. 27 Later values of vector field in the upper part of m.v.a. grow sharply, while values in surrounding areas stay almost the same. Again, it leads to sharp deformation of flow lines on the border of m.v.a. (see Fig. 29 and Fig. 30)

Let us repeat the aspects which will be useful for future analysis:

1. quick growth of velocity is observed without any turbulence

2. therefore (taking the item 1 into account) the emergence of collapses ("blow - up regimes" (b.u.r.) is caused mainly by ratio and not the direction of the vector field

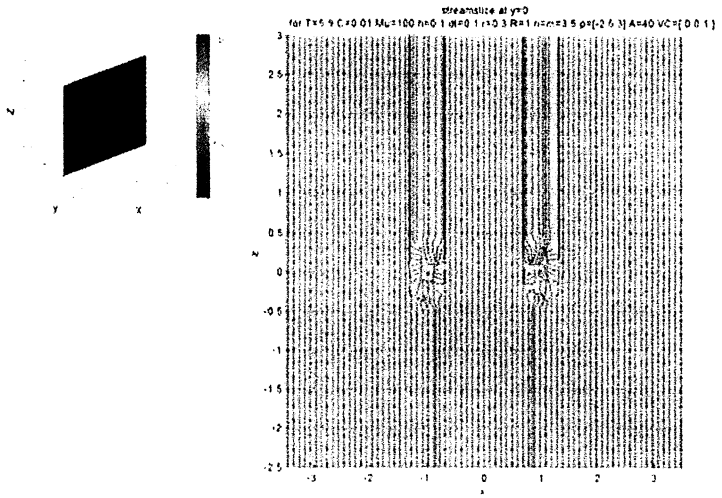

Fig. 32: Sections of flow lines at the moment of sharpening; the torus area has not expanded, instead there are ruptures in flow lines.

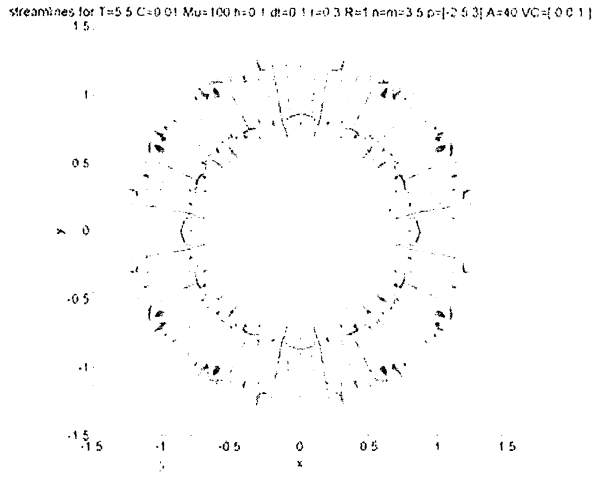

Fig. 33: Emergence of a new toroidal disturbances.

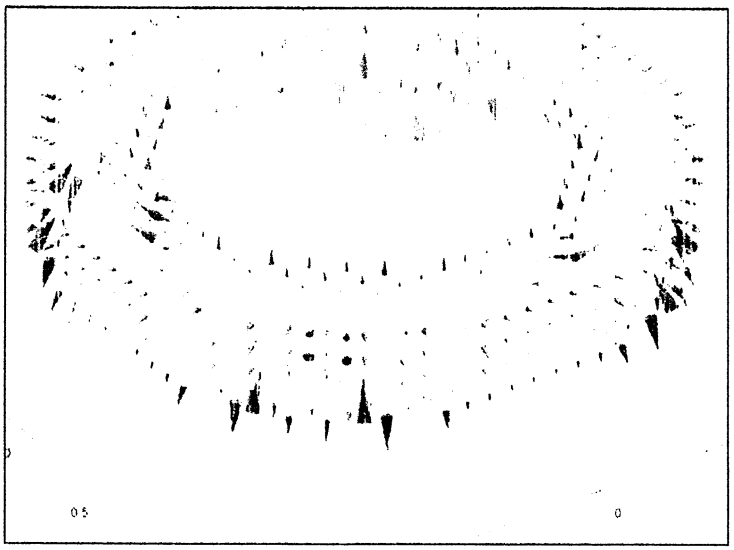

Fig. 34: Dissipation of new vortex and generation of smaller vortices, so-called reduction of characteristic scale.

3. m.v.a., in which sharpening localizes, is placed on the upper border of the torus area and has distinctive transfer to the outer flow, where velocity values are significantly (orders of magnitude) lower than maximal

4. p.2. causes the existence of sharp deformations of flow lines, which can be interpreted as ruptures

5. b.u.r. has local character and does not spread to the whole area (it is related to all data sets, where b.u.r. appears)

Let us consider a typical example of sharpening emergence by another scenario. A distinctive feature of this scenario is that the time of the beginning of the sharp velocity increase is generally lesser than the time of relaxation. In this case, due to the big value of relaxation time, the torus does not have time to expand, saves its structure, and in points, where the ratio is higher than the critical value, velocity growth begins. This causes the emergence of sharp transfer locations between the torus and the stationary flow, because in points, which were located on the initial torus, the

velocity grows to high values, and the stationary flow remains constant. Due to this fact, flow lines deform significantly (they turn by up to 90 degrees - see Fig. 31). Torus area virtually does not expand (see Fig. 32). Initial disturbances disappear at first, subduing to flow line curves, and with time new toroidal disturbances emerge, having a radius lesser than the initial, and the maximal velocity is, as before, located on the boundaries of the initial torus.

Illustration of reduction of characteristic scale effects. A summary of the numerical calculations is as follows:

1. An addition of memory effects to the hydrodynamical models causes the possibility of sharpening emergence, which demonstrates itself by quick velocity growth during a short time period, and is theoretically an indication of unlimited growth of solutions in finite time.

2. There is a necessary condition for the emergence of sharpening

$$\frac{\max_{\vec{x}} \vec{V}(\vec{x}, 0)}{\sqrt{\nu/\mu}} > M_{cr} \tag{83}$$

   Where M_{cr} is a fixed critical value, by experimental data $M_{cr} = 10$.

3. The main role in emergence of collapses is played by the value of absolute velocity and by (83) ratio, and not by the direction of vector field, therefore the existence of vortices would not necessarily cause sharpening. Further, sharpening can emerge even when vortices are absent.

4. M.v.a, where sharpening is located, has a distinct transition area to the outer flow, in which velocity values are significantly(orders of magnitude) lower than maximal, which explains the existence of a sharp deformation of flow lines, interpretable as ruptures

5. In the sharpening area, oppositely directed flows with large velocity values can exist, which can be interpreted as rupture of the vector field.

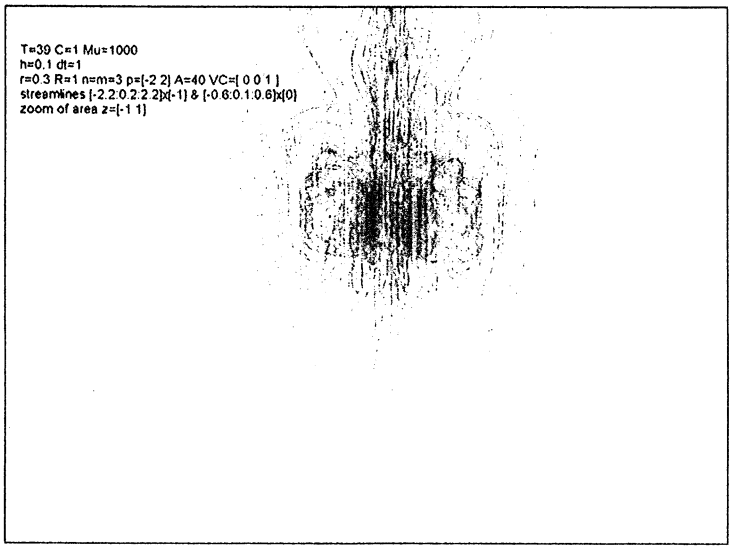

Fig. 35: Emergence of vortices at the moment of crossing of the torus area at the OZ axis.

6. Sharpening always has a local spatial character and its area narrows as time passes.

7. During the evolution process vortex rings emerge and dissipate into smaller rings, this can be interpreted as a reduction of characteristic scales.

8. During evolution, spatial oscillations emerge.

9. The similarity of numeric solutions at some system parameters to experimental snapshots of real fluid flows is determined.

One is able to conclude from these results that memory effects accounting in model hydrodynamic equations, in many cases, essentially change the qualitative and quantitative behaviour of their solutions. The main result is possible new type of fragmentation and vorticity behaviour. Further investigations of systems with memory may bring new unexpected results, especially in related fields of chaos investigations [50–55]. Note that one of

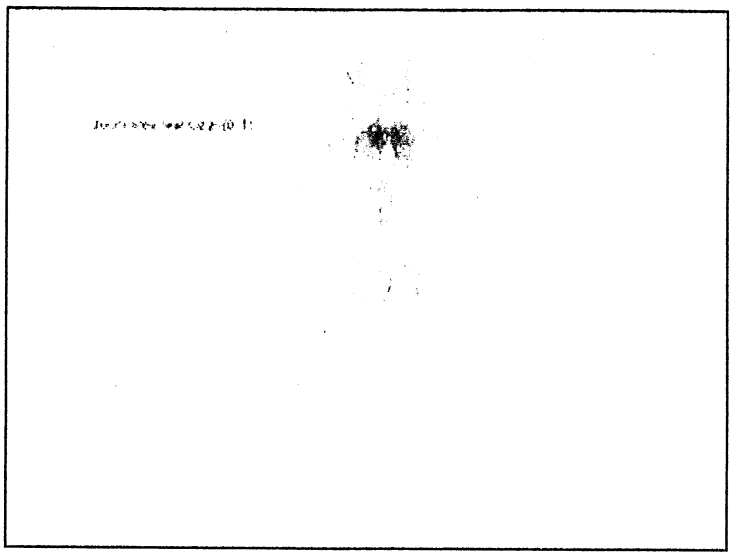

Fig. 36: Dissipation of vortices to few levels along the OZ axis.

the most important conclusions from the proposed investigations is the possibility of vorticity increasing in distributed systems and fragmentations of disturbances (or transfer energy to smaller scales). This is especially important for the general problem of turbulence, sun bursts, and communications. Numerical calculations and investigations of the schemes, presented in this subsection, were carried out by A. Makarenko and his assistant T. Swirskiy.

4. Propagations of nonlinear wave fields in media with oscillating inclusions

Experimental investigations of complex media deformation in a wide range of loading velocities carried out in the last decades testify that media possess two basic features, namely, the discreteness and oscillating motion of discrete elements [56, 57].

For description of wave fields and the processes of media deformation, mathematical models have been offered in [58, 59], in which oscillations of intrinsic oscillators are taken into account in a dynamical equation of state.

Using nonlinear nonlocal models for media exact analytical and complicated numerical invariant solutions describing wave fields in multicomponent media with internal oscillators [60–63] were studied. Let us note that, depending on the media structure and its thermodynamical state, oscillations of structure elements can be taken into account by means of including of additional volumetric forces, caused by structure elements oscillations. It has been suggested in papers [64, 65], the linear mathematical model for structured media taking into account the oscillation of structural elements in volumetric forces but not in dynamical equations of state, as it was the case in papers [58, 59].

Due to the nonlinearity of most real materials, we intend to make some modifications in this linear model. Here, we describe the investigations of resonant regimes of nonlinear wave fields, spreading in the media with oscillating inclusions. The mathematical model consists of two mutually penetrated continua, one of which is the oscillating inclusion. The equations of media motion in one dimensional case have the form [64, 65]:

$$\begin{aligned} \rho\frac{\partial^2 u}{\partial t^2} &= \frac{\partial \sigma}{\partial x} - \int\limits_0^\infty m(\omega)\frac{\partial^2 W}{\partial t^2}d\omega, \\ \frac{\partial^2 W}{\partial t^2} &+ \omega^2\left(1+\tau\frac{\partial}{\partial t}\right)(W-u) = 0, \end{aligned} \tag{84}$$

where ρ is the density, σ is the mechanical pressure, $u(x,t)$, $W(x,t,\omega)$ are the displacements of a basic medium and a typical oscillator with natural frequency ω, τ is the time of relaxation, $m = \int\limits_0^\infty m(\omega)d\omega$ is the total mass of oscillating inclusions. Let us choose the function $m(\omega)$ in the form $m(\omega) = \rho\sum\limits_{j=1}^{n} m_j\delta(\omega-\omega_j)$ corresponding to the model taking into account the finite numbers of oscillators with frequencies ω_j. On the basis of the previous assumptions, we can rewrite equation (84) in the following form

$$\frac{\partial^2 u}{\partial t^2} = \frac{1}{\rho}\frac{\partial \sigma}{\partial x} - \sum_{j=1}^{n} m_j\frac{\partial^2 W_j}{\partial t^2}, \quad \frac{\partial^2 W_j}{\partial t^2} + \omega_j^2\left(1+\tau_j\frac{\partial}{\partial t}\right)(W_j-u) = 0. \tag{85}$$

4.1. Resonant regimes of nonlinear waves propagation in media with oscillating inclusions

Let us consider the peculiarities of resonant regimes within the framework of the mathematical model consisting of equation of motion (85) and the nonlinear equation of state

$$\frac{\partial^2 u}{\partial t^2} = \frac{\partial \sigma}{\partial x} - m_1 \frac{\partial^2 w}{\partial t^2}, \qquad \frac{\partial^2 w}{\partial t^2} + \omega^2 \left(1 + \tau \frac{\partial}{\partial t}\right)(w - u) = 0,$$
$$\sigma = A_1 \frac{\partial u}{\partial x} + A_2 \left(\frac{\partial u}{\partial x}\right)^2 + A_3 \left(\frac{\partial u}{\partial x}\right)^3, \; A_1 = \frac{\alpha_1}{\theta^2 \rho}, \; A_2 = \frac{\alpha_2 h}{\theta^3 \rho}, \; A_3 = \frac{\alpha_3 h^2}{\theta^4 \rho}, \tag{86}$$

where the coefficients α_i are determined in terms of a corresponding elastic module, or extracted from the primary data, θ and h are the scale parameters.

We are interested in the resonant regimes of wave fields propagation along the rod of the length l. It is assumed that our system is resting, the left end of the rod is free, and the right end undergoes the following loading

$$\alpha_1 \frac{\partial u}{\partial x}(x = L) = \frac{\theta}{h} \gamma \sin \alpha t \equiv \phi(t), \; \theta L = l.$$

Using Bogoliubov–Mitropolsky method, we are able to build the amplitude curve of rod oscillations [66, 67]. Consider the case when $A_{2,3}$, τ, γ are the small parameters of the same order ε. To begin with, we reduce the boundary conditions to homogeneous one with the help of the change of variables $U(x,t) = u(x,t) - \dfrac{x^2}{2L\alpha_1}\phi$. Let us state the conditions under which it is possible to observe in the nonperturbed system the non-fading waves with the frequency Ω. Inserting the solution of the form

$$U = \cos\left(\frac{\pi x}{L}\right) \varphi_1 \cos \Omega t, \; w = \cos\left(\frac{\pi x}{L}\right) \varphi_2 \cos \Omega t, \; \varphi_{1,2} = \text{const} \tag{87}$$

to system (86), in the first order approximation we obtain that Ω satisfies the following equation

$$\frac{A_1 \pi^2}{L^2} = \Omega^2 \left(1 + \frac{\omega^2 m_1}{\omega^2 - \Omega^2}\right). \tag{88}$$

Solutions of this equation determine the values of normal modes frequencies for model (86). It follows from the analysis of the graph of the dependence $\Omega(m_1)$ (Fig.37) that in the moment $m_1 > 0$ additionally to the frequency $\Omega_0 = \sqrt{A_1\pi^2 L^{-2}}$ corresponding to the linear classical model of elastic media, a new frequency connected with a partial oscillator appears. With increasing the parameter m_1 the frequency $\min(m_1, \Omega_0)$ decreases monotonically, whereas the frequency $\max(m_1, \Omega_0)$ grows.

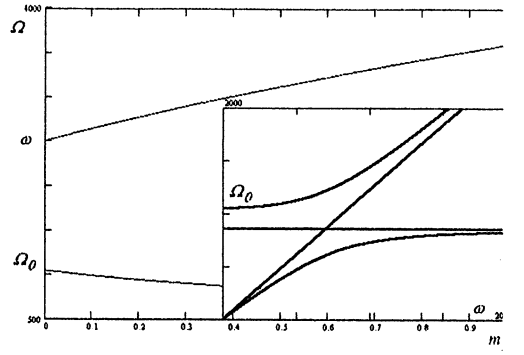

Fig. 37: The diagram of the dependence of normal modes frequencies for model (86) on the parameter m_1 at $\omega = 2500$

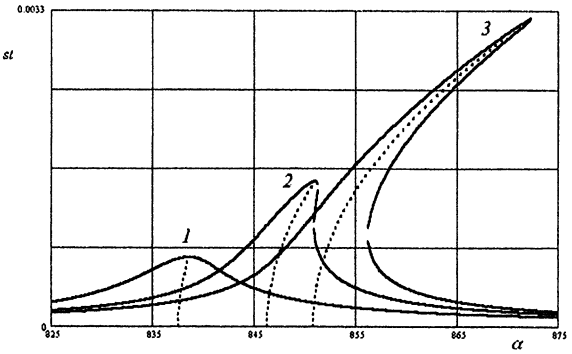

Fig. 38: The resonant curves for the nonlinear model with inclusions at $m_1 = 0.5$ and $1 - \omega = 2500$ s^{-1}, $2 - \omega = 3500$ s^{-1}, $3 - \omega = 5000$ s^{-1}.

At fixed m_1 and changeable ω (Fig.37) the solutions of equation (88) tend to the asymptotic values $\sqrt{\dfrac{A_1\pi^2}{L^2(1+m_1)}}$ and $\sqrt{(1+m_1)\omega}$.

Now, we are going to look for the continuation of solution (87) along the small parameter ε in the resonant case $\Omega - \alpha = \delta\varepsilon$. The dynamics of the amplitude λ and the phase $\alpha t + \vartheta$ of periodic solution (87) are described by the system

$$\lambda' = -\lambda\mu_1 + \mu_4 \cos\vartheta, \quad \vartheta' = \mu_2 + \mu_3\lambda^2 - \frac{1}{\lambda}\mu_4 \sin\vartheta, \tag{89}$$

where

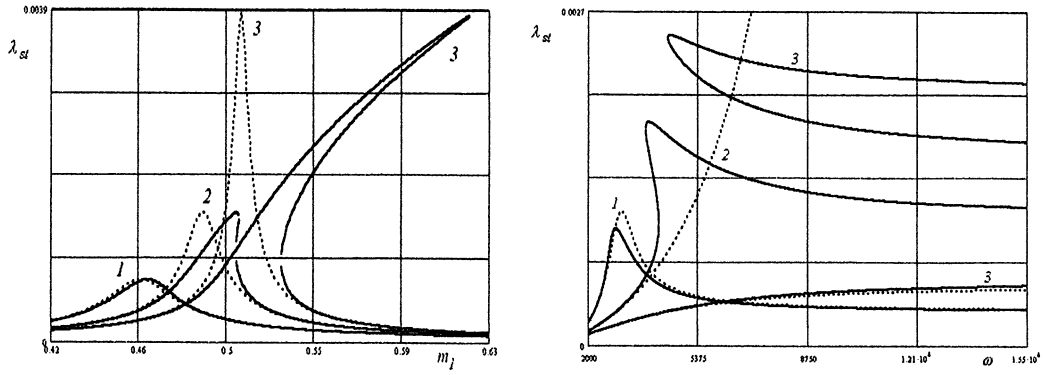

a) b)

Fig. 39: The resonant curves for the nonlinear (solid line) and linear (dashed line) models with inclusions a) at changeable m_1 and fixed ω: $1 - \omega = 2500$ s^{-1}, $2 - \omega = 3500$ s^{-1}, $3 - \omega = 5500$ s^{-1}; b) at changeable ω and fixed m_1: $1 - m_1 = 0.48$, $2 - m_1 = 0.52$, $3 - m_1 = 0.55$.

$$\mu_1 = \frac{\chi_2 \omega^2 \Omega^2 \tau}{2\Delta\left(\omega^2 - \Omega^2\right)}, \mu_2 = \frac{\Omega^2 - \alpha^2}{2\alpha}, \mu_3 = \frac{9A_3\pi^4}{32\alpha\Delta L^4}, \mu_4 = \frac{\gamma L}{\pi^2\alpha\Delta}\left[\alpha^2 + \chi_2\omega^2\right],$$

$$\Delta = 1 + \frac{(m_1 + \chi_2)\,\omega^2}{\omega^2 - \Omega^2}, \chi_2 = \frac{m_1\Omega^2}{\omega^2 - \Omega^2}.$$

Equating the right part of system (89) to zero, we find the fixed values of the amplitude of oscillations

$$\lambda^6 + 2\frac{\mu_2}{\mu_3}\lambda^4 + \frac{\mu_1^2 + \mu_2^2}{\mu_3^2}\lambda^2 - \left(\frac{\mu_4}{\mu_3}\right)^2 = 0. \qquad (90)$$

Let us choose granite as a basic medium with the density $\rho = 2.5 \cdot 10^3$ kg/m^3, the scale coefficients are $\theta = \sqrt{\alpha_1\rho^{-1}} = 884.8277$, $h = 0.1$.

Then $A_1 = 1$, $A_2 = 0.0599$, $A_3 = 0.0081$. This corresponds to the assumption that the nonlinearity is small. We arbitrarily choose other parameters, taking the following example $\tau = 3 \cdot 10^{-4}$ s^{-1}, $L = 3 \cdot 10^{-3}$ m, $\gamma = 0.3 \cdot 10^4$ Pa. Assume that $m_1 = 0,5$ and $\omega = 2500$ $s^{-1} > \Omega_0$. We can then evaluate the normal modes frequencies $\Omega_1 = 837.5659$ s^{-1} and $\Omega_2 = 3125.7169$ s^{-1} on the basis of (88). The dependence of the amplitude

of fixed oscillations at changing α is studied in the vicinity of frequency Ω_1. Solving equation (90) numerically with respect to parameter α, we obtain the graph of a resonant curve (graph 1 in Fig. 38). In a similar way we get the resonant curves at $\omega = 3500\ s^{-1}$ and $\omega = 5000\ s^{-1}$ (graphs 2 and 3 in Fig. 38). The graph of the skeletal curve (the condition of exact resonance) is defined by the relation $\mu_2 + \mu_3\lambda^2 = 0$ (dashed line in Fig.38). Hence, the direction of curve deviation from the vertical depends on the sign of the expression $\frac{A_3}{\Delta(\Omega-\alpha)}$.

In case when $\alpha > \Omega_0$ and increasing the frequency of vibrations of internal oscillators, we observe the deviation of the skeletal curve to the right. This phenomenon is accompanied by the formation of a hysteretic domain, in which the amplitudes of vibrations can suddenly decrease.

Hence, the position and the form of the resonant curve are defined by two connected factors, namely, the oscillating inclusions and the nonlinearity of the carrying medium. A detail investigation of resonant curves at the change of parameter m_1 reveal (Fig.39, *a*) similar effects. It is known that resonant curves can possess the characteristic hysteresis with respect to the direction of the change of the parameter m_1 as soon as a main medium is nonlinear $A_3 \neq 0$.

The studies of influence of parameter ω on the resonant curves show that in special cases (graph 2 Fig. 39, *b*) the linear model can give a wrong estimation of the stationary amplitude values. Note that in this case the skeletal curve deviates to the left and on the resonant curve we can point out the parts corresponding to the hidden regimes (curve 3 Fig. 39, *b*). The hidden regimes can be discovered at slow changes of parameter ω if initial data is chosen in the vicinity of these regimes.

4.2. Propagation of travelling waves in media with oscillating inclusions

In the previous subsection we dealt with resonant regimes connected with boundary conditions. Now we shall discuss the travelling wave regimes which can be detected in the nonlinear model (86). The mathematical model is

written in the following form:

$$\rho\frac{\partial^2 u}{\partial t^2}=\frac{\partial \sigma}{\partial x}-m\rho\frac{\partial^2 w}{\partial t^2},\qquad \frac{\partial^2 w}{\partial t^2}+\omega^2\left(w-u\right)=0, \tag{91}$$

with the classical constitutive equation for the main medium $\sigma = e_1 u_x + e_3 u_x^3$.

The aim of the investigations is to find the exact wave solutions to nonlinear model (91) and numerical modelling of their evolution and interaction.

So, let us consider the travelling wave solutions in the form

$$u=U(s),\quad w=W(s),\quad s=x-Dt, \tag{92}$$

where parameter D is the constant velocity of the wave front. The functions U and W satisfy the system of ordinary differential equations

$$D^2U'=\rho^{-1}\sigma\left(U'\right)-mD^2W',\quad W''+\Omega^2\left(W-U\right)=0, \tag{93}$$

where $\Omega=\omega D^{-1}$. Using the first equation of system (93) and the constitutive equation, we obtain

$$W'=\frac{1}{mD^2}\left(\rho^{-1}\sigma\left(U'\right)-D^2U'\right)=\alpha_1U'+\alpha_3\left(U'\right)^3=\alpha_1R+\alpha_3R^3,$$

where $R=U'$, $\alpha_1=\dfrac{e_1-D^2\rho}{m\rho D^2}$, $\alpha_3=\dfrac{e_3}{m\rho D^2}$. Excluding variable W, one presents the second equation of system (93) in the form of a system

$$R'=Z,\qquad Z'=-\frac{6\alpha_3RZ^2+\Omega^2\left(\left(\alpha_1-1\right)R+\alpha_3R^3\right)}{\alpha_1+3\alpha_3R^2}. \tag{94}$$

Let us remark that system (94) is invariant under the transformation $(R,\,Z)\rightarrow(-R,\,-Z)$. Therefore, the phase space of this system is centrally symmetric. The dynamical system has the fixed points $O\left(0;\,0\right)$ and $A_{\pm}\left(\pm\sqrt{\left(1-\alpha_1\right)\alpha_3^{-1}};\,0\right)$. Linear stability analysis of the fixed points shows that the origin is characterized by the eigenvalues $\lambda_{1,2}=\pm\Omega\sqrt{\left(1-\alpha_1\right)\alpha_1^{-1}}$ and the points $A_{\pm}$ have the eigenvalues $\lambda_{1,2}=\pm\Omega\sqrt{2}\sqrt{\alpha_1-1}$. So, dynamical system (94) has several different types of phase portraits, depending

on parameter α_1. It follows from the analysis of function $\alpha_1(D)$, that increasing D from 0 to $+\infty$ corresponds to decreasing α_1 from $+\infty$ to $-1/m$. Consider typical phase portraits for the following cases.

Case $\alpha_1 \geq 1$ (Fig.40a). There is only one fixed point (0, 0) with pure imaginary eigenvalues. In the sequel, the origin is a center.

Case $0 < \alpha_1 < 1$ (Fig.40b). The origin becomes a saddle with the homoclinic loops depicted with the bold line in the figure. The profile of function $R(s)$ for saddle separatrices is shown in Fig. 41a. The centers $A_{\pm}$ appear in the phase plane. There is an additional set of periodic solutions. These regimes surround the homoclinic loops of saddle point.

Case $\alpha_1 = 0$ (Fig.40c). In this case, system (94) has a peculiarity in the origin. Besides, an analytical expression for the trajectory passing through the origin (see below) exists. The profile of function $R(s)$ for this trajectory is shown in Fig. 41b. This graph differs from left curve essentially.

Case $\alpha_1 < 0$ (Fig.40d). Since α_1 is negative, discontinuities $R^{\pm} = \pm\sqrt{-\frac{\alpha_1}{2\alpha_3}}$ appear in the phase space. Between them there are periodic regimes surrounding the fixed point (0, 0). Trajectories separating periodic and infinite regimes from each other exists. On these separatrices, system (94) can be reduced to the first order integrable differential equation.

To find exact solutions to system (94), let us multiply both sides of system (94) by the expression $(\alpha_1 + 3\alpha_3 R^2)^2$ and change the time variable $(\alpha_1 + 3\alpha_3 R^2)^2 \frac{d}{ds} = \frac{d}{d\theta}$. After these manipulations, system (94) has the form

$$\begin{aligned} R' &= Z\left(\alpha_1 + 3\alpha_3 R^2\right)^2, \\ Z' &= -\left[6\alpha_3 R Z^2 + \Omega^2\left(\left(\alpha_1 - 1\right)R + \alpha_3 R^3\right)\right]\left(\alpha_1 + 3\alpha_3 R^2\right), \end{aligned} \tag{95}$$

where $(\cdot)' = \frac{d(\cdot)}{d\theta}$. It is easy to check that system (95) has the first integral

$$H = \frac{1}{2}Z^2\left(\alpha_1 + 3\alpha_3 R^2\right)^2 + \frac{\Omega^2}{2}\left[\alpha_3^2 R^6 + \frac{4\alpha_1 - 3}{2}\alpha_3 R^4 + \left(\alpha_1^2 - \alpha_1\right)R^2\right] = \text{const}.$$

Take the trajectory, which passes through the fixed point $(0;0)$ at $0 < \alpha_1 <$

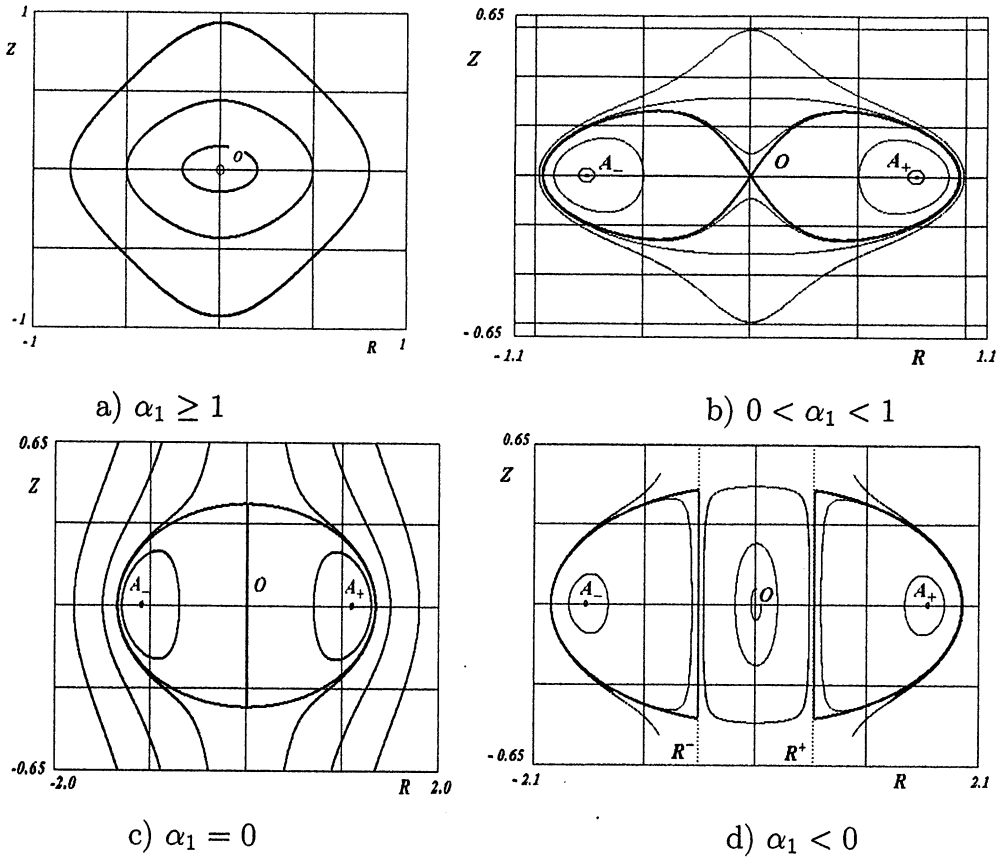

Fig. 40: The phase portraits of dynamical system (94). Here $e_1 = 1$, $e_3 = 0.5$, $\rho = 1$, $\omega = 0.9$, $m = 0.6$ and D varies.

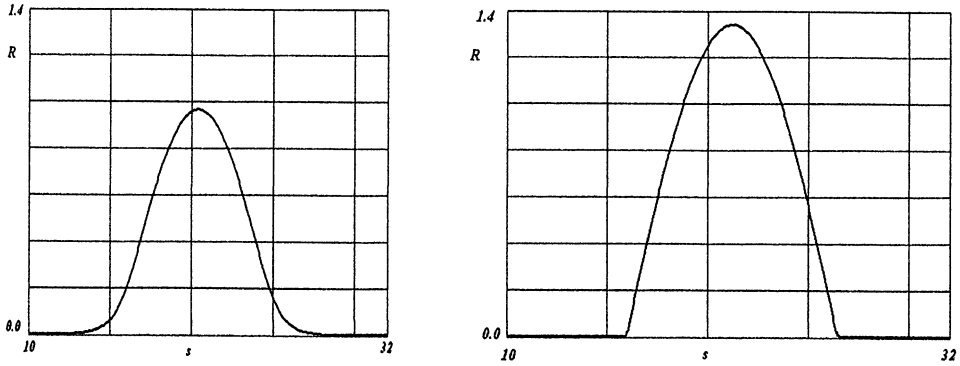

a) b)

Fig. 41: Profiles of soliton-like (a) and compacton (b) solutions of dynamical system (94).

1. Then $H = 0$ and we have

$$Z^2 = -\frac{\Omega^2}{(\alpha_1 + 3\alpha_3 R^2)^2}\left[\alpha_3^2 R^6 + \frac{4\alpha_1 - 3}{2}\alpha_3 R^4 + \left(\alpha_1^2 - \alpha_1\right) R^2\right] \equiv R'^2. \tag{96}$$

Function (96) represents the homoclinic loop of the saddle point $(0;0)$ in the plane $(R;Z)$ (Fig.40b). We can easily obtain the analytical expression of this solution. It follows from relation (96) and system (94), that

$$\int_{s_0}^{s} ds = \frac{1}{2\Omega}\int_{r_0}^{r} \frac{\alpha_1 + 3\alpha_3 r}{r\sqrt{-\alpha_3^2 r^2 + \frac{3-4\alpha_1}{2}\alpha_3 r + \alpha_1 - \alpha_1^2}} dr,$$

where $r = R^2$.

Then

$$s - s_0 = \frac{3}{2\Omega}\arcsin\left(\frac{4\alpha_3 r - 3 + 4\alpha_1}{\sqrt{9-8\alpha_1}}\right) - \frac{1}{2\Omega}\sqrt{\frac{\alpha_1}{1-\alpha_1}}\times$$

$$\ln\left(\frac{1}{r} + \frac{3\alpha_3 - 4\alpha_1\alpha_3}{4\left(\alpha_1 - \alpha_1^2\right)} + \sqrt{\left\{\frac{1}{r} + \frac{3\alpha_3 - 4\alpha_1\alpha_3}{4\left(\alpha_1 - \alpha_1^2\right)}\right\}^2 - \frac{\alpha_3^2\left(9 - 8\alpha_1\right)}{16\left(\alpha_1 - \alpha_1^2\right)^2}}\right)\Bigg|_{r_0}^{r} \tag{97}$$

Solution (97) corresponds to the soliton-like solution with infinite support at $0 < \alpha_1 < 1$ (Fig.41a).

A different homoclinic loop exists at $\alpha_1 = 0$. It follows from equation (96), that

$$R'^2 = \frac{\Omega^2\left(3 - 2\alpha_3 R^2\right)}{18\alpha_3}.$$

Combining the solution of this equation with the trivial one, we get the following solutions

$$R = \begin{cases} \sqrt{\frac{3}{2\alpha_3}}\sin\left(\frac{\Omega s}{3}\right), \frac{\Omega s}{3} \in [0;\pi] \\ 0, \frac{\Omega s}{3} \notin [0;\pi] \end{cases}$$

and

$$U = \begin{cases} 0, \frac{\Omega s}{3} \in [-\infty;0] \\ \frac{3}{\Omega}\sqrt{\frac{3}{2\alpha_3}}\left(1 - \cos\left(\frac{\Omega s}{3}\right)\right), \frac{\Omega s}{3} \in (0;\pi] \\ \frac{6}{\Omega}\sqrt{\frac{3}{2\alpha_3}}, \frac{\Omega s}{3} \in (\pi;\infty) \end{cases}$$

The relation for $R(s)$ defines a nonanalitical solution with compact support or compacton (Fig.40b). This regime can be thought as a limit state for the solution with infinite support (97). At the same time the graph of function $U(s)$ corresponds to the kink-like solution.

In the case $\alpha_1 < 0$ separatrix contours (bold line in figure 40d) are described by the relation

$$Z^2 = \frac{2H\left(R^+, 0\right) - \Omega^2\left[\alpha_3^2 R^6 + \frac{4\alpha_1 - 3}{2}\alpha_3 R^4 + \left(\alpha_1^2 - \alpha_1\right)R^2\right]}{\left(\alpha_1 + 3\alpha_3 R^2\right)^2}.$$

So that we can obtain a nonanalytic solution as above.

Recall that homoclinic solutions can possess the soliton properties. To learn the properties of the homoclinic trajectories, one can investigate the interaction of perturbations by direct numerical simulation of system (91).

Let us construct the numerical scheme for model (91) in the region $\Sigma = [0 \le x \le L] \times [0 \le t \le T]$ with grid lines $x = ih$ and $t = j\tau$, where h, τ are constant. Consider three level numerical scheme. Denote $u = u(t_{n+1})$, $v = u(t_n)$, $q = u(t_{n-1})$, and $K = w(t_{n+1})$, $G = w(t_n)$, $F = w(t_{n-1})$. We use the following difference approximation of derivatives

$$\frac{\partial^2 u}{\partial t^2} \approx \frac{u_i - 2v_i + q_i}{\tau^2}, \quad \frac{\partial^2 u}{\partial x^2} \approx \delta \frac{u_{i-1} - 2u_i + u_{i+1}}{h^2} + (1-\delta)\frac{v_{i-1} - 2v_i + v_{i+1}}{h^2},$$

$$\frac{\partial u}{\partial x} \approx \frac{v_{i+1} - v_{i-1}}{2h}, \quad \frac{\partial^2 w}{\partial t^2} \approx \frac{K_i - 2G_i + F_i}{\tau^2}, \quad w - u \approx \frac{G_i + F_i}{2} - \frac{v_i + q_i}{2}.$$

Thus, if $\delta \neq 0$, then we obtain the three level implicit scheme:

$$A_i u_{i-1} + C_i u_i + B_i u_{i+1} = Y_i, \quad K_i = 2G_i - F_i - \tau^2 \omega^2 \left(\frac{G_i + F_i}{2} - \frac{v_i + q_i}{2} \right), \tag{98}$$

where $A_i = B_i = \frac{\delta}{h^2}\varphi$, $C_i = -2\frac{\delta}{h^2}\varphi - \frac{1}{\tau^2}$, $Y_i = -\left(\varphi \frac{v_{i-1} - 2v_i + v_{i+1}}{h^2}(1-\delta) + \right.$

$\left. m\omega^2 \left(\frac{G_i + F_i}{2} - \frac{v_i + q_i}{2} \right) + \frac{2v_i - q_i}{\tau^2} \right)$, $\varphi = \rho^{-1} \left(e_1 + 3e_3 \left(\frac{v_{i+1} - v_{i-1}}{2h} \right)^2 \right)$.

System of algebraic equations (98) can be solved by the sweep method. The necessary conditions of the sweep method stability ($|A_i| + |B_i| \le |C_i|$) are fulfilled. Let us fix the values of the parameters $e_1 = 1$, $e_3 = 0.5$, $\rho = 1$, $\omega = 0.9$, $m = 0.6$, $D = 0.9$, and the parameters of the numerical scheme $L = 30$, $N = 400$, $\delta = 0.3$, $h = L/N$, $\tau = 0.05$. As initial data for numerical simulation the regime from figure 41a is chosen. The result of numerical integration by means of scheme (98) are presented in Fig.42a. We would like to stress on the selfsimilar character of solution movement for 200τ time units.

Consider the collision of two kink-like solutions. Then, the initial data is presented in the form

$$y = \{y_0, y_1, \ldots, y_{N-1}, y_{N-1}, \ldots, y_1, y_0\},$$

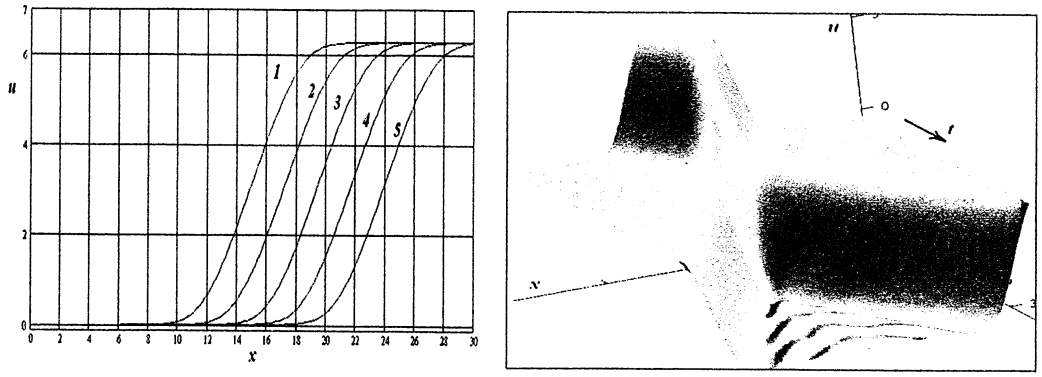

a) b)

Fig. 42: The movement of the single kink-like solutions (a) from figure 41a and the collision (b) of two kink-like solutions.

where $y \in \{u, v, q, K, G, F\}$.

The representation of kink-like perturbations collision are shown in Fig. 42b. The occurrence of a visible ripple after the collision points out the non elastic character of kink-like solutions' interaction. Note that the simulation of compacton solutions displays similar properties, but the neutrally stable scheme (98) does not correctly approximate some of the details of wave movement, due to the singularity taking place near the origin.

Therefore, nonlinear mathematical model (91) possesses the localized wave solutions. These regimes appear due to the nonlinearity and incorporating the dynamics of oscillating inclusions. The obtained solutions have the properties close to the soliton waves. This stimulates the investigations of model (91) further.

4.3. The spatially nonlocal model of media with oscillating inclusions

In this subsection we consider the influence of spatial nonlocality on the structure of wave solutions of model (91). We use the following equation of

state with spatial nonlocality:

$$p-p_0=\Phi\left(\frac{V-V_0}{V_0}\right)+\Gamma\varepsilon_r\left\{\tau_{TV}\left(p_{xx}-\frac{V_x}{V}p_x\right)+\frac{\tau_{Tp}}{V_0\chi T_0}\left[V_{xx}-\frac{1}{V}\left(V_x\right)^2\right]\right\} \tag{99}$$

Applying known relations $\varepsilon=\frac{V-V_0}{V_0}$, $\sigma=-\left(p-p_0\right)$, we rewrite equation (99) in the form

$$\sigma=E_1\varepsilon+E_3\varepsilon^3+\theta\left(\sigma_{xx}-\sigma_x\frac{\varepsilon_x}{\varepsilon+1}-\eta\left[\varepsilon_{xx}-\frac{\left(\varepsilon_x\right)^2}{\varepsilon+1}\right]\right) \tag{100}$$

and use it to close system (91). Consider the wave solutions of (92) type. Substituting (92) into equations (91) and (100), we obtain the dynamical system

$$D^2U''=F'-m_1D^2W'', \tag{101}$$

$$W''+\Omega^2\left(W-U\right)=0, \tag{102}$$

$$F=E_1U'+E_3\left(U'\right)^3+\theta\left(F''-F'\frac{U''}{U'+1}-\eta\left[U'''-\frac{\left(U''\right)^2}{U'+1}\right]\right), \tag{103}$$

where $\Omega=\omega D^{-1}$.

Integrating equation (101)

$$F=D^2\left(U'+m_1W'\right)$$

and excluding the variable F, we get the dynamical system

$$W''+\Omega^2\left(W-U\right)=0,$$

$$D^2\left(U'+m_1W'\right)=E_1U'+E_3\left(U'\right)^3+\theta\left(F''-F'\frac{U''}{U'+1}-\eta\left[U'''-\frac{\left(U''\right)^2}{U'+1}\right]\right). \tag{104}$$

Introducing new variables $R=U'$, $Z=W'$, we can rewrite system (104) as follows:

$$Z''+\Omega^2\left(Z-R\right)=0,$$

$$D^2\left(R+m_1Z\right)=E_1R+E_3R^3+$$

$$\theta\left(D^2\left[R''+m_1Z''\right]-D^2\left[R'+m_1Z'\right]\frac{R'}{R+1}-\eta\left[R''-\frac{\left(R'\right)^2}{R+1}\right]\right). \tag{105}$$

Coordinates of fixed points of dynamical system (105) satisfy the system of algebraic equations

$$Z = R, \quad D^2 (R + m_1 Z) = E_1 R + E_3 R^3.$$

Solving this system, we get:

$$Z_1 = R_1 = 0$$

and

$$Z_2 = R_2 = \pm\sqrt{\frac{D^2 (1 + m_1) - E_1}{E_3}}.$$

Let us write down system (105) in the form

$$\begin{gathered} Z' = Y, \quad Y' = -\Omega^2 (Z - R), \quad R' = X, \\ X' = \frac{1}{\theta (D^2 - \eta)} \Big(-E_1 R - E_3 R^3 + \frac{X^2 \{D^2 - \eta\} \theta + D^2 \theta m_1 XY}{R + 1} + \\ + \theta m_1 D^2 \Omega^2 \{Z - R\} + D^2 \{R + m_1 Z\} \Big) \end{gathered} \tag{106}$$

The matrix of linearization of this system at the stationary point has the form:

$$J = \begin{pmatrix} 0 & 1 & 0 & 0 \\ -\Omega^2 & 0 & \Omega^2 & 0 \\ 0 & 0 & 0 & 1 \\ J_{41} & 0 & J_{43} & 0 \end{pmatrix},$$

where $J_{41} = \dfrac{m_1 (D^2 + \omega^2 \theta)}{(D^2 - \eta) \theta}$, $J_{43} = \dfrac{D^2 - E_1 - m_1 \omega^2 \theta}{(D^2 - \eta) \theta}$ at the point $(Z_1; R_1)$ and $J_{41} = \dfrac{m_1 (D^2 + \omega^2 \theta)}{(D^2 - \eta) \theta}$, $J_{43} = \dfrac{2E_1 - D^2 (2 + 3m_1) + m_1 \omega^2 \theta}{(D^2 - \eta) \theta}$ at the point $(Z_2; R_2)$. Eigenvalues of the matrix J satisfy the biquadratic equation

$$\lambda^4 + \lambda^2 \left(\Omega^2 - J_{43}\right) - (J_{43} + J_{41}) \Omega^2 = 0.$$

Differentiating the expression

$$D^2 (R + m_1 Z) = E_1 R + E_3 R^3$$

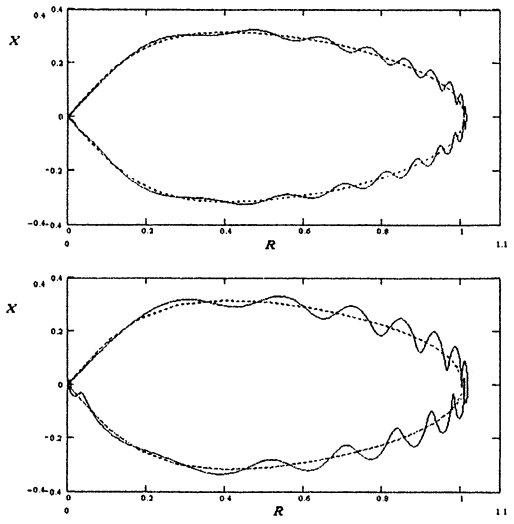

a) $\theta = 0.01$ b) $\theta = 0.016$

Fig. 43: The homoclinic loop form of the fixed point O of dynamical system (107) at different values of the parameter θ. The dashed line obtained at $\theta = 0$ corresponds to the case of neglecting of spatial nonlocality effects.

in the case $\theta = 0$, we can obtain from equation (105) the following system

$$Z' = Y, \quad Y' = -\Omega^2 (Z - R), \\ R' = \frac{Y}{\alpha_1 + 3\alpha_3 R^2}, \tag{107}$$

where $\alpha_1 = \dfrac{E_1 - D^2}{m_1 D^2}$, $\alpha_3 = \dfrac{E_3}{m_1 D^2}$.

The investigations of system (107), presented in the previous subsection, proved the existence of the homoclinic loop in the phase space of the dynamical system. In the plane $R - R'$ the graph of the loop is defined by function (96). The phase space of system (107) and the graph of function (96) are presented in Fig. 40b, 41a at $D = 0.9$, $\omega = 1$, $m_1 = 0.8$, $E_1 = 1$, $E_3 = 0.7$.

Let us consider wether the homoclinic loop survives after the incorporation of the nonlocal effects. We are going to numerically integrate dynamical

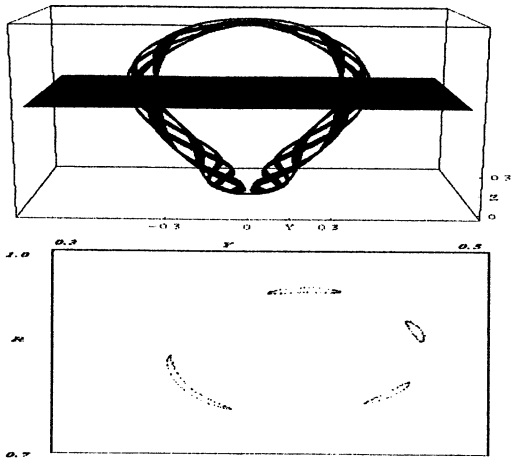

Fig. 44: The torus in the phase space of dynamical system (107) at $\theta = 0.7$ and the Poincare diagram. The initial data $(0.6; 0.3; 0.8; 0.4)$.

system (106) at small θ. We fix the parameters $\eta = 0.105$, $\theta = 0.001$ and choose the initial data $(10^{-6}; 0; 0; 0)$. The stationary point $(Z_1; R_1)$ with the eigenvalues $(\pm 16.577i; \pm 1.708)$ of the matrix J is a saddle. The fixed point $(Z_2; R_2)$ is characterized by the eigenvalues $(\pm 47.118i; \pm 0.85i)$ therefore it is a center. The integration of system (106) with parameters fixed above shows that the homoclinic loop is saved. Increasing parameter θ causes the change of the homoclinic loop form (Fig.43) and creation of torus which undergoes the next bifurcations (Fig.44, 45).

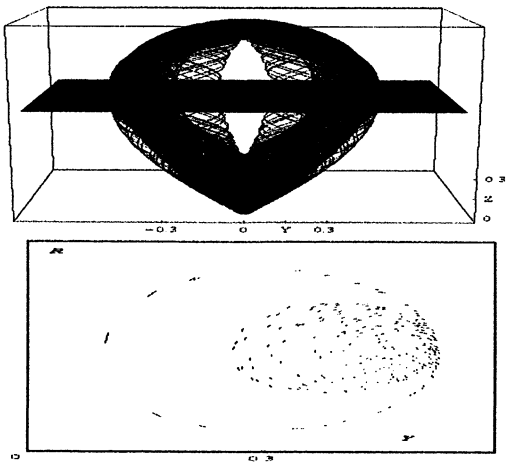

Fig. 45: The torus phase portrait and the Poincare section by the plane $Z = 0.8$ at $\theta = 0.8$ obtained by the numerical integration with the initial data $(0.109691391; 0.122529212; 0.342078078; -0.140624676)$.

Bibliography

[1] Danylenko V.A., Danevich T.B., Makarenko O.S., Moskaliuk N. M., Skurativskiy S.I. and Vladimirov V.A., Algebra-invariant models for nonlinear nonlocal media // Algebras, Groups and Geometries, 2012. – Vol. 29, No. 3. – PP. 309–376.

[2] Danylenko V.A., Danevich T.B., Makarenko O.S., Moskaliuk S. S.(jn), Skurativskiy S.I. and Vladimirov V.A., Group analysis of reaction-diffusion-convection nonlinear equations // Algebras, Groups and Geometries, 2013. – Vol. 30, No. 3. – PP. 275–366.

[3] Danylenko V.A., Danevich T.B., Makarenko O.S., Moskaliuk V. S., Skurativskiy S.I. and Vladimirov V.A., Exact solutions and wave patterns within some non - local hydrodynamic - type model// Algebras, Groups and Geometries, 2014. – Vol. 31, No. 4. – PP. 363–436.

[4] Berezhnev I.A., Nikolaev A.V., On the propagation of strong nonlinear pulse in blocked-hierarchic media // Phys. Earth Planetary Int., 1988. – Vol.50. – PP.83–87.

[5] Danylenko V.A., Vladimirov V.A., Korolevich V.Yu. Nonlinear models of multi-component relaxing media // Dopovidi Acad. Sci. Ukraine, 1992. – No. 1 – PP. 89–93.

[6] Nakoryakov V.E, Pokusajev B.R. and Schreiber I.D. Evolution of waves in gaseous-liquid mixtures, Inst. for Thermal Physics, Novosibirsk, 1983.

[7] Danylenko V.A., Kudinov V.M., Makarenko A.S. The influence of the memory effects for the dissipative structure creations under the high-rate processes. – Kiev, Ukraine. Preprint, IES - 83 - 1, 1983. – 60 p. (in Russian).

[8] Day W. A. The thermodynamics of simple materials with fading memory, Springer-Verlag, Berlin, 1972.

[9] Danylenko V.A., Kudinov V.H., Makarenko A. S. The influence of the memory effects for the burning and explosion processes // Phys. of burning and explosion, 1984 – Vol. 20, No.3. – PP. (In Russian). Translated in Journ. Eng. Phys., Consultant Bureau, NY, 1984, Vol.47, No.5.

[10] Danevych T.B,, Danylenko V,A., Korolevich V.J., Sorokina V.Y., Vladimirov V.A. The equations of hydrodynamics for active media. Symmetries, qualitative analysis and wave structures evolution

[11] Danylenko V.A., Vladimirov Y.A., Korolevich V.Yu. The nonlinear models of multicomponent relaxing media. Dynamic of wave structures and qualitary analysis. Part 1, Preprint. Ukr. Geophys. Inat., Kiev, 1990. – 40 p. (in Russian).

[12] Zubarev D.N. Nonequlibium statistical thermodynamics, Moscow, Nauka, 1975. – 320 p.

[13] Danylenko V.A., Kudinov V.M., Makarenko A.S. The ignition and burning of despersive systems // Doklady of Ukr.A.S., Ser.A., 1985. – No. 5. – PP. 69–72.

[14] Samarskii A.A., Qalaktionov Y.A., Kurdyumov S.P., Michajlov A.L. The blow-up regimes in the problems for the quasilinear parabolic equations, Moscow, Nauka, 1987.

[15] Kurdyumov S.P. Evolution and self-organization law in complex systems // Inter. Journal of Morden Physics. C, 1990. – Vol.1, No.4. – PP.299–327.

[16] Vladimirov V.S. The equations of mathematical physics, Moscow, Nauka, 1976. – 528 p.

[17] Frank-Kamenetski D.A. Diffusion and heattransfer in chemical kinetics, Moscow, Nauka, 1967. – 492 p.

[18] Zeldovich Ja.B., Barenblatt G.I., Librovich V.B., Machviladze G.M. The mathematical theory of combustion and explosions, Moscow, Nauka, 1980. – 478 p.

[19] Makarenko A.S. Of the special features of the heat and mass convection description in high-rate processes // Type-scrip. registrated in AISEII, II., N 6882-B 87, 1987. – 40 p. (in Russian). Resume: Jorn. of Engineer Physics. Consultants Bureau, NY, 1988. – Vol.54, No.2.

[20] Newell A.O., Rand D.A., Russell D. Turbulent dissipation rates and the random occurrence of coherent events // Physics Letters, Ser. A., 1988. – Vol.132, No. 2,3. – PP.112–123.

[21] Landau L.D., Lifshitz E.M. Hydrodynamics, Nauka, Moscow, 1986. - 736 p.

[22] Zubarev D., Tishchenko S. Nonlocal hydrodynamics with memory // Physica, 1972. – Vol.59, No.2. – PP.285–304.

[23] Picirelli R. Theory of the dynamics of simple fluids for large spatial gradients and long memory // Physical Review, 1968. – Vol.175, No.1. – PP.77–98.

[24] Resibua P., De Lener M. Classical kinetic theory of fluids and gases, Moscow, Mir, 1980.

[25] Loyciansky L.G. // Izv. Akad. Nauk USSR Ser. Fluid Mech. 2 (1982) 5.

[26] Joseph D.D., Preziozi L. Heat Waves // Review of Modern Physics, 1989. – Vol. 61, No. 1. – PP.41–73.

[27] Oskolkov A.P. Initial-boundary value problems for equations of motion of Kelvin–Voight fluids and Oldroyd fluids // Boundary value problems of mathematical physics. Part 13, Work collection, Trudy Mat. Inst. Steklov., 179, 1988. – PP.126-–164.

[28] Luikov A.V. Application of irreversible thermodynamics methods to investigation of heat and mass transfer // Inzhenerno-Fiziceskii Zhurnal, 1965. – Vol.IX, No.3. – PP.287–304. (Translation in International Journal of Heat and Mass Transfer, 1966. – Vol.9, No.2. – PP.139–152.)

[29] Astarita G., Marucci G. Principles of non-newtonian fluid mechanics, McGraw-Hill, 1974.

[30] Wilkinson Y.L. Non-newtonian fluids, Moscow, Mir, 1964.

[31] Burgers J.,M. The Nonlinear Diffusion Equation, Reiedl, Dordrecht, 1974.

[32] Karpman V.I. Nonlinear waves in dispersive media, Moscow, Nauka, 1973.

[33] Dodd R.K., Eilbek J.C., Gibbon J.D., Morris H.C. Solitons and Nonlinear Wave Equations, Academic Press, London, 1984.

[34] Makarenko A.S., Moskalkov M.N. Some solution of relaxed media model equations // KPI, Kyiv, 1992.

[35] Pyatkov S.B., Riudyak V.Ya., Smagulov Sh. Of the propertiesof the solution of hyperbolic approximation of Navier-Stokes aquations //Chislennye metody meoh. eploshnoy sredy, Movosibirsk, 1982. – Vol.13, No.13. – PP.104–113.

[36] Danylenko V.A., Christenyuk V.O., Korolevich V.Yu. and Makarenko A.S.

[37] Rudyak V. Ya., Yanenko N.W. Some nonlocal model of fluid mechanics // Math. Modelling, 1985. – Vol.6. – PP.401–412.

[38] Makarenko A.S., Moskalkov M., Levkov S. On blow-up solutions in turbulence // Phys. Lett. A, 1997. – Vol. 23. – PP.391–397.

[39] Starr P. Physics of negative viscosity phenomena, Moscow, Mir, 1972.

[40] Yasnikov G.P, Galperin L.G., Kutiavin Z.I. // Inzh.-Fiz. J., 1980. – Vol.39. – P.334.

[41] Jou D., Perez-Garcia C.,Garcia-Colin L.S., Lopez de Haro M., Rodriguez R. F. Generalized hydrodynamics and extended irreversible thermodynamics // Phys. Rev. A, 1985. – Vol.31, No.4. – PP.2502–2508.

[42] Rosenau P., Hyman J. Compactons: solitons with finite wavelength // Phys. Rev. Letter, 1993. – Vol. 70, No.5. – PP.564–567.

[43] Larkin N.A., Novikov V.A., Yanenko N.N. The nonlinear equations of changable type, Novosibirsk, Nauka, 1983. – 270 p.

[44] Bartucelli M., Conetantin P., Doering C.H. Hard turbulence in a finite dimensional dynamical system // Phys. Letters A., 1989. – Vol.142, No 6,7. – PP. 349-353.

[45] Sharkovski A.N., Maistrenko Yu.L., Romanenko E.Yu. The difference equations and their applications, Kiev, Naukova dumka, 1986. -– 280 p.

[46] Makarenko A.S., Swirsky T. Modeling self-origin of collapses in hydrodynamics with memory. // Proc. of the XV-th Int. Hutsulian Workshop "Category theory and applied systems analysis in decision-making problems" (april,2004, Kyiv; september, 2005, Sevasopol, Ukraine), Kyiv, 2006. – PP.183–206.

[47] Samarskii A.A. Numerical schemes theory, Moscow, Nauka, 1977.

[48] Makarenko A.S. Toward the analysis of numerical schemes dispersion for Klein-Gordon equation // Numerical methods for continuum mechanics (Novosibirsk), 1982. – Vol.13, No.3. – PP.81–90.

[49] Makarenko A.S., Moskalkov M.N. One approach to numerical oscillations reducing // Computational and applied mathematics, Kiev, 1980. – No.41. – PP.65–71.

[50] Boldrighini C. and Franceschini N. Five-dimensional truncation of the plane incompressible Navier-Stokes equations // Comun. Math. Phys., 1979. – Vol.64, No.2. – PP.159-170.

[51] Burczlaff J., Zakrzewski W. CP^2 soliton scattering: the collective coordinate approximation // Nonlinearity,1998. – Vol.11, No.5, – PP.1311-1320.

[52] Gonchenko S., Turaev D., Šilnikov L. On models with non-rough Poincaré homoclinic curves // Physica D, 1993. – Vol.62, No.1-4. – PP.1–14.

[53] Ladyzhenskaya O.A. The mathematical quations of viscous incompressible fluid dynamics, Moscow, Nauka, 1970. – 288 p.

[54] Kuleshov V.A., Makarenko A.S. On the dispersive turbulance in a some descrete and distributed systems. Type-scrop registrated in AISHCI, Moscow, No.7491, 1985, – 44 p. (in Russian). Resume in J. Engrg. Phys. Consultant Bureau, NY, 1985. – Vol.48, No.4 – P.664.

[55] Temam R. Infinite-dimensional dynamical systems in mechanics and physics, Springer-Verlag, New York, 1988.

[56] Rodionov V.N. Essay of geomechanics, Moscow, Nauchnij mir, 1996. – 64 p.

[57] Sadovskiy M.A. Selfsimilar of geodynamical processes // Vestnik AS USSR. – 1986. – No. 8. – PP.3–11.

[58] Danevych T. B., Danylenko V.A. Nonlinear nonlocal models of multicomponent relaxing media with interior oscillators // Dop. NAS of Ukraine. - 2005. - Vol.1. - PP.106-110 (Ukr.).

[59] Nikolajevskiy V.N. Viscoelastisity with internal oscilations as a possible model of saismic media // Doclady AS USSR, 1985. – Vol.283, No.6. – PP.1321–1324.

[60] Danevych T.B., Danylenko V.A. Exact analitical solutions of nonlinear equations for dynamics of relaxing media with spatial and temporal nonlocalities. // Dop. NAS of Ukraine . - 2004. - No.3. - P. 110 - 114.

[61] Danevych T.B., Danylenko V.A. Exact analitical solutions of nonlinear equations for dynamics of nonlocal media taking into account of temperature terms and the nonstationarity of generalized thermodynamical force. // Dop. NAS of Ukraine . - 2004. - No.4. - P. 106 - 112.

[62] Danylenko V.A., Skurativskiy S. I. Chaotic invariant solutions of nonlinear nonlocal models for multicomponent media with internel oscilators // Dop. NAS of Ukraine, 2006. – Vol.9. – P. 111–115.

[63] Danylenko V.A., Skurativskyy S. I. Invariant chaotic and quasi-periodic solutions of nonlinear nonlocal models of relaxing media // Reports of mathematical physics, 2007. – Vol.59, No. 1. – PP. 45–51.

[64] Palmov V.A. On some model of media with complex structure // Journal of Applied Mathematics and Mechanics, 1969. – Vol.4. – PP.768–773.

[65] Slepjan L.I. The wave of deformation in rod with amortized mass // Mechanics of Solids, 1967. – No. 5. – PP.34–40.

[66] Bogolyubov N. N., Mitropolskyy Yu.A. Asimptotical methods in the theory of nonlinear oscilations. – Moscow: Nauka, 1974. – 504 p.

[67] Pisarenko G.S. Vibration of mechanical systems involving imperfectly elastic materials, Kyiv, Naukova dumka, 1970. – 357p.